Electronic components & applications

Vol. 3, No
February 19

ISSN 0141–6219

Electronic components & applications

Volume 3, No. 2 February 1981

Fibre-optics, current in computers and inter-city telephony may soon replace the solid copper link to the subscriber. If so, with a million gigahertz carrier, the way is open to an almost unlimited number of communications channels into our homes. On Page 87 we review the state of fibre-optic hardware. The telephone network also figures in an article on Page 110 where a microprocessor-based interactive peripheral system for Prestel is described. Prestel and its like, while not improving tv programmes do provide an alternative – information. They are also capable of putting more power within the grasp of the private citizen (and of authority!) than ever before.

What with increased channels and interactive systems, technology is taking us to where far-reaching social decisions will be needed. But, who knows? If the Tower of Babel was anything to go by they are decisions we may be spared.

Contents

Integrated circuits for car radios

B. P. BAHNSEN and A. GARSKAMP

Car radio manufacturers are currently basing the design of the f.m. section of the radio on either the ratio detector or the quadrature detector configuration. Which of these concepts is chosen depends on many criteria such as the manufacturer's cost structure, traditional design philosophies and the cost and availability of components in the country where the radio is assembled. Our comprehensive range of car radio integrated circuits shown in Fig. 1 therefore includes an optimally matched pair of f.m. circuits for i.f. amplification/detection and PLL stereo decoding for each concept. It also includes an impulse interference absorption circuit for the f.m. channel, a choice of two a.m. channels, a choice of three audio power output stages, and a cassette player motor control circuit with radio/cassette supply switching, tape-end indication and motor stop. All these circuits

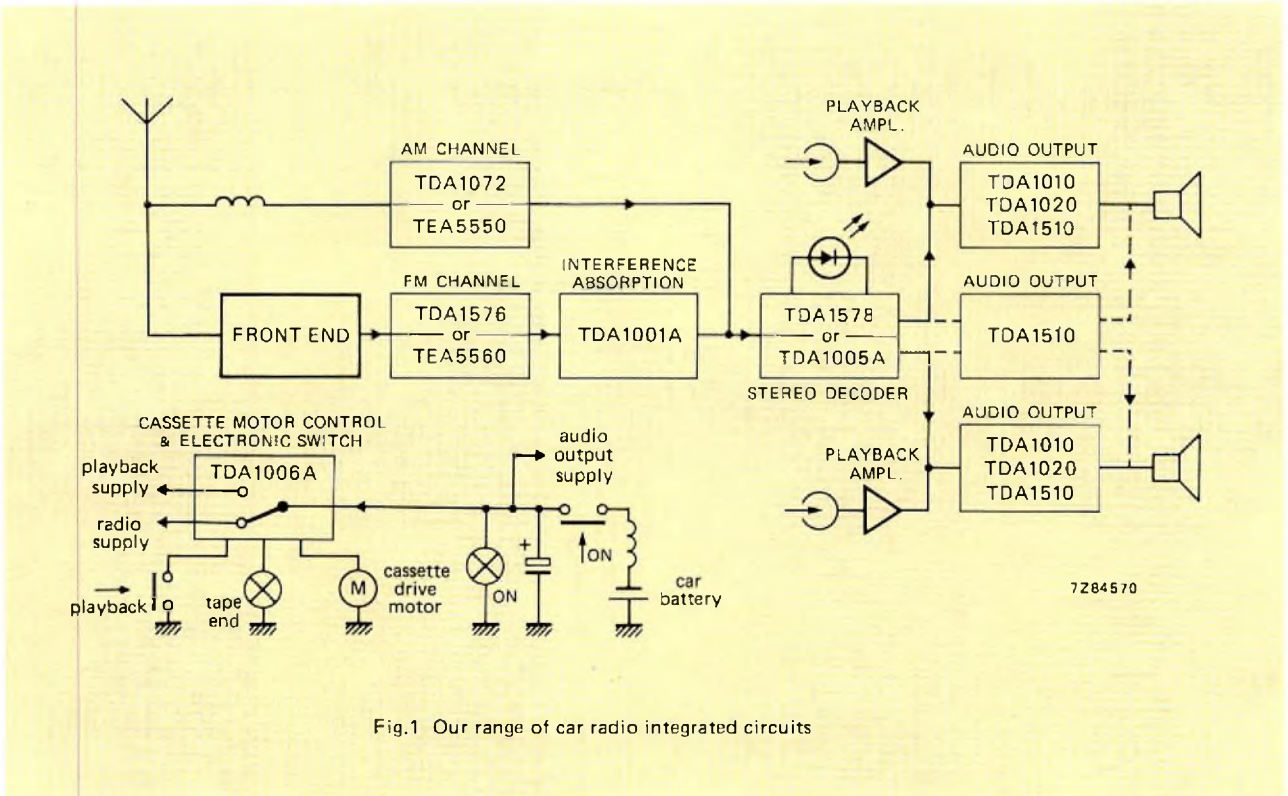

Fig.1 Our range of car radio integrated circuits

are specifically designed for use in car radios. This total system approach has minimised the number of peripheral components and switching contacts required, without degrading the performance of the circuits or decreasing the flexibility which allows them to be used with discrete circuits or with other integrated circuits outside our car radio range.

REQUIREMENTS FOR CAR RADIOS

Car radios operate in a hostile environment. Unlike home radios, they must be immune to wide variations of supply voltage (10,5 V to 16 V for normal operation; 8 V to 24 V for transients) and load dump, temperature (−30°C to +75°C) and aerial signal level (microvolts to volts). They must also be able to withstand severe mechanical shock whilst travelling over rough terrain and more gentle continuous vibration during normal driving. Furthermore, as many of the radio components as possible must be integrated both for high reliability and because the available space in the radio is being reduced by the incorporation of extra facilities. The latter problem is particularly acute in radio/cassette players. This article will show how our range of car radio integrated circuits can meet the following requirements:

Signal level considerations

- The r.f. section of the a.m. channel must have effective a.g.c. to provide low distortion during the reception of exceptionally strong signals.
- An a.g.c. range of about 90 dB is required to accommodate the wide range of aerial input levels.
- In the f.m. channel, precautions must be taken against the generation of hiss and sudden stereo/mono switching. Our system of field strength dependent control of muting and stereo channel separation solves this problem.
- Effective limiting must be provided in the f.m. i.f. stages or detector to ensure suppression of a.m. signals, especially whilst receiving weak signals.
- Automatic audio level control (smoothly controlled muting) must be provided to reduce interstation noise.
- The radio must have high sensitivity and low noise for satisfactory reception of weak aerial signals.

Interference suppression

- Interference due to ignition systems, neon signs and atmospherics must be suppressed. Our interference absorption circuit TDA1001A is ideal for this purpose.
- The radio must be protected against lightning induced surges.
- Suppression at the a.m. i.f. must be provided to eliminate interference due to broadcasts from sources such as ships, airports and navigational aids.
- A double-tuned aerial circuit can provide good image rejection.
- Whistles (tweets) due to the reception of signals close to the 2nd and 3rd harmonics of the i.f. must be adequately suppressed.

Audio fidelity and power

- The i.f. selectivity and bandwidth must be such as to allow faithful reproduction of modulation frequencies up to 3 kHz for a.m., and up to 12 kHz for f.m.
- Audio output stages must be available to supply a wide range of output powers to suit all classes of radios and power boosters. They must also incorporate standby switching to minimise noise and high currents due to switching transients.
- The integrated audio power circuits must require the use of only a few small passive components and the packages must be so designed that, where possible, they can be easily mounted on the case of the radio to provide extra heatsinking. They must have a wide range of useful gain and good ripple rejection and must also be protected against load dumping, loudspeaker short-circuit and excess dissipation so that they will not be damaged during manufacture and testing of the radio, or during its use.

Tuning systems

- To provide vibration immunity and simplify tuning mechanisms and preset station controls, facilities must be provided for permeability tuning or variable capacitance diode tuning.
- Buffered, constant, low-level local oscillator outputs must be available to facilitate microcomputer control of tuning, preset station selection and digital frequency indication. Variable capacitance diode tuning facilities are also required for this purpose.

CAR RADIO CIRCUIT DESIGN PHILOSOPHY

F.M. channel

It is well known that the necessary a.m. suppression for low noise in the f.m. channel of a car radio can be achieved if the i.f. amplifier is followed by a ratio detector. This type of balanced f.m. demodulator however, requires a lot of passive components including two h.f. capacitors, a matched pair of diodes and an electrolytic capacitor. It must also incorporate two tuned LC circuits that need alignment after the circuit has been assembled.

Despite its good performance in car radios, the ratio detector does not therefore lend itself to integration and consequently occupies a considerable amount of circuit-board area.

To maximise the integration of the f.m. detector and minimise the required adjustments without compromising performance, we have developed the TDA1576 integrated i.f. amplifier/detector circuit for the f.m. channel. This circuit incorporates a double balanced phase-shift detector which is entirely integrated and does not need external adjustment of balance. Only a single adjustment of an external 90° phase-shift network is required to achieve satisfactory performance. This type of quadrature detector however, does not provide a.m. suppression except for a signal at the zero-crossing of the demodulation curve. It is therefore preceeded by an i.f. amplifier with excellent low-level limiting characteristics. A field-strength dependent muting system is used to reduce interstation noise whilst tuning and to reduce noise under conditions of weak signals or rapidly varying signal strength. To economically exploit the full high performance of this system, the TDA1576 should be used in conjunction with the PLL stereo decoder TDA1578 because this circuit contains the muting system for control by signal-strength or detuning-dependent voltages from the TDA1576.

For those manufacturers who are not deterred by the discrete components of the ratio detector, the inherent high a.m. suppression of this type of detector can be exploited in conjunction with the simpler f.m. i.f. amplifier integrated circuit TEA5560. Since the ratio detector provides good a.m. suppression without the need for low-level limiting in the i.f. amplifier, the gain of the TEA5560 can be relatively low. This results in low interstation noise and a smooth tuning characteristic. Furthermore, since the i.f. circuits are isolated from the ratio detector by LC circuits, the a.f.c. can easily be applied because the detector output is without a d.c. offset component.

The TEA5560 also contains level detectors which generate a signal-strength dependent voltage that can be applied to the PLL stereo decoder TDA1005A to obtain smooth control of stereo channel separation and/or audio high-frequency response. The space saving 9-pin SIL package of the TEA5560 compensates for the additional circuit board area required by the components of the ratio detector.

A.M. channel

Market research has revealed that two types of a.m. channel are required to meet the needs of the broad range of present day car radio designs. Both types must of course satisfy the standard car radio performance requirements with respect to signal-to-noise ratio, high-level signal handling and distortion. They must be suitable for use with variable capacitance tuning diodes and either ceramic or LC i.f. filters and also be attractive for use in straightforward conventional radios. One type however must also be suitable for use in radios with features such as voltage controlled multi-band tuning to frequencies of up to 27 MHz, digital frequency display, frequency synthesis and microcomputer control. Our car radio integrated circuit range includes the TEA5550 and the TDA1072 to meet these requirements.

Although these circuits can be used with either of our f.m. channel circuits, for the sake of completeness, we have included the description of the TEA5550 in the section of this article devoted to the radio with a ratio detector for f.m. The TDA1072 is included in the description of the radio with a quadrature detector for f.m.

Audio power circuits

Despite the comparatively low voltage available in a car, a range of integrated audio power output circuits must be available to provide continuous sinewave output powers of between 5 W and 24 W for both mono and stereo operation. Both single and dual amplifier circuits are therefore required and, for higher powers, bootstrapping facilities must be provided; and, for output powers of greater than 12 W, dual circuits must be capable of operating in the bridge-tied load configuration. Our car radio range of integrated circuits therefore includes the following audio output stages:

TDA1010: Preamplifier and power amplifier for up to 6 W continuous sinewave power into a 4Ω or 9 W into a 2Ω loudspeaker. Encapsulated in an inexpensive 9-pin SIL package with a thermal resistance of 12 °C/W.

TDA1020: Preamplifier and power amplifier for continuous sinewave power of 7 W into a 4Ω loudspeaker or 12 W into a 2Ω loudspeaker. Pin compatible with the TDA1010 but with an improved performance specification and a thermal resistance of 8 °C/W.

TDA1510: Dual power amplifier for continuous sinewave power of 2 x 7 W into 4Ω loudspeakers or 2 x 12 W into 2Ω loudspeakers. In the bridge-tied load configuration, this circuit can provide up to 24 W into a 4Ω loudspeaker. Encapsulated in a 13-pin power SIL package with a thermal resistance of only 3 °C/W.

AM/FM RADIO WITH RATIO DETECTOR FOR FM

A.M. channel TEA5550

The a.m. receiver circuit TEA5550, connected as a medium-wave a.m. channel as shown in Fig. 2, performs all the a.m. channel functions between the aerial and the audio amplification stages of the car radio. It has the high performance required by car radios with regard to large signal handling and signal-to-noise ratio. Its ability to be used with ceramic i.f. filters, variable capacitance diode tuning up to 8 MHz, single-pin d.c. controlled on/off switching (a.m./f.m. selection) and very few peripheral components make it the ideal choice for the simpler type of high performance car radio.

Aerial input signals of up to 1.5 V, modulated to 80%, can be handled with distortion of less than 10%. A double balanced mixer provides low noise and high common-mode rejection. The LC filter at the mixer output prevents the generation of mixing products when the radio is detuned whilst receiving strong signals. It also prevents the local oscillator signal breaking through to the i.f. amplifier if ceramic filters are used. The oscillator is tuned by a tank circuit connected between the positive supply rail and a single pin of the TEA5550. The sensitive low-distortion envelope detector with emitter-follower output delivers the audio signals to pin 10 and also generates a well-defined a.g.c. voltage for the i.f. amplifier and mixer. The a.g.c. starting point can be adjusted at pin 14, from which the a.g.c. is also available for connection to external circuits. The a.m. channel can be muted by connecting a positive voltage to the a.g.c. decoupling point at pin 11, thereby inhibiting the local oscillator, applying full a.g.c. to the i.f. amplifier and switching off the emitter-follower that delivers the audio output to pin 10. The circuit can be supplied from an unstabilised source because an internal voltage stabiliser with an 8 V integrated reference diode supplies all of the internal circuits and can also provide up to 20 mA from pin 9. In this application, the internal voltage stabiliser is not used because the power supply is derived from the external stabiliser shown in Fig. 4.

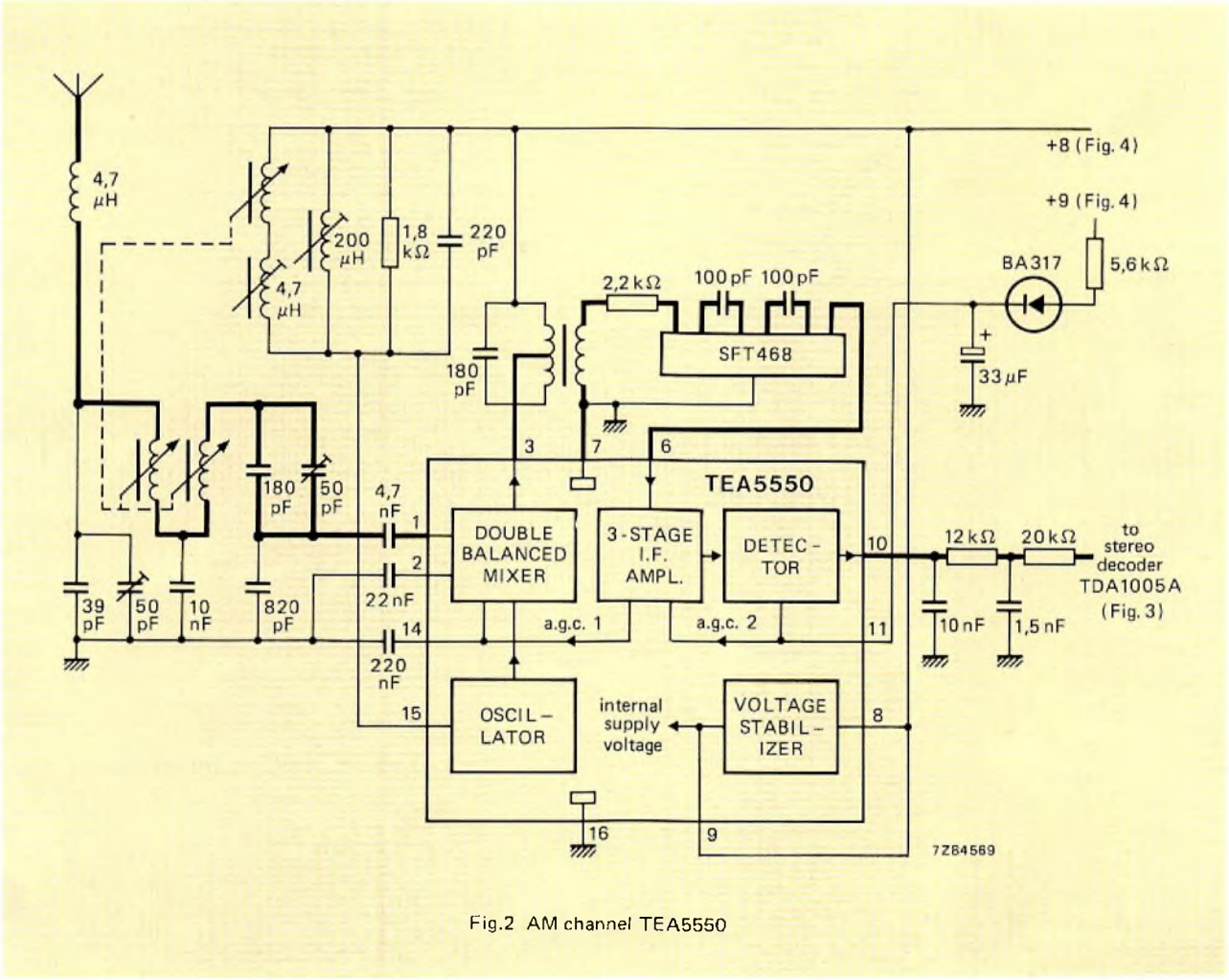

Fig.2 AM channel TEA5550

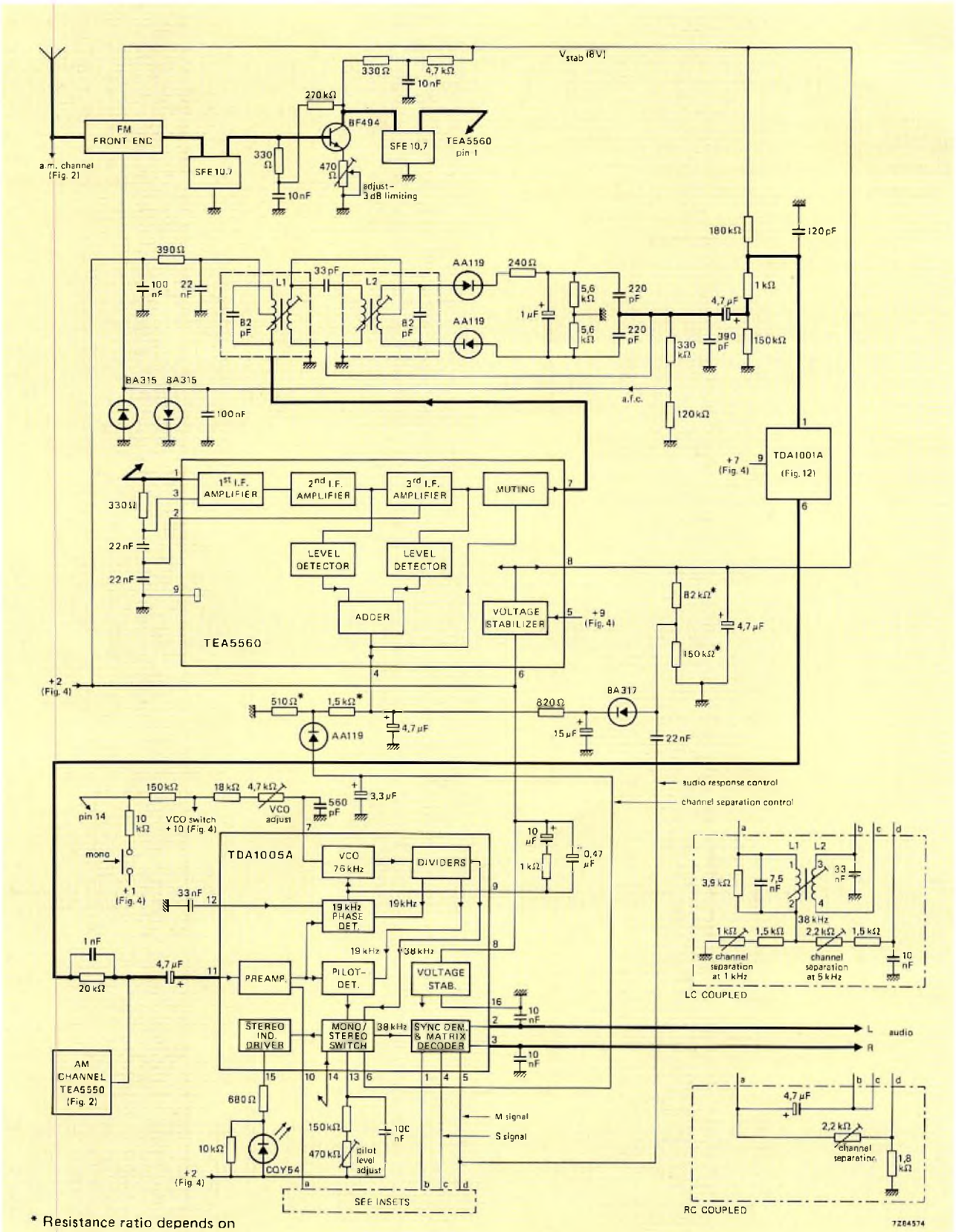

* Resistance ratio depends on specified 3 dB limiting level; values given here relate to performance given in Fig.6.

Fig.3 The r.f. section and stereo decoder of the car radio with a ratio detector for f.m.

F.M. i.f. system TEA5560

As shown in Fig.3, the TEA5560 incorporates three balanced differential stages of i.f. amplification which require very few external components. This results in a 150 μV input sensitivity 3 dB before limiting. In this application, an external preamplification stage with adjustment of overall i.f. gain is used. The external stage also allows the overall circuit design to meet the selectivity requirements of various classes of radio.

Alternatively, gain adjustment can be provided by connecting a variable voltage to pin 5. The outputs from the second and third i.f. stages are internally applied to level detectors to derive a d.c. voltage for controlling an internal interstation noise muting circuit, and for external field strength dependent control of smooth stereo/mono switching (stereo channel separation) and high-frequency audio response at the stereo decoder TDA1005A. The output from the final i.f. stage is applied via a muting circuit to an external ratio detector which provides a high signal-to-noise ratio (>70 dB for V_i = 1 mV and Δf = 22.5 kHz) and a typical 50 dB suppression of interfering a.m. signals, even under conditions of low field strength. An integrated voltage stabiliser supplies the internal circuits and also provides an 8 V output (15 mA max.). The circuit also incorporates stand-by switching which can be activated by a switch connected between pins 5 and 8. The switch is not used in this application because the supply switch is in the circuit shown in Fig.4. The integrated standby switch is on when a voltage is applied to pin 5. Since the a.m. channel is muted when a voltage is applied to the a.g.c. decoupling point at pin 11 of the TEA5550 (Fig.2), a.m./f.m. switching can be achieved with a simple changeover switch contact.

For simple mounting, the TEA5560 is encapsulated in a space-saving plastic SIL package with nine leads.

PLL stereo decoder TDA1005A

To achieve an easily adjusted stereo decoder system with few peripheral components, the TDA1005A shown in Fig. 3 extracts the L–R stereo information by phase comparing the detected stereo multiplex signal with a stable regenerated 38 kHz sub-carrier from a phase-locked loop (PLL). The VCO of the PLL has a guaranteed capture range of 3.5% of its tuned frequency and has a temperature coefficient of 400 p.p.m./°C without applying compensation. The TDA1005A is characterised by its many facilities and excellent suppression of both adjacent channel interference and beat frequency components within the audible frequency spectrum. It also causes very little harmonic distortion and exhibits a low spread of stereo/mono switching level.

The composite demodulated stereo input signal from the TEA5560 is buffered by an emitter follower in the preamplifier block and fed to the phase comparator in the PLL. In the PLL, the VCO frequency (76 kHz) is halved to 38 kHz in the divider block and halved again by a flip-flop to provide two antiphase 19 kHz signals. One of these signals is the other input to the PLL phase comparator. The output from this phase comparator maintains the VCO frequency at precisely 76 kHz.

The MPX input signal and the second 19 kHz signal from the flip-flop in the final part of the divider are applied to the inputs of the pilot presence detector. When the PLL is locked, the output from the pilot presence detector activates the mono/stereo switch which has two functions. One function is to light the stereo lamp via the stereo indicator driver; the other function is to switch the 38 kHz output from the output from the first part of the divider (regenerated subcarrier) to the decoder block where it is used for synchronous demodulation of the L and R stereo signals.

For LC coupled frequency-division multiplex decoding (see Fig.3 inset), the subcarrier component (L–R, 23 kHz to 53 kHz) is separated from the MPX signal by a band-pass filter and applied as the other input to the synchronous demodulator at pin 4. The output from the demodulator is therefore the L–R and –(L–R) stereo information. The resonance curve of the band-pass filter provides the de-emphasis. The main (L+R, 0 to 15 kHz) component of the MPX signal is applied to the input of an amplifier at pin 5. De-emphasis is provided by the time constant of the components between pins 10 and 5. The L+R information from the main signal amplifier is matrixed with the L–R and –(L–R) information from the synchronous demodulator to provide the L and R audio signals at pins 2 and 3.

For RC coupled decoding with relaxed specification for spurious outputs (see Fig.3 inset), the MPX signal is fed directly from pin 10 to pin 5 and, via d.c. decoupling capacitor to pins 1 and 4. In this case, de-emphasis is applied by the capacitors at output pins 2 and 3. Features of the TDA1005A are:

- The upper limit of the audio-frequency response can be lowered (de-emphasis) by connecting a capacitor between pin 5 and the common return. This facility, which improves the signal-to-noise ratio during the reception of weak signals can be made dependent on signal strength by connecting the capacitor via an active element controlled by the level detector output from the TEA5560.

- The transition from stereo to mono (channel separation) can be smoothly controlled as a function of signal strength by controlling the voltage at pin 6 with the level detector output from the TEA5560.

- To prevent interference from the VCO when the radio is operating on a.m., the VCO can be switched off by connecting pin 7 to the common return or, via a 100 kΩ resistor, to the positive supply rail. Alternatively, pin 9 can be connected, via a 100 kΩ resistor, to the common return.
- The system can be switched to mono (stereo override) by connecting pin 14 to the common return.
- The circuit has a built-in gain of 7 dB (RC coupled demodulation) or 10 dB (LC coupled demodulation) which is also useful during a.m. reception.

Interface circuits

In the circuit shown in Fig.3, a discrete r.f. preamplifier transistor is used, tuned at its base and collector by ceramic filters. Besides allowing adjustment of the limiting level, the potentiometer in the emitter lead of the transistor also allows compensation for the spread of the limiting −3 dB level and spread of the outputs from the level detectors in the TEA5560.

To control the stereo channel separation as a function of signal strength, the level detector output from pin 4 of the TEA5560 is used to apply control voltages between 0.65 V (mono) and 1.3 V (full stereo) to pin 6 of the stereo decoder TDA1005A. The potential divider connected to pin 4 of the TEA5560 determines the control starting point. The values shown in the diagram cause control to start when the aerial input falls to about 200 μV. At this signal level, the signal-to-stereo noise ratio has reduced from 67 dB to 55 dB. The control causes the stereo channel separation to reduce smoothly so that it reaches 0 dB (mono) when the aerial input has fallen to 20 μV. At this point the signal-to-noise ratio is 57 dB. The values of the resistors in the potential divider can be changed to allow the control to start for aerial input voltages within the range 90 μV to 200 μV, which will cause mono operation (0 dB channel separation) for aerial input levels of 18 μV and 50 μV respectively. If the manual stereo override facility is used at pin 14 of the TDA1005A, the voltage at pin 6 will be internally reduced to the level required to cause mono operation. A diode is therefore connected between pin 6 of the TDA1005A and the potential divider junction to prevent the channel separation control voltage inhibiting the stereo override function.

To ensure high sensitivity and low noise for satisfactory reception of weak aerial signals, the high-frequency audio response is controlled as a function of signal strength by the level detector output from pin 4 of the TEA5560 (0.25 V to 5.7 V for aerial inputs of 5 μV to 600 μV). This is achieved by connecting the control voltage to one side of a 22 nF capacitor, the other side of which is connected to the M-signal input at pin 5 of the TDA1005A. A potential divider connected

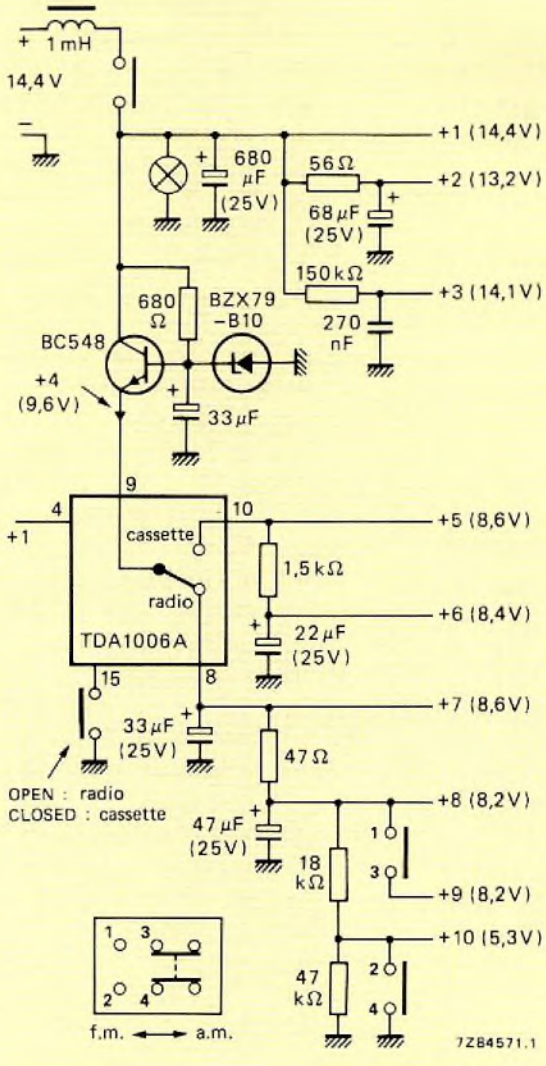

Fig.4 Power supply and switching circuit

to the 8 V stabilised supply at pin 8 of the TEA5560 connects about 3.5 V to the anode of a diode to set the upper limit of the control voltage. This causes the control to start at an aerial input of 200 μV and gradually increase the normal 50 μs de-emphasis so that it reaches 75 μs when the aerial input level has fallen to 30 μV. Although the control voltage is decoupled by the 4.7 μF capacitor connected to pin 4 of the TEA5560, the additional RC filter (820Ω/15 μF) is necessary to prevent noise from the level detector in the TEA5560 being injected into pin 5 of the TDA1005A, thereby degrading the overall signal-to-noise ratio of the radio.

Power supplies and switching

The stabilised power supplies and switching for the complete a.m./f.m. stereo car radio with cassette player are derived as shown in Fig. 4. The supplies are connected as follows:

+1 (14.4 V) Power amplifier in TDA1010 (pin 3).
+2 (13.2 V) TEA5560 pin 6 and TDA1005A pin 8.
+3 (14.1 V) Preamplifiers in TDA1010 (pin 5).
+4 (9.6 V) TDA1006A pin 5.
+5 (8.6 V)
+6 (8.4 V) Discrete cassette player playback amplifiers.
+7 (8.6 V) TDA1001A pin 9.
+8 (8.2 V) TEA5550 pins 8 and 9.
+9 (8.2 V) Switched supply to TEA5560 pin 5 and TEA5550 pin 11.
+10 VCO muting to TDA1005A.

PERFORMANCE OF THE COMPLETE RADIO

General

Supply voltage range	10.2 to 16	V
Operating ambient temperature range	−30 to +75	°C
F.M. frequency range	87.5 to 104	MHz
A.M. frequency range	510 to 1650	kHz
F.M. i.f.	10.7	MHz
A.M. i.f.	468	kHz
F.M. aerial input impedance	75	Ω asym.

A.M. characteristics

V_{supply} = 14.4 V, T_{amb} = 25 °C, f_0 = 1 MHz, m = 0.3, f_{mod} = 1 kHz unless otherwise specified.
Dummy aerial as shown in Fig.5.

Aerial input voltage		
for (S+N)/N = 6 dB	3.6	μV
for (S+N)/N = 20 dB	21	μV
for (S+N)/N = 26 dB	42	μV
for P_o = 500 mW	5.2	μV
Signal-to-noise ratio		
for V_{in} = 1 mV	50	dB
A.G.C. range		
V_{in}/500 mV for 10 dB variation of a.f. output	90	dB
R.F. signal handling capability		
at m = 0.8, T.H.D. < 10%	1.5	V
Total harmonic distortion		
over most of the a.g.c. range, m = 0.8, f_{mod} = 400 Hz	1.2%	
R.F. bandwidth B_{3dB}	25	kHz
R.F. + i.f. bandwidth B_{3dB}	4.2	kHz
Fidelity (− 3 dB)	30 Hz to 1.8	kHz
I.F. suppression		
tuned frequency 600 kHz, V_{in} = 20 μV	75	dB
Image rejection		
tuned frequency 1400 kHz, V_{in} = 20 μV	65	dB
Overall performance spread:		
for supply voltage variation 10.5 V to 16 V	±1	dB

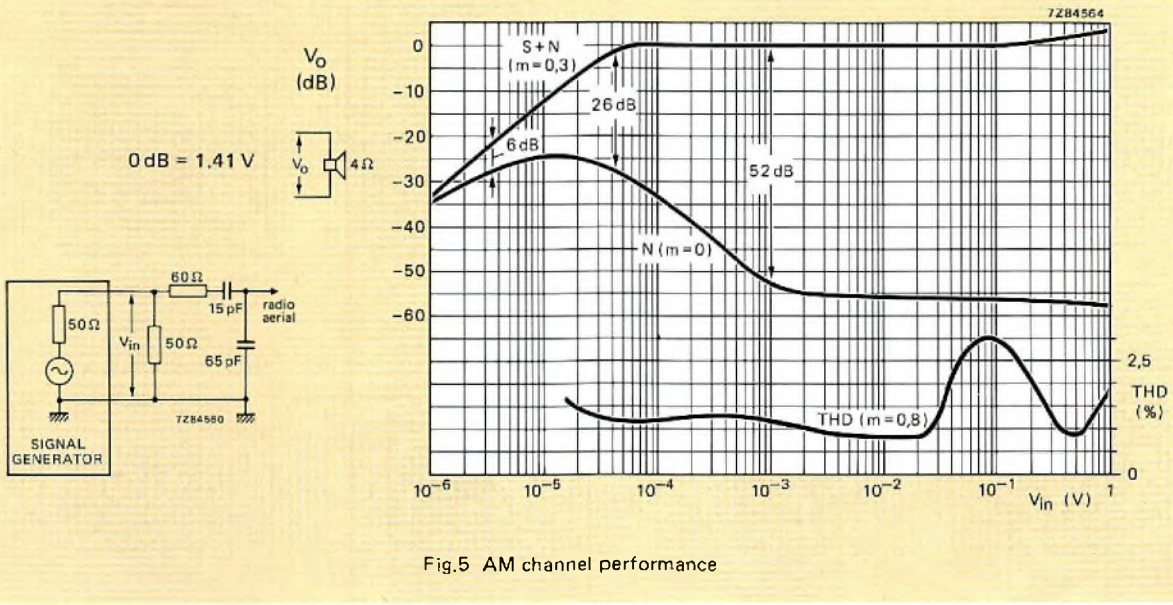

Fig.5 AM channel performance

F.M. characteristics

V_{supply} = 14.4 V, T_{amb} = 25 °C, f_o = 98 MHz, Δf = ±22.5 kHz, f_{mod} = 1 kHz unless otherwise specified.
Dummy aerial as shown in Fig.6.

Aerial input voltage (Z_s = 75 Ω asymmetrical);		
for −3 dB limiting (adjustable):	10-30	μV
for (S+N)/N = 26 dB:	2.2	μV
Signal-to-noise ratio;		
over most of the frequency range:	65	dB
R.F. signal handling capability;		
for Δf_{osc} = 50 kHz		
(dependent on type of front-end):	800	mV typ.
A.F. output over most of the signal range;		
measured at: ratio detector output:	200	mV
TDA1001A output:	220	mV
TDA1005A input:	100	mV
TDA1005A output:	200	mV
A.M. suppression;		
over most of the signal range	50	dB
Total harmonic distortion over most of the signal range;		
Δf = 22.5 kHz	0.25%	
Δf = 40 kHz	0.5%	
Δf = 75 kHz	1.6%	
I.F. selectivity S_{300}:	50	dB
I.F. bandwidth B_{3dB}:	170	kHz
Overall performance spread;		
for supply voltage variation 10.5 V to 16 V:	±2	dB

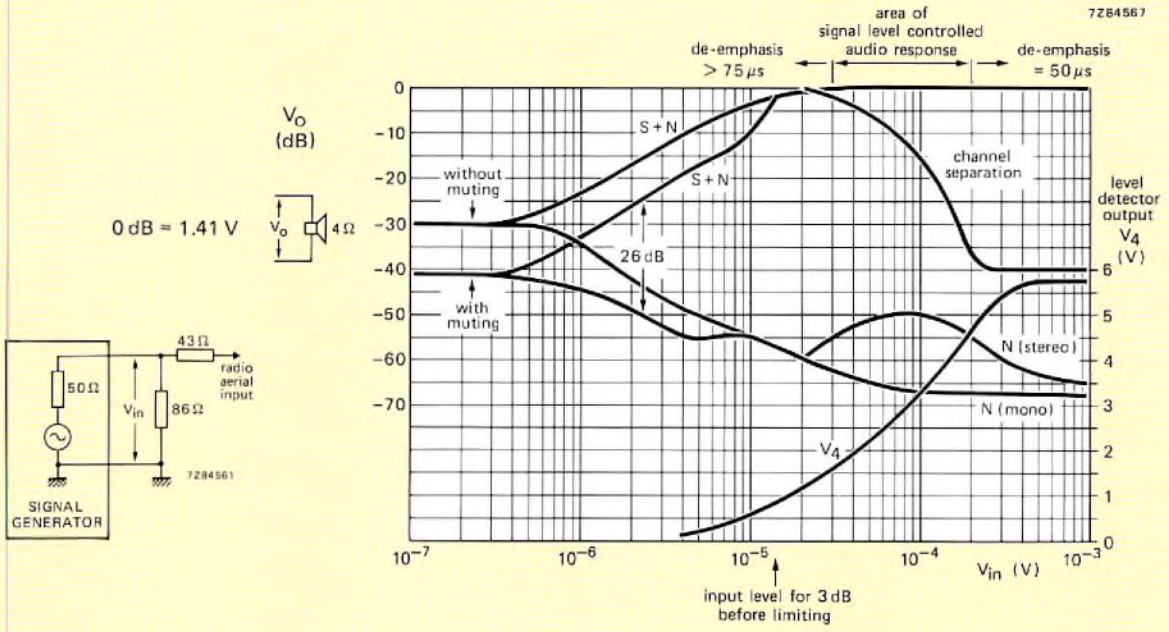

Fig.6 Weak signal performance of the f.m. channel

A.M./F.M. RADIO WITH QUADRATURE DETECTOR FOR F.M.

A.M. channel TDA1072

The a.m. receiver circuit TDA1072, connected for medium-wave operation as shown in Fig. 7, performs all the a.m. channel functions required between the aerial and the audio amplification stages of the radio. Its low distortion handling of a wide dynamic range of input signals and its many additional features make it suitable even for use in fully comprehensive high-performance car radios.

Input signals of up to 2.1 V, modulated to 80%, can be handled with less than 10% distortion and the dis-

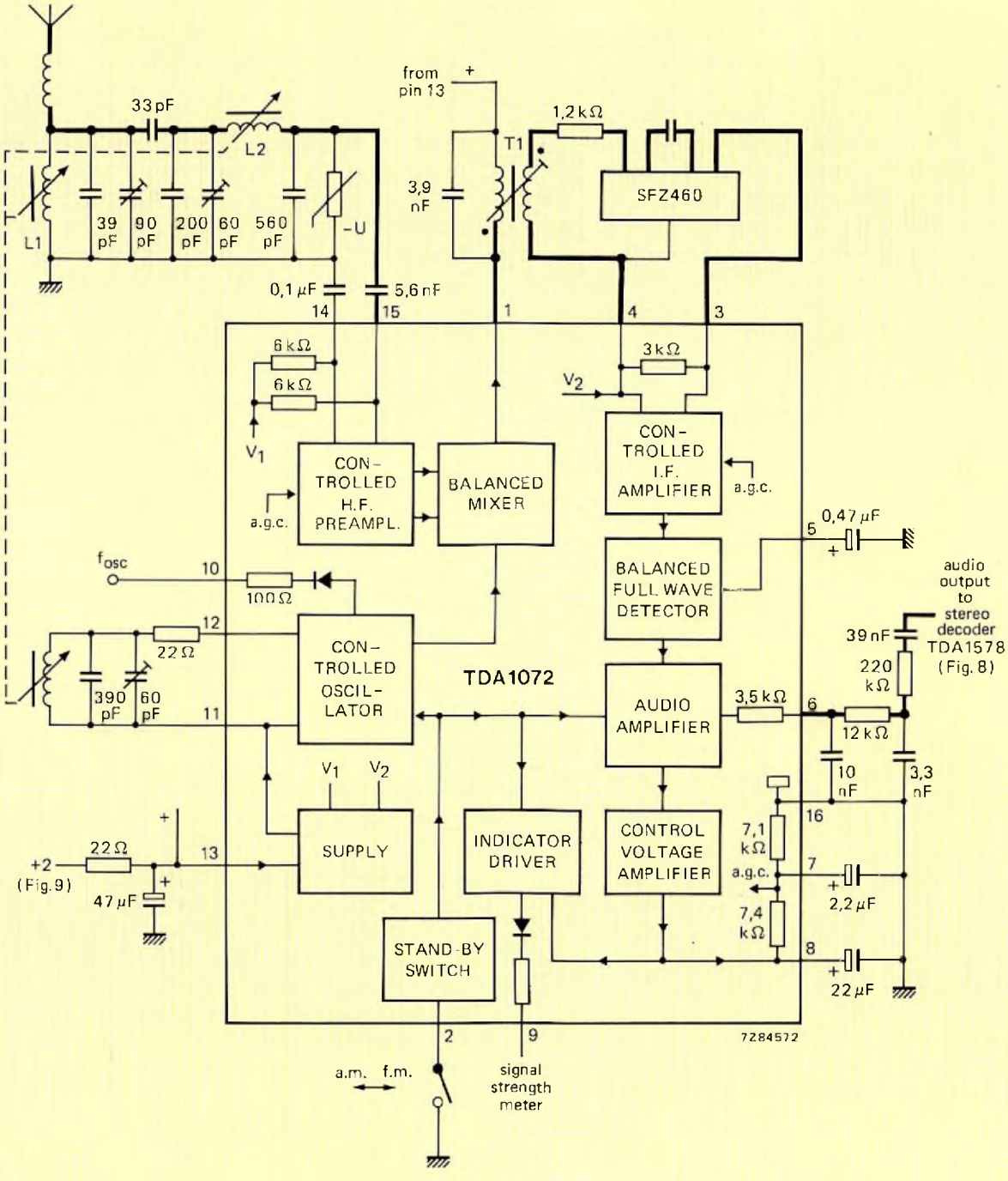

Fig.7 AM channel TDA1072

tortion remains low (0.5%) even during weak signal conditions. This is mainly due to the use of a balanced full-wave detector with internal i.f. filter. Although the permeability tuned band-pass filter is asymmetrically coupled to the r.f. preamplifier, the i.f. rejection is 60 dB at 520 kHz and 110 dB at 1620 kHz with the unloaded Q of the permeability tuned filter of 50. The fully symmetrical mixer is essential to achieve this performance.

The i.f. selectivity is concentrated in a hybrid filter comprising a tuned LC circuit followed by a 2nd-order ceramic filter at the output from the mixer. The LC circuit prevents the intermodulation distortion which would be generated if the radio were detuned during the reception of a strong signal. The a.g.c. loop contains a 2nd-order filter comprising two internal resistors and two external capacitors at pins 7 and 8. The filter component values are chosen to reduce harmonic distortion of low-frequency modulation without causing too much delay of the a.g.c. The starting levels of the a.g.c. for the three controlled stages (r.f. preamplifier and two i.f. stages) are determined internally and are therefore independent of the spreads of external components.

Both for mixing and for using variable capacitance diode tuning, it is desirable that the amplitude of the local oscillator signal should be independent of tuned frequency, even if the radio incorporates long and short-wavebands in addition to the medium-wave. The TDA 1072 local oscillator output at pin 12 is therefore controlled at a typical level of 140 mV up to a frequency of 50 MHz. A buffered output from the oscillator is also available at pin 10 for driving a frequency synthesiser (e.g. for microcomputer-controlled tuning and/or digital frequency indication). This output can provide up to 2 mA and has a source resistance of 150 Ω.

A buffered output signal which is a logarithmic function of the aerial input voltage can provide up to 1.2 mA from pin 9 for driving a signal strength indicator. With an aerial input of 500 mV, the typical signal strength output is 2.8 V. The TDA1072 can be switched on and off (a.m./f.m. selection) by an internal standby switch activated by connecting pin 2 to the common return. As required for car radio, the signal handling performance of the TDA1072 varies by less than 1 dB over the entire temperature and supply voltage operating ranges specified for the circuit.

Integrated f.m. i.f. circuit and quadrature detector TDA1576

This circuit is designed for optimum performance with minimum peripheral components, as shown in Fig. 8.

The completely integrated four-stage symmetrical limiting i.f. amplifier provides a 22 μV sensitivity 3 dB before limiting and a signal-to-noise ratio of 75 dB ($\Delta f = \pm 22.5$ kHz) with an input voltage of 1 mV. The i.f. amplifier limiting level and the signal-to-noise ratio are almost constant for input impedances of between 50 Ω and 300 Ω. The a.m. suppression is 50 dB ($\Delta f = \pm 22.5$ kHz) over most of the input signal range. A voltage which is a logarithmic function of the input voltage is provided for driving a signal strength indicator and/or controlling stereo channel separation in the TDA1578 as a function of signal strength. An internal standby switch allows the circuit to be switched on and off (a.m./f.m. switching) by connecting pin 5 to the common return. The i.f. amplifier is followed by a fast-acting muting circuit and a quadrature detector which is entirely integrated except for the simple 90° phase-shift network. The circuit generates much less noise during tuning and the reception of rapidly fluctuating signals than conventional high-gain systems with quadrature detectors. This is due to the fast-acting muting circuit which can be controlled by the previously mentioned field-strength dependent control voltage. Alternatively, when the TDA1576/TDA1578 combination is used, the muting circuit in the TDA1576 can be inhibited and a muting attenuator in the TDA1578 can be controlled by the field-strength dependent voltage, and/or by the detuning detector output derived from the quadrature detector S-curve. Other features of the TDA1576 include a symmetrical a.f.c. output with low spread and d.c. offset shift, electronic smoothing to eliminate hum in the audio output and a reference voltage output for use with the field-strength dependent and detuning control voltages. This reference voltage has a temperature dependence matched to the temperature dependence of the muting attenuator and the smooth mono/stereo switching in the PLL stereo decoder so that the temperature dependence of these functions is negligible.

PLL stereo decoder TDA1578

The TDA1578 shown in Fig. 8 is a time-division multiplex stereo decoder designed for optimum performance with minimum peripheral components. The stereo decoding function is similar to that previously described for the PLL stereo decoder TDA1005A operating in the RC coupled mode and will not therefore be explained again. The circuit incorporates internal suppression of adjacent channel interference (114 kHz), suppression of interference from traffic warning identification signals (57 kHz), and electronic filtering of hum on the supply line.

At input pin 6, the level of the signals from the f.m. and a.m. detectors can be matched by the use of input current matching resistors. This eliminates the need for a switching contact and individual level-matching potentiometer networks. The overall gain of the decoder is

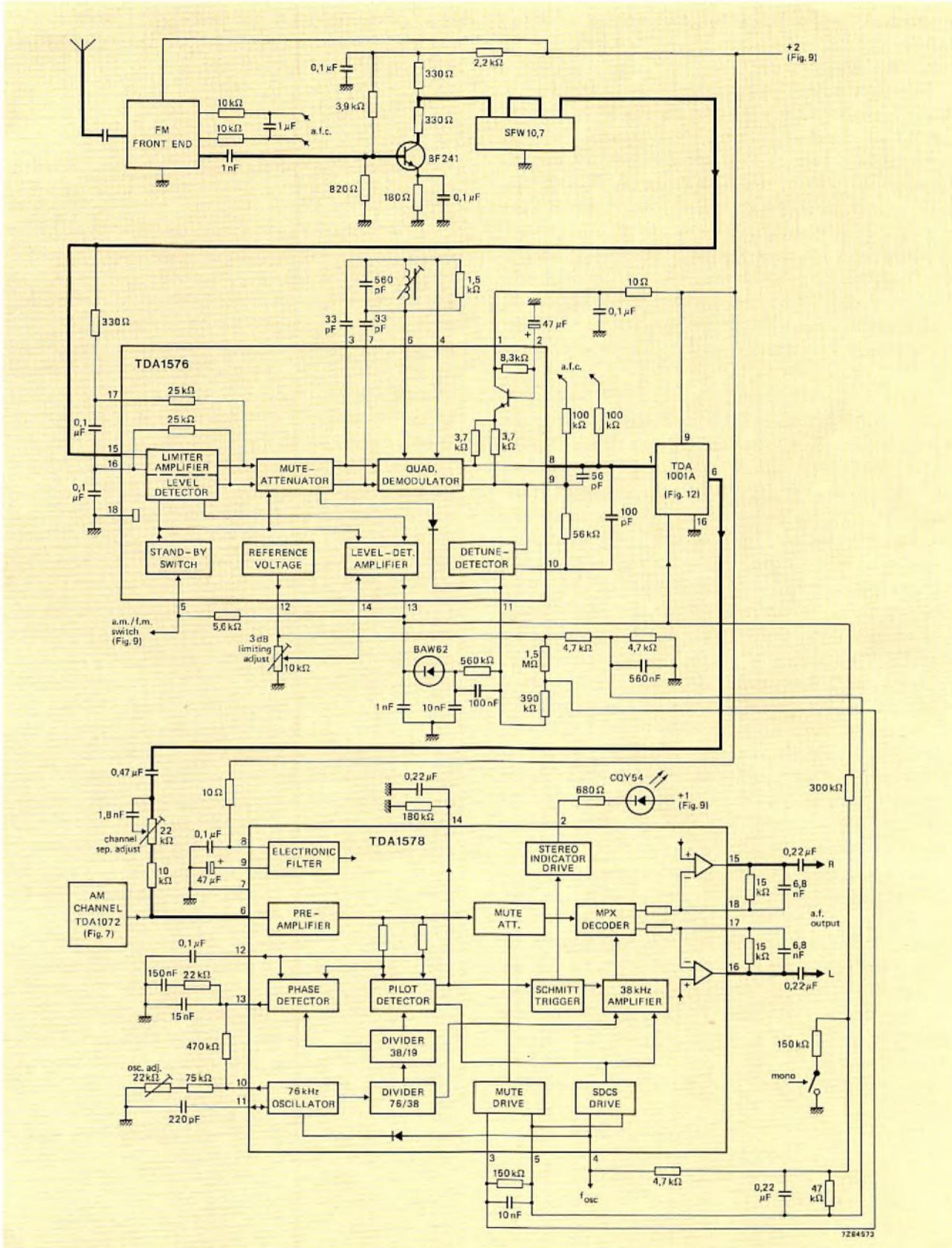

Fig.8 The r.f. section and stereo decoder of the car radio with a quadrature detector for f.m.

determined by the values of the external resistors. In the application shown in Fig.8, the overall gain is 10 dB ± 0.5 dB.

The pilot tone presence detector is followed by a Schmitt trigger which switches on the MPX decoder and the pilot indicator when a stereo signal is received. The switching level of this Schmitt trigger is proportional to the level of the supply voltage. When the circuit is used in conjunction with the TDA1576, the switching level is compensated for supply voltage variations because the audio output level from the quadrature detector exhibits the same degree of supply voltage dependence. Stereo override can be achieved by simply connecting pin 14 to the common return, thereby inhibiting the output from the pilot tone presence detector.

The circuit also incorporates an audio attenuator before the MPX decoder. This attenuator has externally adjustable slope and level and, in the TDA1576/TDA 1578 combination reduces noise during the reception of rapidly changing signal levels and suppresses interstation noise. If the control voltage between pins 3 and 5 is varied between 0 V and −500 mV, the attenuation varies between 0 dB and 60 dB. The voltage at pin 5 is the reference voltage from the TDA1576 and the control voltage can be the field-strength dependent voltage and/or the output from the detuning detector in the TDA1576. The slope of the attenuation characteristic is set by the two external resistors connected to pin 3. When the muting system is in use, the mute indicator driver can control a LED connected to pin 1. The indicator lights when the muting is less than 1 dB and is switched off when the muting exceeds 6 dB. If the muting system is controlled by the output from the detuning detector in the TDA1576, the lamp will light when the radio is correctly tuned.

Smooth control of mono/stereo switching (control of channel separation) can be achieved by applying a control voltage between pins 4 and 5. With the same voltage on pins 4 and 5 the channel separation is at least 38 dB. This reduces to 0 dB when the voltage difference between pins 4 and 5 is increased to 200 mV. The pilot presence detector switches off (mono) when there is a difference of 275 mV between pins 4 and 5, and switches on (stereo) when the voltage difference reduces to 250 mV. The slope of the mono/stereo characteristic is controlled by the resistors connected between pins 4 and 5. The channel separation control function will be field-strength dependent if the pin 4 control voltage is derived from the TDA1576. During a.m. reception, the VCO need not be switched off because it has a symmetrical triangular waveform and the oscillator capacitor presents a very small load. If 6 V is applied to pin 4, it becomes a test point at which the VCO output signal is available for alignment purposes. The uncompensated temperature coefficient of the free-running frequency of the VCO is typically zero with spreads to 100 p.p.m./°C.

Interface circuits

In the circuit of Fig. 8, special care has been taken to reduce the number of adjustable components required by minimising the spread of sensitivity to temperature and supply voltage variations. A discrete r.f. preamplifier stage is used to ensure good a.m. suppression, even during the reception of weak signals, and to compensate for the insertion loss of the ceramic filter. This additional amplification causes h.f. limiting even with aerial signals as small as 2 μV. It also, however, increases the overall noise level of the circuit. The noise is reduced again by controlling the audio muting circuit (progressive attenuator) at pin 3 of the TDA1578 stereo decoder with field-strength dependent and detuning dependent control voltages from the TDA1576. The control voltages from pins 13 and 11 of the TDA1576 are referred to the reference level at pin 12. This reference level is also applied to the level detector at pin 14 via a potentiometer which is the only component that requires adjustment to compensate gain spreads in the f.m. front-end, ceramic filter and i.f. amplifier. The starting point of the muting (−3 dB) occurs at an aerial input level of 15 μV and the interstation noise (no signal) is fixed at 30 dB below the level of strong signals. These parameters and the response time of the muting are determined by the values of the peripheral fixed resistors and capacitors in the control lines. Hiss due to rapid changes of signal strength can also be eliminated by correct choice of the RC time constants in the control lines. The effect of the muting on the weak signal performance of the f.m. channel is shown in Fig. 11.

With an aerial input level of 20 μV, the signal-to-noise ratio has reached 50 dB and a controlled smooth transition from mono to stereo operation starts. This function is controlled by the signal-strength dependent voltage level from pin 13 of the TDA1576. This control voltage is applied to the signal-dependent channel separation (SDCS) block at pin 4 of the TDA1578. Full channel separation is achieved when the signal level at the aerial reaches 300 μV. The stereo signal-to-noise ratio remains almost constant at 50 dB throughout the control range.

Stereo override is achieved by the switch and resistors connected between pin 4 of the TDA1578 and the common return. The characteristics of the automatic channel separation control are determined by the values of the peripheral components in the control line connected to pin 4 of the TDA1578.

Power supplies and switching

The power supplies and switching for the complete a.m./f.m. stereo car radio are derived as shown in Fig. 9. The supply voltages are connected as follows:

+ 1 (14.4 V) Audio amplifiers and supply for stereo indicator connected to pin 2 of TDA 1578.

+ 2 (9.3 V) F.M. front-end, discrete r.f. amplifier, TDA1576, TDA1001A, TDA1578, TDA1072.

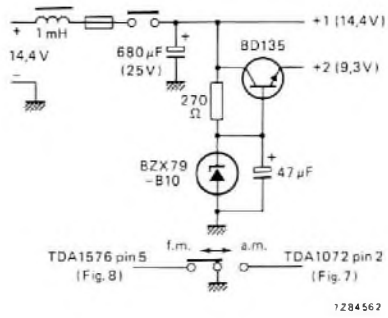

Fig.9 Power supply and switching circuit for the car radio with a quadrature detector for f.m.

PERFORMANCE OF THE COMPLETE RADIO

General

Supply voltage range	10.5 to 16	V
Operating ambient temperature range	−30 to +80	°C
F.M. frequency range	87.5 to 108	MHz
A.M. frequency range	510 to 1620	kHz
F.M. i.f.	10.7	MHz
A.M. i.f.	460	kHz
F.M. aerial input impedance	150	Ω asym.

A.M. characteristics

V_{supply} = 14.4 V, T_{amb} = 25 °C, f_0 = 1 MHz, m = 0.3, f_{mod} = 400 Hz unless otherwise specified.
Dummy aerial as shown in Fig.10.

Aerial input voltage		
for (S+N)/N = 6 dB	5	µV
for (S+N)/N = 20 dB	27	µV
for (S+N)/N = 26 dB	64	µV
Signal-to-noise ratio		
for V_{in} = 1 mV	48	dB
A.G.C. range		
V_{in}/500 mV for 10 dB variation of a.f. output	92	dB
V_{in}/500 mV for 6 dB variation of a.f. output	91	dB
R.F. signal handling capability		
at m = 0.8, T.H.D. = 3%	1.3	V
T.H.D. = 10%	2.1	V
Total harmonic distortion		
over most of the a.g.c. range, m = 0.8	0.5%	
R.F. bandwidth B_{3dB}	18.5	kHz
R.F. + i.f. bandwidth	3.9	kHz
Fidelity (− 3 dB)	30 Hz to 1.75	kHz
I.F. suppression		
tuned frequency = 510 kHz	64	dB
= 1 MHz	101	dB
= 1.62 MHz	>110	dB
Image rejection		
tuned frequency = 510 kHz	80	dB
= 1 MHz	71	dB
= 1.62 MHz	62	dB

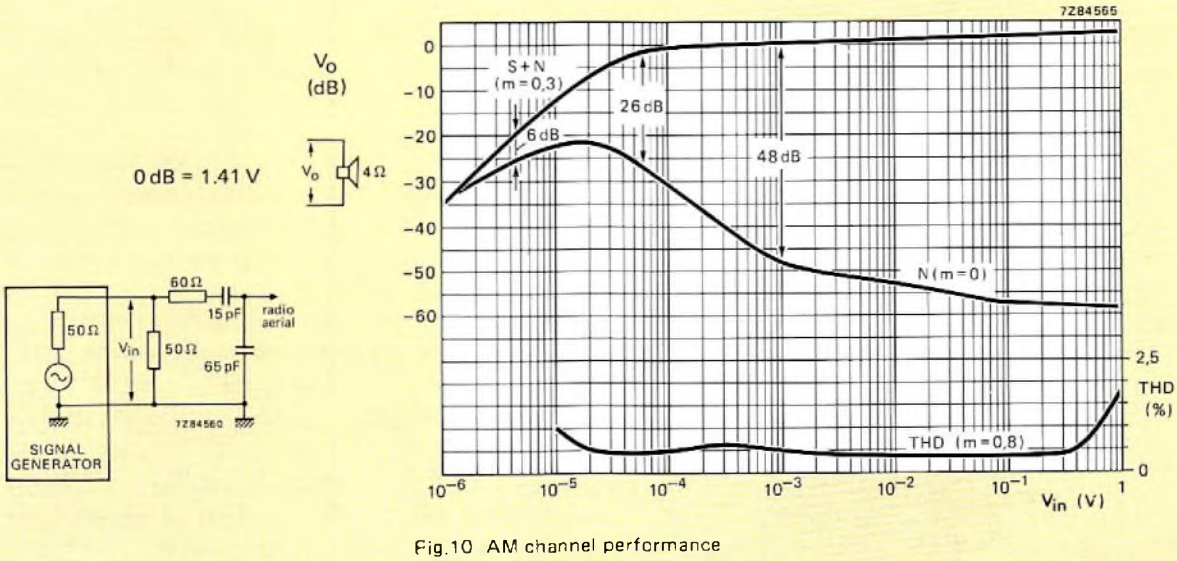

Fig.10 AM channel performance

F.M. characteristics

V_{supply} = 14.4 V, T_{amb} = 25 °C, f_o = 98 MHz, Δf = ±22.5 kHz, f_{mod} = 1 kHz unless otherwise specified
Dummy aerial as shown in Fig.11.

Aerial input voltage (Z_s = 150 Ω)		
for −3 dB limiting (adjustable)	10-30	μV
for (S+N)/N = 26 dB	3.3	μV
	(Z_s = 75 Ω) 2.2	μV
Signal-to-noise ratio		
over most of the frequency range	65	dB
R.F. signal handling capability		
for Δf_{osc} = 50 kHz		
(dependent on type of front-end)	800	mV typ.
A.F. output over most of the signal range		
measured at: quadrature detector output	80	mV
TDA1001A output	85	mV
TDA1578 output	250	mV
A.M. suppression:		
over most of the signal range	50	dB
Total harmonic distortion		
Δf = ±22.5 kHz	0.15%	
Δf = ±40 kHz	0.25%	
Δf = ±75 kHz	0.8%	
I.F. selectivity S_{300}	70	dB
I.F. bandwidth B_{3dB}	160	kHz

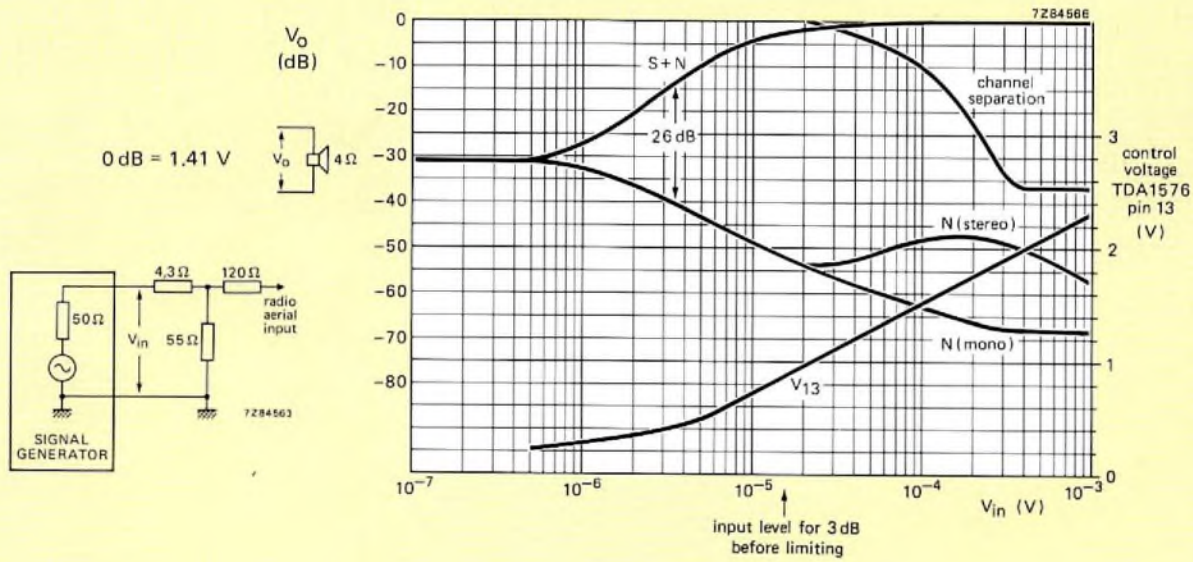

Fig.11 Weak-signal performance of the f.m. channel

INTERFERENCE ABSORPTION CIRCUIT TDA1001A

The high-quality reception capability of the f.m. channel of a car radio is often marred by the intrusion of h.f. interference radiated by vehicle ignition systems, neon signs, atmospherics and tyre static. This type of interference is characterised by brief pulses with steep flanks and a repetition rate dependent on the nature of the source. Although such interference can be minimised by accurate i.f. alignment, precise tuning, a well-balanced detector and the installation of suppression components in the electrical system of the car, it cannot be entirely eliminated by these means. We therefore developed our well-known interference absorption integrated circuit TDA1001 for incorporation between the detector and stereo decoder of the f.m. channel.

In accordance with our policy of constantly reviewing the performance required from our components in the light of our customers' experience, we have now considerably improved the circuit and allocated it the new type number TDA1001A. As shown in Fig. 12, the operation of the TDA1001A is based on the use of a high-pass filter separating the interference from the audio signal. The interference pulses are then used to trigger a one-shot. In this way, gating pulses are obtained to interrupt the audio signal after it has been delayed by a low-pass filter. During the gating periods,

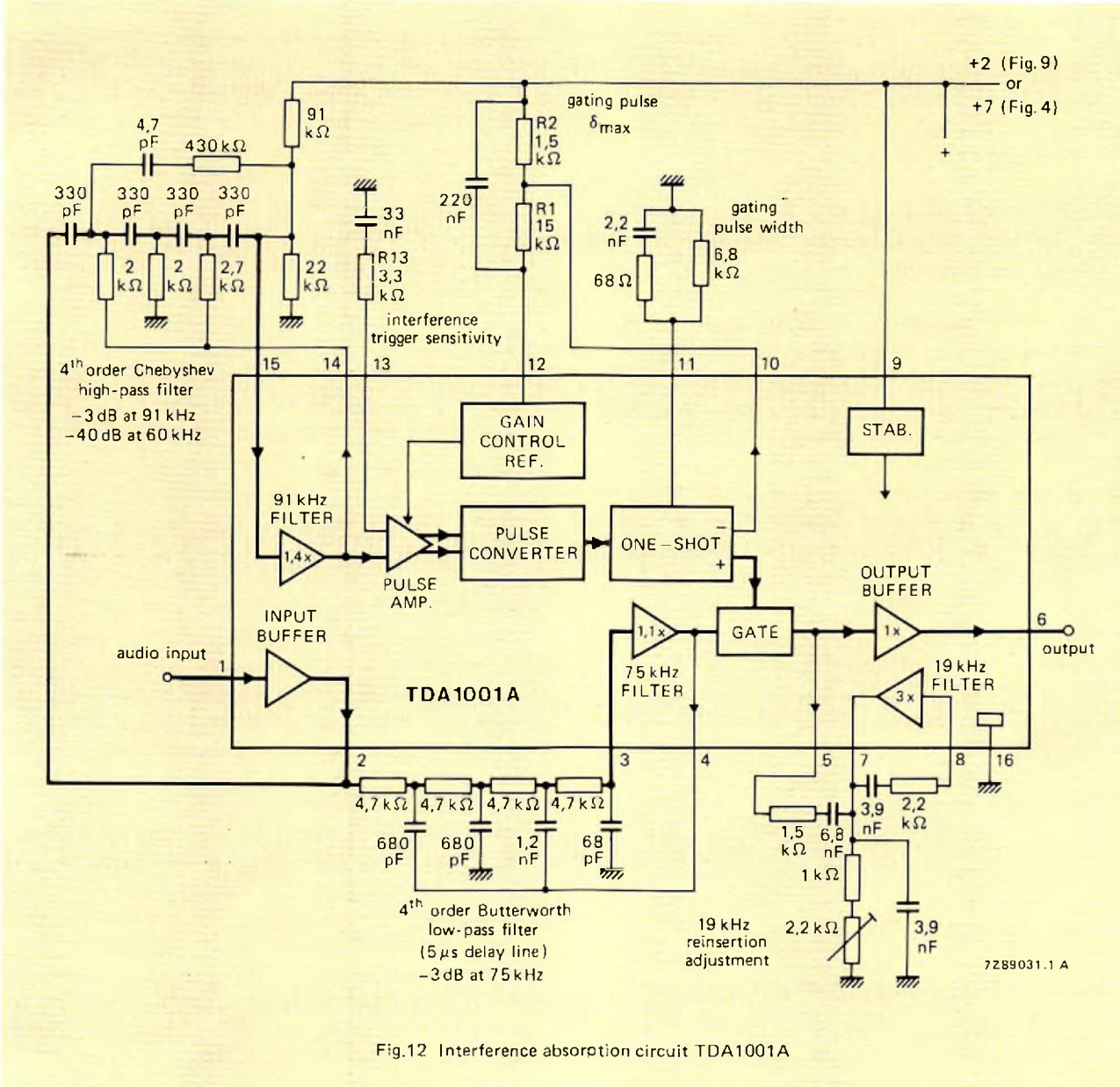

Fig.12 Interference absorption circuit TDA1001A

the output level is maintained by the RC network connected to pin 5. A 19 kHz resonant circuit can be completed by the components connected between pins 7 and 8 to sustain the stereo pilot tone during suppression. A gain control circuit decreases the trigger sensitivity for high duty factor interference, thereby preventing excessive audio distortion.

The differences between the TDA1001A and its predecessor are:

- The relationship between the trigger sensitivity and the noise at the input of the TDA1001 is subject to a rather wide spread due to the tolerance of internal components. The influence of the spread of values of internal components has been eliminated in the TDA1001A.
- Interference pulses are unable to trigger the TDA1001 in the presence of high-level noise because the noise-operated gain control circuit continues to reduce the trigger sensitivity as the noise level increases. In the TDA1001A the trigger sensitivity remains constant if the noise level exceeds a predetermined threshold.
- The active filters in the TDA1001 have an open-loop gain of 60 dB and their stability is defined by a phase margin of about 45° and a gain margin of about 6 dB. In the TDA1001A, the open-loop gain of the active filters has been reduced to about 40 dB resulting in improved stability defined by a phase margin of about 70° and a gain margin of about 20 dB.

The main features of the TDA1001A are:

- Operates from a supply of 8 V to 15 V d.c.
- Can function in ambient temperature between −30 °C and +80 °C.
- After interference absorption, the peak-to-peak amplitude of the residual pulse on the audio signal waveform is less than 4 mV.
- The typical overall gain of 0.8 dB allows simple incorporation of the IC in existing radio circuits.
- Continues to absorb interference spikes during extremely high level noise at the input.
- Prevents degradation of the audio signal during the suppression of intensive (high repetition-rate) interference by limiting the maximum interference absorption rate.
- Includes a facility for regenerating the 19 kHz stereo pilot tone whilst interference is being absorbed.
- The very high trigger sensitivity of the circuit can be fully exploited in radios with low-noise demodulators or can be reduced by selection of the value of an external resistor.

AUDIO CIRCUITS

Preamplifier and power amplifier TDA1010

Figure 13 shows two integrated circuits TDA1010 connected as a stereo car radio power amplifier which can deliver up to 2 x 6.4 W (continuous sinewave with less than 10% distortion) into 2Ω loudspeakers or up to 2 x 6.2 W into 4Ω loudspeakers. Increased power drive can be achieved by simply connecting a 220Ω resistor between pins 3 and 4. This increases the output power into 2Ω loudspeakers to 9 W. In the TDA1010, the preamplifier and power stage are separate and the input and output connections to both are available externally. This arrangement allows volume control and/or tone control to be effected either before the preamplifier or between the two stages. The voltage gain of the power amplifier is 30 dB with internal feedback so that no external a.c. decoupling capacitor in the feedback path is required. The voltage gain of the preamplifier is 24 dB but this can be reduced by connecting a resistor between pins 7 and 9. The ripple rejection is 42 dB for ripple frequencies between 1 kHz and 10 kHz.

The upper limit of the frequency response is externally limited by C_4. The circuit is protected against thermal overload if it raises the temperature of the crystal above 150 °C. It is also safe in the event of increased supply voltage up to 24 V. The 9-pin SIL plastic encapsulation incorporates a cooling tab which extends from the edge of the package opposite the pins. The SIL package provides a thermal resistance of 12 °C/W between crystal and tab. The circuit can be mounted at the edge of a circuit board, which facilitates easy attachment to the chassis of the radio with a single bolt or screw.

Preamplifier and power amplifier TDA1020

The performance of the circuit in Fig.13 can be increased by replacing the TDA1010 with TDA1020 integrated circuits. The TDA1020 is pin-compatible with the TDA1010 and is similarly constructed. The TDA1020 however can provide up to 12 W with less than 10% distortion into a 2Ω loudspeaker and up to 7 W into a 4Ω loudspeaker. Without bootstrapping, the power output available for a 4Ω loudspeaker is at least 4.5 W. The voltage gain of the power amplifier is 30 dB and the voltage gain of the preamplifier is 18 dB but this can be reduced by connecting a resistor between pins 7 and 9. The ripple rejection is 52 dB for ripple frequencies between 1 kHz and 10 kHz. The upper limit of the frequency response is limited by C_4. The circuit is protected against a.c. short-circuit of the output, against load dump which causes the supply voltage to increase to not more than 45 V and against excess supply voltage up to 28 V. The TDA1020 also incorporates a standby switching facility for muting and on/off switching without switching transients. Standby switching is activated by a simple low-current changeover switch contact which switches R_1 between pin 3 and the common return. The 9-pin SIL encapsulation provides the same simple mounting as described for the TDA1010 but the thermal resistance between the crystal and the cooling tab is reduced to 8 °C/W.

Dual power amplifier TDA1510

To meet the demand for higher output powers with a comprehensive range of protections and hi-fi frequency response, the dual power amplifier TDA1510 can be connected in bridge configuration to obtain a mono power output of up to 24 W from the limited supply voltage available from the car battery. Since the TDA1510 is a dual circuit, it can also be used as a stereo power amplifier for outputs up to 2 x 12 W.

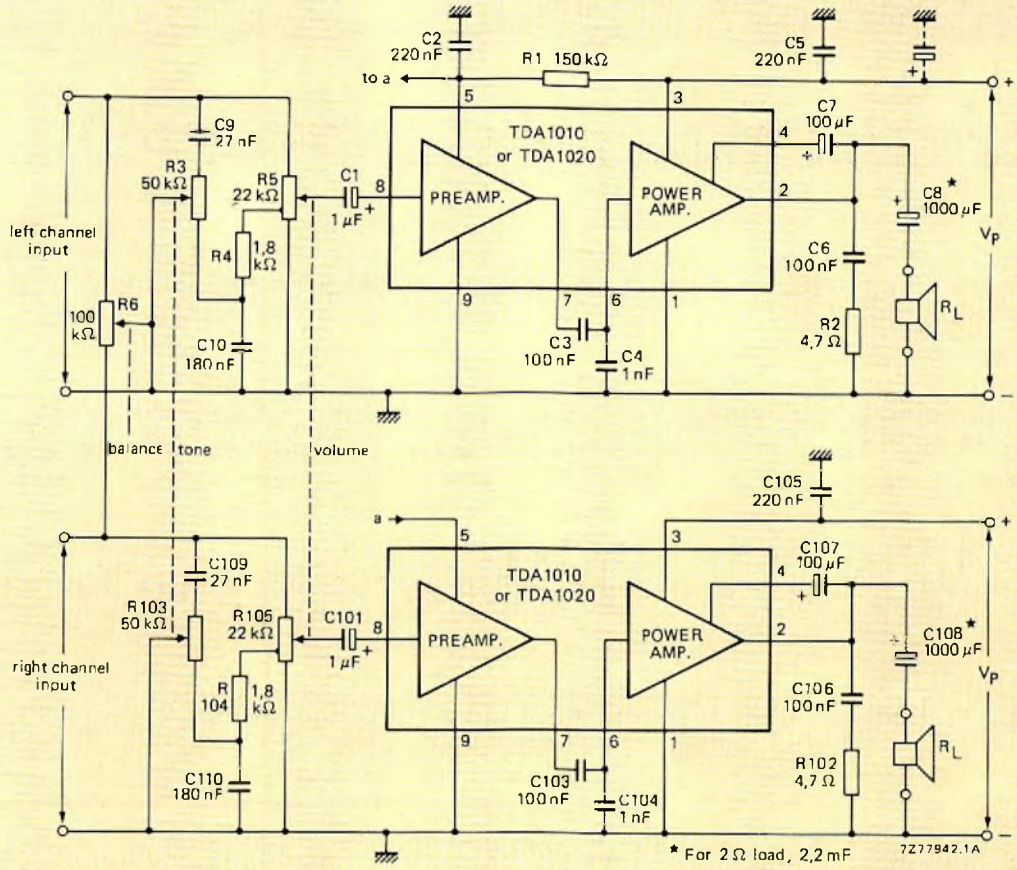

Fig.13 Stereo car radio power amplifier using 2 x TDA1010 or 2 x TDA1020. For the TDA1010, $C_3/103 = 100$ nF, $C_4/104 = 1$ nF. For the TDA1020, $C_3/103 = 150$ nF, $C_4/104 = 3.3$ nF. For the mono operation, $R_1 = 300$ kΩ

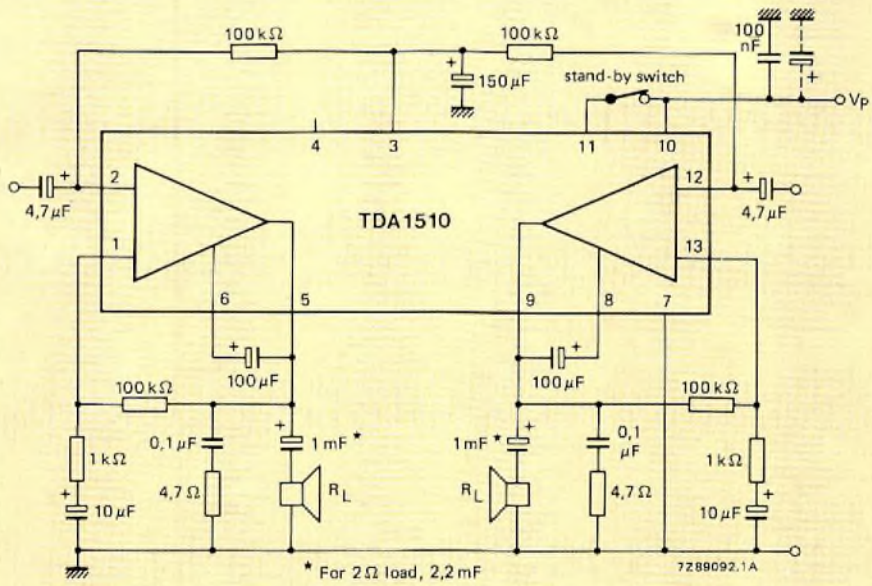

Fig.14 TDA1510 connected as a stereo car radio power amplifier for outputs of 2 x 7 W to 2 x 12 W with $V_p = 14.4$ V

In stereo configuration, the TDA1510 can deliver up to 2 x 6 W (continuous sinewave with less than 10% distortion) into 4Ω loudspeakers. With bootstrapping as shown in Fig.14, the output increases to 2 x 7 W into 4Ω loudspeakers or 2 x 12 W into 2Ω loudspeakers. The closed loop gain of each amplifier is 40 dB (externally adjustable between 26 dB and 56 dB). The frequency response is 20 Hz to more than 20 kHz. The circuit is protected against load dump and thermal overload which raises the crystal temperature above 150 °C. It also has SOAR protection and will not be damaged if the outputs are a.c. short-circuited. Rejection of 1 kHz ripple is 50 dB. The 13-pin power SIL plastic encapsulation provides the same ease of mounting as the previously described circuits and provides an extremely low thermal resistance between the crystal and the cooling tab. The TDA1510 also incorporates a standby switching facility for muting or on/off switching without switching transients. The internal switch is activated by a simple low-current switch contact connected between pins 10 and 14.

In bridge configuration, as shown in Fig.15, the TDA1510 can deliver up to 24 W of continuous sinewave power with less than 10% distortion into a 4Ω load with bootstrapping (18 W with not more than 0.5% distortion). The closed loop gain of the bridge amplifier is 40 dB (externally adjustable between 32 dB and 56 dB). The frequency response of the circuit shown is 20 Hz to more than 20 kHz but can be modified with external components. The −3 dB power bandwidth is 20 Hz to more than 20 kHz. Particular features of this amplifier bridge are the low d.c. offset (less than 50 mV) between the two outputs, and the protection which can be provided for the loudspeaker by simply connecting pin 4 to pin 3. This ensures that the d.c. potential between the two outputs cannot exceed 1 V if one output terminal is connected to the common return.

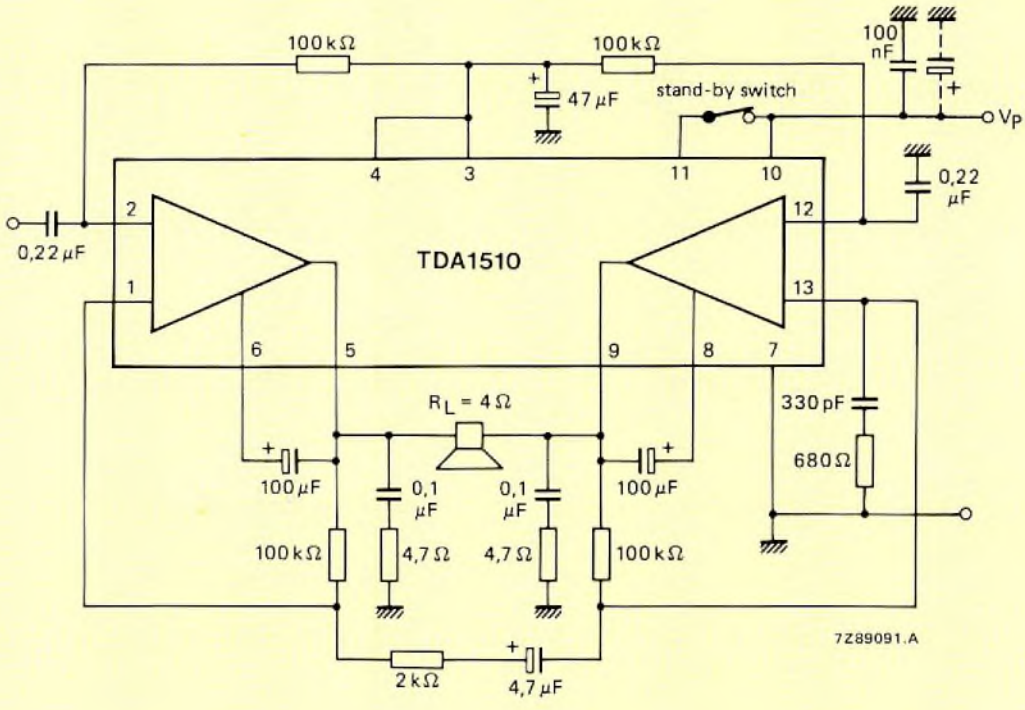

Fig.15 TDA1510 with bridge-tied load (BTL) for power outputs up to 24 W with V_p = 14.4 V

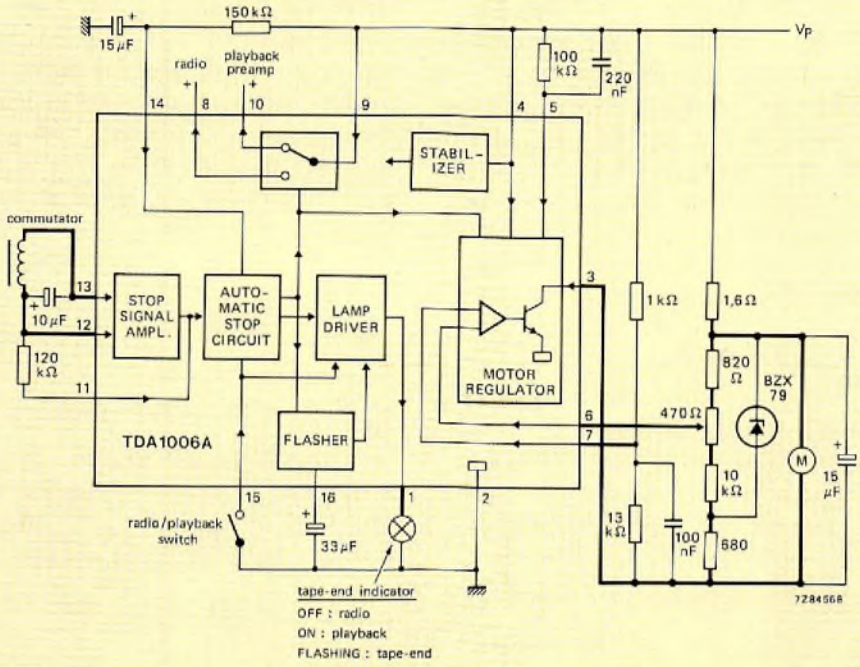

Fig.16 Motor regulator and tape-end indicator TDA1006A

TDA1006A - MOTOR REGULATOR WITH AUTOMATIC TAPE-END INDICATOR

The TDA1006A shown in Fig. 16 stabilises the speed of the capstan drive motor of a car radio/cassette player against variations of mechanical load, supply voltage and temperature variations of the magnetic material and windings of the motor. It also provides a flashing lamp indication when the end of the tape is reached. It then automatically stops the motor and operates an integrated switch to transfer the supply voltage from the playback head preamplifiers to the radio circuits.

The back e.m.f. generated by the motor is proportional to its speed and is compared with a reference voltage by a difference amplifier, the inputs to which are at pins 6 and 7. The output from the difference amplifier controls the motor current via pin 3 to maintain the back e.m.f. (and therefore the motor speed) constant at a level determined by the setting of the 470 Ω potentiometer. The motor speed control can regulate motor current up to 250 mA. The component values shown are for a motor with an armature resistance of 27 Ω and a back e.m.f. of between 7.2 V and 8.3 V at a speed of 3000 r.p.m.

The motor control is only applied as long as the motor is rotating as indicated by a pulse train or sinusoidal waveform between pins 12 and 13 (high sensitivity input 3.5 mV typ.) or between pins 11 and 2 (low sensitivity input ±6 V). The inputs to the stop signal amplifier can be motor commutator pulses or can be derived by hysteresis slip-coupling. When the motor stops (tape-end), the automatic stop circuit is activated. This circuit changes over the internal supply voltage switch to the radio position, inhibits the motor control and enables the lamp driver which causes the lamp connected to pin 1 to flash repetitively until the user sets the switch connected to pin 15 to the radio position. The lamp is then extinguished. The lamp drive output at pin 1 is not more than 1.85 V below V_p and a current of up to 40 mA is available. When the motor is running, the lamp is permanently on. The automatic supply voltage switch between pins 8, 9 and 10 can pass up to 45 mA with a voltage drop of less than 1.35 V in the radio position. In the playback position, the switch can handle a playback preamplifier current of up to 20 mA with a voltage drop of less than 1.2 V.

MICROPROCESSOR-CONTROLLED CAR RADIO

Figure 17 shows how the previously described car radio with quadrature detector for f.m. can be microprocessor controlled. The tuning system uses a phase-locked loop frequency synthesiser to maintain stable, accurate tuning of the a.m. or f.m. channel. The local-oscillator signals from the f.m. front-end and from the a.m. channel

TDA1072 are passed to a frequency divider with a programmable division ratio in the PLL synthesiser. The output from the divider is compared with a crystal-controlled reference frequency. The result of the comparison, which represents the tuning error, is amplified and filtered before being used to modify the tuning voltage applied to the variable-capacitance diodes in the appropriate oscillator tuned circuit. The listener can change the tuned frequency by keying-in the required broadcast frequency, or by manual or search tuning. These commands cause the microprocessor to calculate the appropriate division ratio for the programmable divider after adding or subtracting the i.f. of the a.m. or f.m. channel. The stop pulses required when a station is detected during search tuning are generated in a very simple manner for both reception channels by using the TDA1576 as a balanced phase detector for both a.m. and f.m. For this purpose, the TDA1576 detector circuit incorporates an additional tuned circuit which is resonant at the a.m. i.f. During a.m. or f.m. search tuning, the TDA1072 and/or TDA1576 is switched on by the microprocessor and the zero crossing of the S-curve at the output of the TDA1576 is located by the LM 293 threshold detector to identify the correct tuning point. If a.m. is being received, the TDA1576 is then switched off by the microprocessor and normal reception continues via the a.m. channel TDA1072.

FURTHER INFORMATION

For further information on the integrated circuits, refer to our data handbook Bipolar ICs for radio and audio equipment. Loose data sheets are available for the more recently released integrated circuits.

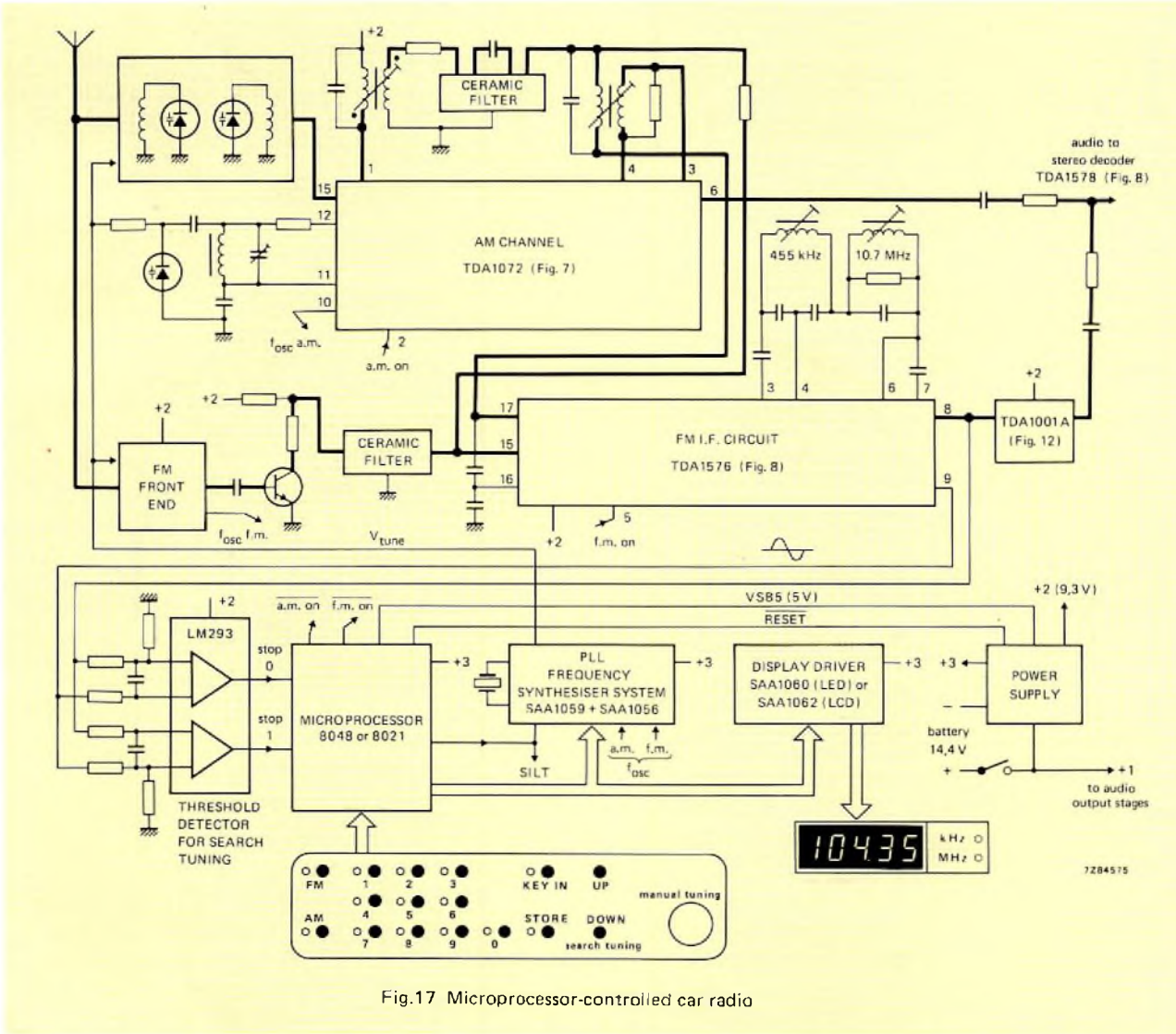

Fig.17 Microprocessor-controlled car radio

Fibre-optic communications

H. J. M. OTTEN

The idea of using light as a medium of communication is by no means new: indeed, the technology celebrates its centenary about now (Ref.1). For most of its history, the development of optical communications centred on the use of beams of light, but success was limited. Suitable light sources were a problem until the advent of the laser; practical ranges were limited by atmospheric conditions and beam-alignment accuracy (Ref.2). Thus, although the idea was sporadically revived for short-range applications, it was not until the rapidly-developing technologies of semiconductor optoelectronics and fibre-optics were married that the full potential of optical communications could be realised.

As with most new technologies, interest in fibre-optics has centred on the most technically-demanding applications: long-distance wideband links for telephony, data, and TV signals. However, as is often the case, technological spin-off from the main endeavour has provided a basis for the use of fibre-optic communication techniques in a range of applications that are likely, in total, to represent the dominant market.

The reason for the widening interest in fibre-optic communications is not hard to find; an optical fibre is almost the ideal transmission line:

- it is made from abundant, low-cost materials
- its bandwidth is larger than that of any other line
- it has a low weight per unit length
- it is an electrical insulator
- it is immune to electromagnetic interference and, thus
- it is also immune to crosstalk from adjacent fibres and
- it is virtually immune to tapping.

Several different types of optical fibre, in various forms, are now available commercially; most have attenuations well below 10 dB/km. To accompany them, connector systems and splicing aids have been developed.

Unlike electrical transmission lines, optical fibres require light sources and photodetectors to interface them with electronic equipment. These are, however, little if any more complicated than the drivers and multiplexers used with wideband cables. A variety of semiconductor generators and detectors have been developed that are very suitable for short and medium-range applications. Most are in packages designed for easy connection to optical fibres.

It is now possible to assemble from commercially-available components optical communications systems that are ideal for use in hostile or hazardous environments, or where large potential differences exist, or where earth loops must be avoided. Applications range from factory instrumentation, through multi-terminal data systems to vehicle control. It is with such practical, local fibre-optic systems that this article is concerned.

OPTICAL-FIBRE TRANSMISSION

Optical fibres rely for their operation on the phenomenon of total internal reflection. If a ray of light propagating within a medium of refractive index n_1 approaches the boundary with a second medium of refractive index n_2 at an angle less than a critical angle

$$\theta = \arccos(n_2/n_1) \quad \text{(Snell's Law)}$$

it will not pass through the boundary but will be reflected back into medium n_1, provided that $n_1 > n_2$, as shown in Fig.1.

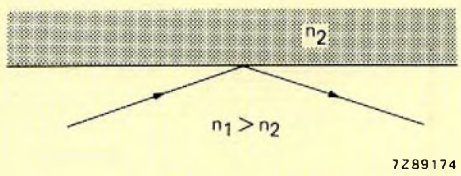

Fig.1 If a ray of light propagation within a medium of refractive index n_1 approaches the boundary with a second medium of refractive index n_2 at an angle less than the critical angle, it will not pass into the second medium but be reflected back into n_1

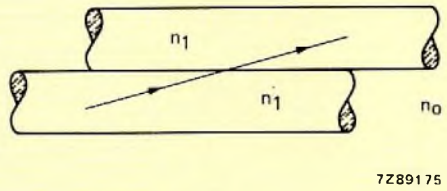

Fig.2 Single fibres are not practical: if two touch, light passes from one to the other

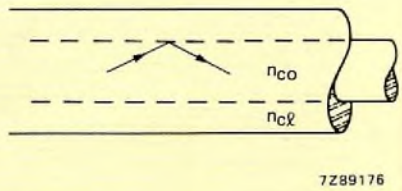

Fig.3 The simplest practical optical fibre has a core of refractive index n_{co} surrounded by a cladding layer of refractive index n_{cl}. Two fibres of this construction can touch without light escaping from one to the other

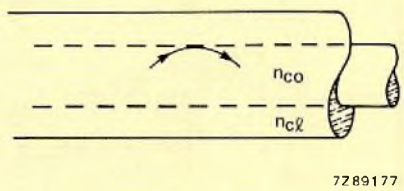

Fig.4 In a graded-index fibre, the refractive index of the core decreases towards the boundary with the cladding. Light crossing the axis of the fibre is gradually refracted as it approaches the boundary; this property is called self focusing

Thus, light propagating within a rod of transparent material will be reflected from the walls of the rod if it approaches them at an angle less than the critical angle for the material and the surrounding medium (usually air). Unfortunately, such a simple arrangement is unsuitable for most fibre-optic applications: if two rods touch, as would happen within a cable, light passes from one to the other, Fig.2. This would lead to excessive losses, crosstalk and lack of security.

Practical optical fibres

In practice, optical fibres for communications purposes are made with a core of higher refractive index than that of the material near the walls, so that they are self contained. The angle at which light can enter the fibre and be trapped is reduced, but losses due to light escaping and crosstalk are eliminated, and the fibre is almost proof against tapping.

Two basic types of optical fibres are commercially available. The simplest is the step-index fibre which consists of a central core surrounded by a cladding layer of lower refractive-index material. Light will be trapped within the core if it approaches the boundary with the cladding at an angle less than

$$\theta_c = \arccos(n_{cl}/n_{co}) \qquad (1)$$

where n_{cl} is the refractive index of the cladding and n_{co} the refractive index of the core, Fig.3.

In the second type of fibre, the refractive index of the core decreases with increasing distance from the axis of the core. Again, light will be trapped if the conditions of Eq.1 are satisfied. However, due to the refractive-index profile of the core, light crossing the core axis at less than the critical angle is progressively refracted back towards the centre, Fig.4. This property of graded-index fibres is called self focusing. The difference between the refractive index at the axis and at the boundary of the core is about 1%.

Depending on the radius a of the fibre core and refractive indices of core and cladding, light waves propagate through a fibre in one or more modes, much as microwaves in a waveguide (Ref.3). The number of modes N that can be sustained by a fibre at a given free-space wavelength λ_0 is a function of the normalised fibre frequency V:

$$N \approx \tfrac{1}{2}V^2 \qquad (2)$$

$$V = \frac{2\pi a}{\lambda_0}\sqrt{(n_{co}^2 - n_{cl}^2)} = \frac{2\pi a n_{co}}{\lambda_0}\sqrt{(2\Delta)} \qquad (3)$$

where $\Delta = (n_{co} - n_{cl})/n_{co}$ is the relative refractive index difference.

Figure 5 shows the modes present at different V numbers, and the V number as a function of core radius for $\lambda_0 = 900\,nm$ and n_{co} greater than n_{cl} by 1% (Ref.4). Note that hybrid mode HE_{11} has no cut-off frequency. Thus, for $V < 2.405$ there exists only one propagating mode; the corresponding fibre is called a monomode fibre.

Figure 6 shows the relation between the refractive index difference and core radius a of this kind of waveguide. For a 1% index difference $a = 1.8\,\mu m$. To avoid such very small core size and thus extreme connector accuracy the index difference is usually reduced to about 0.1%, bringing the core radius to about $5\,\mu m$.

On the other hand, when $V \gg 2.405$, many modes propagate and the fibre is termed multimode. Figure 7 shows cross-sections and index profiles of usual fibre types.

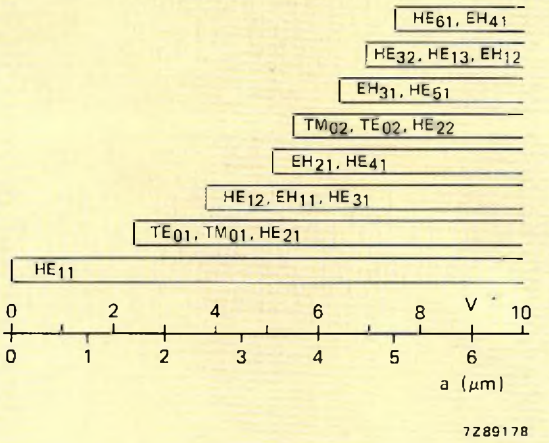

Fig.5 As the radius a and normalised frequency V of a fibre decrease, so does the number of modes of propagation possible within it. Here, the core radius is given for a wavelength of 900 nm, $n_{co} = 1.5$, $\Delta = 0.01$

Optical-fibre characteristics

From the point of view of the system designer, the most important characteristics of an optical fibre are colour dispersion, mode dispersion, numerical aperture and attenuation. Colour and mode dispersion together set the maximum fibre length or maximum repeater spacing as a function of signal frequency or data bit rate. Numerical aperture and attenuation set the maximum fibre length in terms of the available light power.

Mode dispersion

In step-index fibres, different modes correspond to different angles of reflection from the core/cladding boundary, and, thus, different speeds of propagation through the fibre because path length depends on reflection angle. Since refractive index is the ratio of the velocity of light in a medium to its velocity in free space, c, it follows that phase velocities due to the different propagation modes lie between two limits:

$$\frac{c}{n_{co}} \leqslant v_{ph} \leqslant \frac{c}{n_{cl}} \qquad (4)$$

where v_{ph} is the phase velocity. The spread of phase velocities results in pulse spreading which, in turn, limits the upper frequency of modulation for a given fibre length.

In practice, due to deviations from the ideal, the degree of pulse spreading in step-index fibres is always less than that predicted by Eq.4. Irregularities in the core/cladding boundary lead to mode conversion: fast propagation modes, corresponding to low angles of reflection, are converted to slower, higher-angle, modes; slow, high-angle, modes are converted to faster, lower-angle modes. The net result is a narrowing of the phase velocity spread (Fig.8).

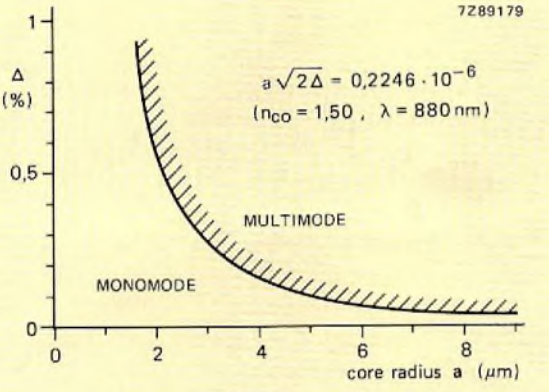

Fig.6 The boundary between monomode and multimode fibre operation as a function of refractive-index difference Δ for a wavelength of 880 mm. Very small cores for monomode operation can be avoided by reducing Δ. The curve shown is for $n_{co} = 1.50$

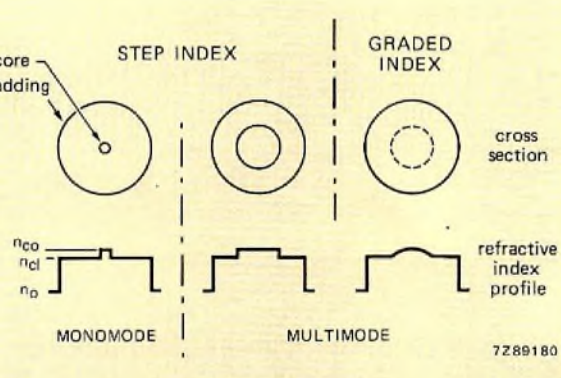

Fig.7 Refractive-index profiles of the three basic types of optical fibre

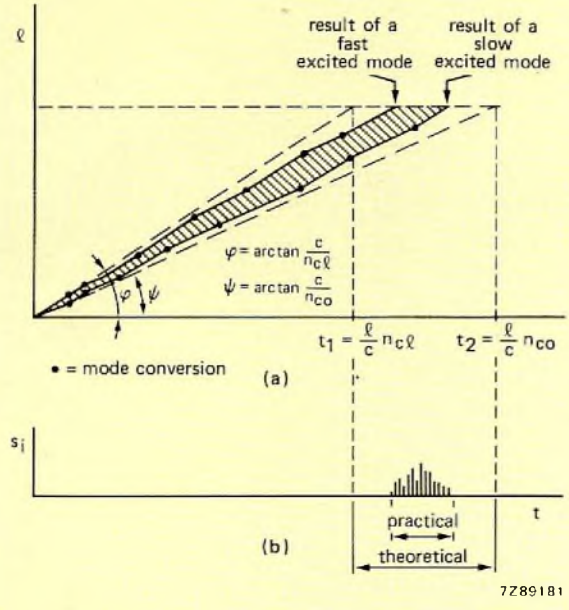

Fig.8 Owing to mode conversion at core-cladding boundaries, actual phase-velocity spreads (a) and consequent pulse dispersion (b) in step-index fibres are always less than theory predicts

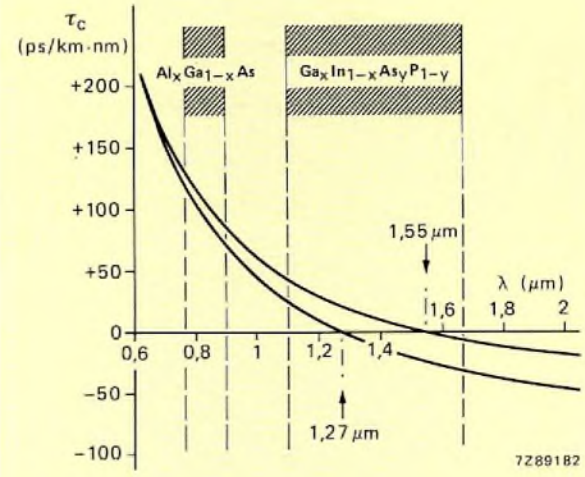

Fig.9 Colour dispersion τ_c as a function of wavelength λ for two types of optical fibre. Both curves pass through points of zero colour dispersion, offering the prospect of greatly-improved optical fibre performance at the longer wavelengths at which the zeros occur. The shaded bands indicate the radiation spectra of two semiconductor light source materials

Perfect step transitions in refractive index cannot be achieved in practice either, so that a continuous transition from n_{co} to n_{cl} takes place about the core/cladding boundary. Within this transition zone, some self-focusing similar to that in a graded-index fibre takes place.

Mode dispersion in graded-index fibres is less than that in step-index fibres due to path-length differences being reduced by the self-focusing action. Calculation shows that the phase-velocity spread is least when the core refractive-index profile approximates a parabola (Ref. 5).

For step-index fibres, the maximum phase delay due to mode dispersion is given by

$$\frac{\Delta t}{t} = \Delta \qquad (5)$$

where t is the time required to traverse a given length of fibre, and Δt is the maximum phase-difference time. For graded-index fibres, the maximum phase delay is given by

$$\frac{\Delta t}{t} \approx \Delta^2 . \qquad (6)$$

Mode dispersion can result in phase-delay differences of up to 50 ns/km for step-index fibres, but only about 0.5 ns/km for graded-index fibres; both for multi-mode fibres.

Colour dispersion

Colour dispersion is the variation of phase velocity with wavelength in a transparent medium whose refractive index depends on wavelength. It is interesting to note that the colour dispersion of silica fibres passes through zero at a wavelength above 1 μm. Figure 9 shows the colour dispersion as a function of wavelength of two fibres (Ref. 7 and 8) which pass through zero at 1.27 μm and 1.55 μm. At these wavelengths only mode dispersion remains and monomode fibres, which avoid this phenomenon, behave virtually as an infinite bandwidth transmission line. A survey of typical mode and colour dispersion data is given in Table 1.

TABLE 1
Typical dispersion values for silica fibres

	monomode	multimode	
		graded-index	step index
mode dispersion	0	0.5 ns/km	50 ns/km
colour dispersion	60 ps/km.nm	100 ps/km.nm	60 ps/km.nm

Numerical aperture

Since there is a maximum angle at which light can strike the core/cladding boundary and be reflected back, there must also be a maximum angle at which light can enter the core of an optical fibre and be trapped. This is illustrated by Fig.10, where it can be seen that, with θ_c as defined in Eq.1, and from Snell's Law,

$$\frac{\sin\theta_a}{\sin\theta_c} = \frac{n_{co}}{n_0} \qquad (7)$$

For a fibre-to-air interface, $n_0 = 1$, so

$$\sin\theta_a = n_{co}\sin\theta_c = \sqrt{(n_{co}^2 - n_{cl}^2)} \approx n_{co}\sqrt{(2\Delta)} \; . \qquad (8)$$

Angle θ_a is termed the acceptance angle of the fibre; the quantity $\sin\theta_a$ is the numerical aperture NA.

The numerical aperture determines the power that can be coupled from a light source into an optical fibre. Where the diameter of the emitting area of the source D_e is less than or equal to the diameter of the fibre core D_c, and source and fibre are in contact, the theoretical optical power P_O coupled into a step-index fibre is, assuming a Lambertian source,

$$P_O = \frac{\pi^2}{4} D_e^2 R_0 (NA)^2 \; . \qquad (9)$$

When D_e is greater than D_c, so that the emitting area overlaps the fibre core,

$$P_O = \frac{\pi^2}{4} D_c^2 R_0 (NA)^2 \qquad (10)$$

where R_0 is the on-axis radiance of the source in both cases. (In this article, SI units are used throughout. Ref.6 is a brief guide to optical SI units.)

Equations 9 and 10 apply only when the light rays lie in a plane containing the axis of the fibre (meridional rays). However, for an extended source, some rays not in a plane with the fibre axis will also be accepted by the fibre (helical rays). This about doubles the power actually coupled for a fibre of NA = 0.2 (Ref.9).

In practice, source and fibre will not be in perfect contact and there will be a power loss in consequence. In most cases, this loss will be a least 2 dB.

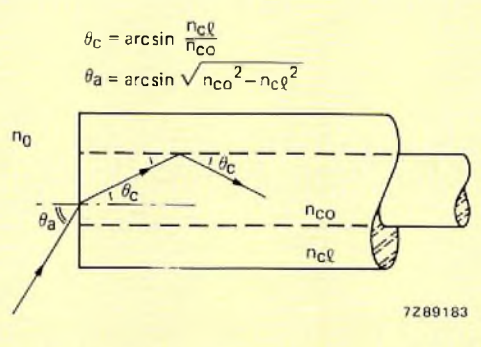

Fig.10 There is a maximum angle, the acceptance angle, at which light can enter and be trapped in the core of a fibre. This angle is set by the refractive indices of core and cladding

Attenuation

Attenuation, or rather its reduction, is the key to the current success of fibre-optic techniques. Materials research has reduced the attenuation of optical fibres from well over 1000 dB/km to less than 10 dB/km. Specimens have been produced with attenuations approaching 0.2 dB/km. There are two main causes of loss in optical fibres: absorption and scattering.

Absorption is still the principal cause of loss. It is caused by metallic ion impurities in the core material. Many of these ions have electron transition energies corresponding to light wavelengths in the region 0.5 μm to 2 μm.

Light passing through a fibre will be scattered by inclusions and dislocations in the material that are small compared to the wavelength of the light. Scattering can also be caused by local temperature gradients. Rayleigh scattering due to the molecules of the material themselves is independent of light intensity but varies with $1/\lambda^4$.

Very high grade glasses have Rayleigh scattering losses of about 0.9 dB/km at a wavelength of 1 μm. This must be regarded as close to the practical limit at that wavelength. Figure 11 shows the attenuation of a low loss monomode fibre as a function of wavelength (Ref.10).

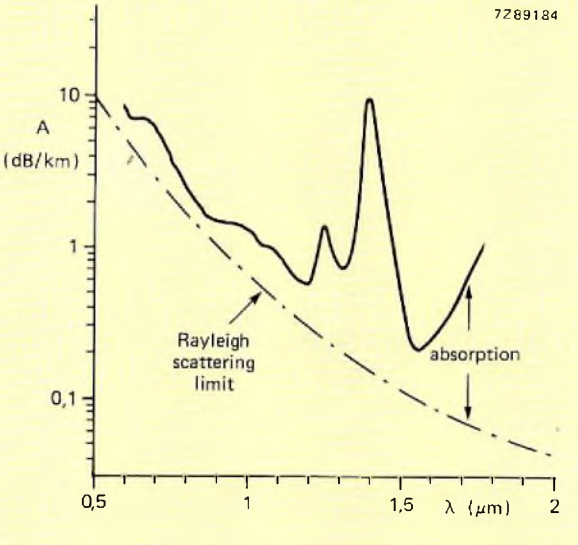

Fig.11 The attenuation a of a low-loss monomode fibre as a function of wavelength. Peaks are due to absorption by metallic or hydroxyl ions

Optical-fibre specifications

We are now able to list those optical-fibre properties that must be known if basic quantitative design is to be undertaken. They are:

- dimensions
- mechanical properties
- optical attenuation
- dispersion
- numerical aperture
- minimum modulation bandwidth
- wavelength at which optical characteristics are measured.

By way of example, Table 2 lists the principal characteristics of graded-index optical fibre, type 8222 075 20161 manufactured by Philips' Glass Division by a chemical vapour-deposition process (Ref. 11).

TABLE 2
Characteristics of Philips' graded-index optical fibre type 8222 075 20161

bandwidth	$\geqslant$ 500 MHz.km
attenuation (850 nm)	$\leqslant$ 5 dB/km
pulse dispersion	$\leqslant$ 1 ns/km
numerical aperture	0.23 ± 0.02
core diameter	50 μm
cladding diameter	100 μm

LIGHT SOURCES

Fibre-optic communications systems require sources of light of adequate brightness capable of being modulated at the desired frequency. The choice, in practice, lies between the semiconductor laser and the light-emitting diode. These devices are attractive in that their drive requirements are compatible with semiconductor practice, they are compact and robust, and, of great importance, they have the long-life and high-reliability potential that characterises well-made semiconductor devices. In the case of the LED, this potential is well on the way to being realised: useful lives of the order of 100 000 h can now be achieved.

Figure 12 shows three important transitions that occur in semiconductors.

Spontaneous emission, which takes place in a LED, is a transition of an electron from the conduction band to the valence band while generating a photon with an energy equal to the band-gap energy:

$$h\nu = eV_{gap} . \qquad (11)$$

When the electron density in the conduction band is very high, an incoming photon of the right wavelength can activate the generation of another photon. This situation is termed population inversion and accounts for the phenomenon *stimulated emission*, which is the mechanism of semiconductor lasers.

Semiconductor lasers

Figure 13 shows the wavelengths at which light sources made from various semiconductor compounds can emit. Binary compounds are mostly of the III-V type (GaAs, InP, GaSb). By replacing a fraction of one element by another equivalent element a ternary compound such as $Al_xGa_{1-x}As$, $In_{1-x}Ga_xP$ or $GaAs_ySb_{1-y}$ is obtained. Similarly, quaternary compounds such as $In_{1-x}Ga_xAs_yP_{1-y}$ and $Al_xGa_{1-x}As_ySb_{1-y}$ can be made. Varying x and y changes the bandgap (and emitting wavelength)

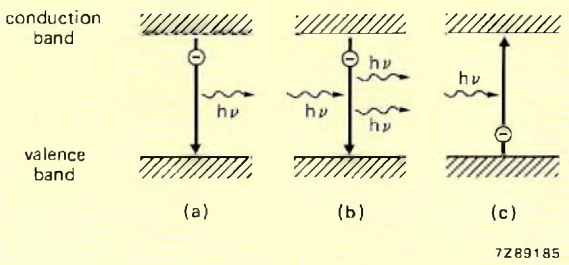

Fig.12 The three principal electron transitions in semiconductors involving photons. Spontaneous emission (a), the mechanism used in LEDs, is the emission of a photon by an electron falling from the conduction to the valence band. When the electron density in the conduction band is high, an incoming photon can activate the generation of another photon by stimulated emission (b). Absorption (c) of a photon by an electron in the valence band causes it to rise to the conduction band to give rise to a photocurrent or voltage

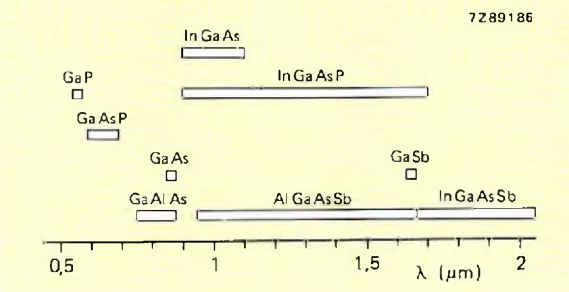

Fig.13 The wavelengths at which various semiconductor compounds can be used in light sources

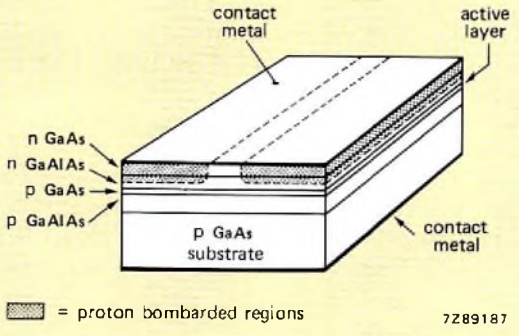

Fig.14 The five-layer double-heterojunction structure used for LEDs and lasers operating in the region 800 nm to 900 nm wavelength. The active region is defined by proton bombardment during processing

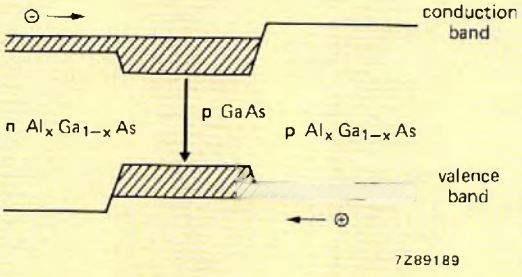

Fig.15 The band structure of a GaAs-$Al_xGa_{1-x}As$ laser

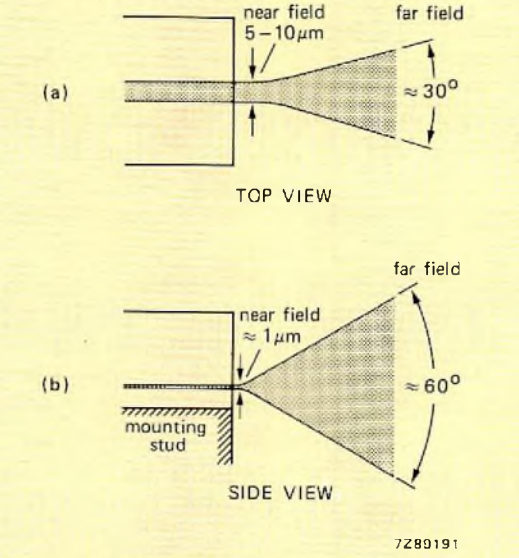

Fig.16 Horizontal (a) and vertical (b) radiation pattern of a double-heterojunction laser showing near and far-field patterns

and lattice parameter of the material. Good lattice matching between structure layers is necessary for long device life. GaAs and $Al_xGa_{1-x}As$ are the most attractive materials for lasers in the 0.78 to 0.9 μm wavelength range. Currently, the investigation of InP-$In_xGa_{1-x}As_yP_{1-y}$ compounds for longer wavelengths is being actively pursued. Most currently available lasers, and modern, high-intensity LEDs use the five-laver double-heterojunction structure shown in Fig.14. The active, light-generating region is the central p-type GaAs layer. This is sandwiched between two layers of higher bandgap energy that effectively confine the emission process. Reference 12 is a useful, comprehensive discussion of semiconductor lasers.

In lasers, the lower refractive-index of these confining layers converts the active layer into a slab optical waveguide. The ends of this waveguide are flat so that some of the light generated is reflected back into the active region to stimulate further emission. The dimensions of the waveguide are so chosen that it acts as a Fabry-Perot optical resonator for the laser frequency.

The active region can further be defined by proton bombardment, which forms two semi-insulating layers across the active layer. Finally, the outermost GaAs layers ensure good electrical contact. Figure 15 shows a band structure of a GaAs-$Al_xGa_{1-x}As$ laser.

Light is emitted from the rectangular flat ends of the active layer of the double-heterojunction structure. The near-field pattern of the light beam is rectangular; it then diverges, as shown in Fig.16. Light from the rear of the waveguide can be coupled to a detector and used to monitor and control the laser output.

The forward characteristics of the 375CQY development-type laser are given in Fig.17. Its V_F/I_F characteristic is similar to that of a LED; the light-output/I_F characteristic is, however, rather different. Up to the knee of the curve, at about 120 mA forward current,

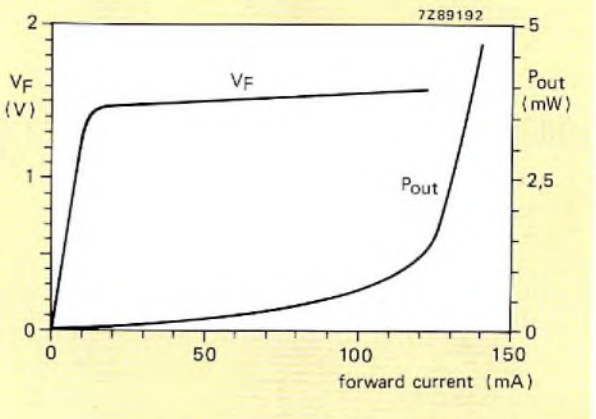

Fig.17 Forward V_F/I_F and light output/I_F characteristics of the 375CQY semiconductor laser

spontaneous emission, such as happens in a LED, takes place only. At a well-defined threshold current I_{th}, which is 120 mA for these devices, lasing commences and light-output increases rapidly with current. This non-linear behaviour of lasers generally restricts them to pulse-modulation applications.

The outputs spectrum of a semiconductor laser consists of one or more clase-spaced narrow emission lines. It is possible to achieve a pure, monochromatic, coherent light source when the device oscillates in a *single longitudinal mode*. These structures are attractive in ultra-high-speed applications since colour dispersion of the fibre to which the laser is coupled is zero.

A very stable laser structure is obtained when the device oscillates in a *single transversal mode*. Then, the steep part of the modulation characteristic shows no kinks and the linearity is adequate for high-performance analogue transmission.

By way of example, Table 3 summarises the principal properties of the 375CQY laser. This c.w. device, a good example of the new generation of semiconductor lasers, is provided with a fibre tail especially for fibre-optic applications. The small emitting area (about 1 μm by 5 μm), the ultra-high brightness and fast response make the laser suitable for long-distance, high-bit-rate applications using thin monomode or graded-index fibres with low mode and colour dispersion.

TABLE 3
Principal characteristics of the 375CQY semiconductor laser (typical values)

threshold current at T_j = 60 °C	150 mA
radiant output power at T_j = 60 °C	3 mW
forward voltage	2 V
peak emission wavelength	840 nm
spectral line width	4 nm
response time (above threshold)	1 ns
fibre tail core diameter	50 μm
fibre tail cladding diameter	100 μm

Light-emitting diodes

High-radiance, double-heterojunction LEDs emit sufficient light for medium-range (up to about 1 km) applications with large-diameter, high-NA fibres. They can be modulated at frequencies approaching 100 MHz, and their linear current/output characteristic makes them suitable for analogue modulation and multiplexing.

A LED die is a Lambertian source: its radiation pattern is spherical (Ref.6). For fibre-optic purposes, the major characteristic is the on-axis radiant intensity. This determines how much light can be coupled into a fibre of given diameter and NA. Since a fibre of fairly large diameter is usually necessary in order to couple sufficient light, and since the spectrum of a LED is much broader than that of a laser, both mode and colour dispersion are important in setting the maximum range or repeater spacing.

There are three basic, practical types of LED.

Top emitting devices where the substrate is soldered onto the stud (header) and the radiating area is on top of the chip, Fig.18(a). Due to the relatively long thermal path between active area and heatsink, current density is limited to about 1 kA/cm^2 and, thus, the radiance will not exceed 3 to 5 W/sr cm^2.

Burrus or bottom-emitting devices, Fig.18(b), where the device is mounted upside down to obtain low thermal resistance. For good chip-to-fibre coupling, a hole is etched in the substrate enabling the fibre to penetrate very close to the active area. Current density and radiance of these devices are considerably higher, 20 kA/cm^2 and 50 to 100 W/sr cm^2. However, the production process is much more involved.

Edge-emitting devices have a structure similar to that of a semiconductor laser shown in Fig.13. Low thermal resistance is also obtained by upside-down mounting, Fig.18(b). Special measures are taken to avoid stimulated emission.

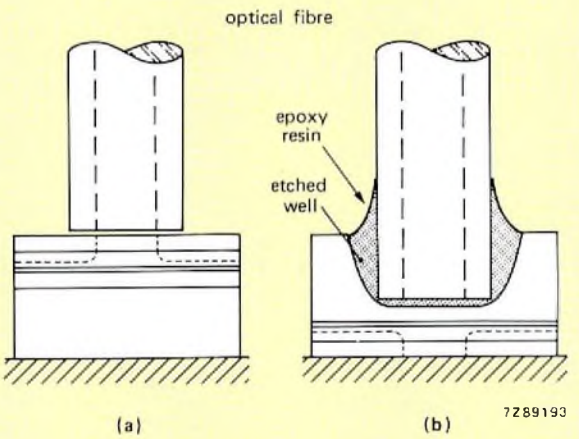

Fig.18 Typical LED structures:
(a) top-emitting; (b) Burrus or bottom-emitting. Actual semiconductor structures may be identical to that of Fig.14

The CQX60 family of high-radiance, top-emitting LEDs incorporates a double-heterojunction die developed especially for fibre-optic communication. A number of versions are available, with various speed and radiance combinations and encapsulations. Brief data on the CQX61 high-speed version are given in Table 4.

TABLE 4
Principal characteristics of the CQX61 LED (typical values)

on-axis radiant intensity (I_F = 50 mA)	300 μW/sr
wavelength at peak emission	830 nm
forward voltage at I_F = 100 mA	1.9 V
light rise time	10 ns
light fall time	10 ns

PHOTODETECTORS

When a photon of energy greater than the bandgap energy is absorbed in a semiconductor it raises an electron from the valence to the conduction band. This is the basis of the operation of semiconductor photodiodes, Fig.12(c). A condition for absorption is that

$$h\nu \geqslant eV_{gap} . \qquad (12)$$

For the purposes of fibre-optic-system design, the principal characteristics of a photodetector are:

- quantum efficiency, the proportion of incident photons converted into current
- response time, which sets bandwidth
- internal multiplication factor, the ratio between primary photocurrent and output current
- noise
- practical considerations, such as operating voltage and encapsulation.

For the reasons given in connection with light sources, semiconductor devices are also the preferred choice for detectors in fibre-optic systems.

Table 5 lists response time and internal current multiplication factor M for the main types of semiconductor photodetectors. It is apparent that the best available performance for wideband links is currently that offered by silicon p-i-n and avalanche diodes.

TABLE 5
Internal multiplication factor M and response time for various types of semiconductor photodetector

detector type	M	response time (s)
photoconductor	10^5	10^{-3}
p-n diode	1	10^{-6}
p-i-n diode	1	10^{-9}
phototransistor	10^2	10^{-5}
avalanche photodiode	10^3	10^{-9}
field-effect transistor	10^2	10^{-7}

Figure 19 shows the responsivity and quantum efficiency of various types of semiconductor photodetectors. Silicon is evidently the most suitable material for use with GaAs-AlGaAs light sources. For longer-wavelength sources, InP-InGaAsP seems the most promising material.

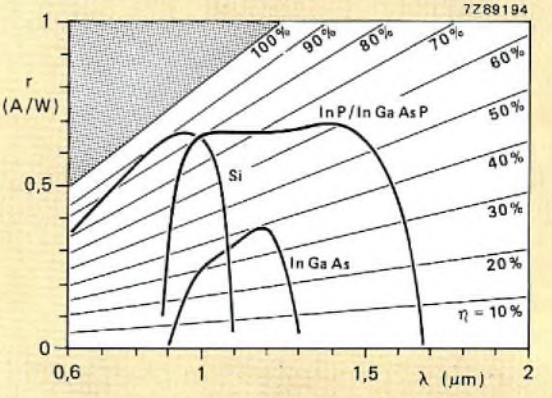

Fig.19 Responsivity r and quantum efficiency η of semiconductor photodetectors in various semiconductor materials. Silicon is evidently the most suitable material for detectors operating with GaAs-AlGaAs light sources emitting at around 900 nm

P-I-N diodes

Silicon p-i-n diodes, Fig.20, are sufficiently sensitive for most short range applications. They have the additional advantages of being both comparatively cheap and rugged devices. Moreover, they operate with low bias (5 V to 10 V).

For fibre-optic applications, photodetector structures are generally optimized for the LED or laser wavelength to be used. In this way, quantum efficiencies

$$\eta = \frac{I_p h\nu}{eP_p} \qquad (13)$$

where I_P is the photocurrent and P_P the optical power, approaching 90% can be achieved in the region 0.75 μm to 0.9 μm wavelength, with modulation bandwidths of several hundred megahertz.

Table 6 gives brief data for the BPW44 p-i-n diode. This device is intended for use with sources emitting at 830 nm; it is a development type of which samples only are available.

Avalanche photodiodes

Avalanche photodiodes (APD) combine detection of light with internal amplification by avalanche multiplication. They are operated with a reverse bias close to the breakdown voltage (about 200 V) so that photon-liberated electrons passing through the high field gradient

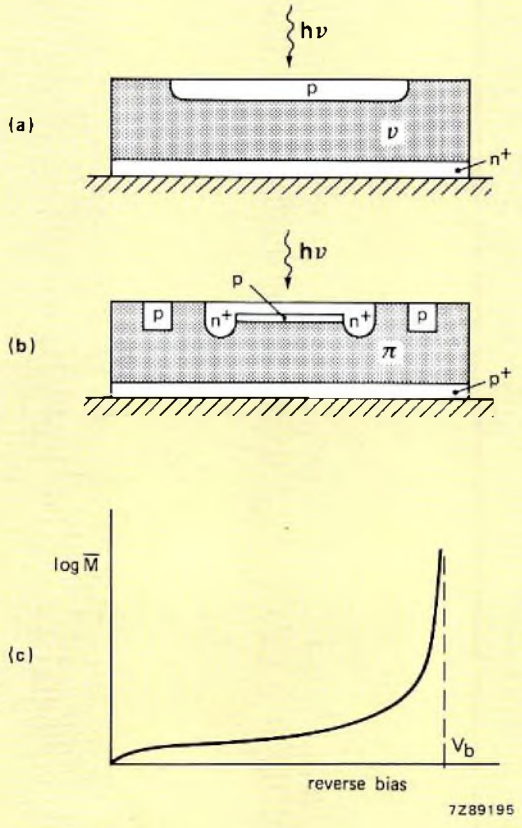

Fig.20 Cross sections of (a) p-i-n diode and (b) avalanche diode photodetectors with (c) typical avalanche multiplication factor $\bar{M}$ as a function of reverse bias characteristic

TABLE 6
Principal characteristics of the BPW44 p-i-n photodiode (typical values)

sensitivity at 830 nm	0.4 A/W
wavelength at peak response	830 nm
dark current	100 pA
capacitance	2.5 pF
rise time	0.2 ns

about the junction gain sufficient energy to create new electron-hole pairs by impact ionisation. The amplification of an avalanche diode is strongly dependent on the bias (Ref. 13).

Since the process by which gain is achieved is stochastic, excess noise is generated by random gain fluctuations. The excess-noise factor F_e of an avalanche diode is a function of average gain $\bar{M}$, Fig.20. For this reason, there is a value of $\bar{M}$ and, hence, of operating bias, for which detector signal-to-noise ratio is optimum for a given bandwidth, modulation method and optical power combination.

Due to their very high sensitivity, avalanche diodes are the preferred detectors in long-distance fibre-optic communication systems using semiconductor light sources.

Table 7 gives brief data on the 368BPY development-type avalanche photodiode, samples of which are available. This device is supplied with a similar fibre tail to that of the 375CQY laser. Both fibre tails use the fibre detailed in Table 2.

TABLE 7
Principal characteristics of the 368BPY avalanche photodiode (typical values)

wavelength at peak response	800	nm
quantum efficiency at 800 nm	93	%
avalanche breakdown voltage	200	V
dark reverse current	5	nA
responsivity (M = 100)	60	A/W
pulse response time (FWHM*)	0.44	ns
effective noise factor	0.02	
fibre-tail core diameter	50	μm
fibre-tail cladding diameter	100	μm

* Full width at half maximum.

DEVICE PACKAGES

Optimum coupling between an optical fibre and a laser, LED, or photodetector requires that the end of the fibre be positioned accurately close to the active region of the semiconductor die. This is a job for which the device manufacturer is best equipped, especially since positioning the fibre involves exposing the die to possible contamination.

Light sources and detectors are now available in packages that already incorporate a length of optical fibre one end of which is in close proximity to the active region of the die. Two of these are shown in Fig.21. That of Fig.21(a) has a pigtail of fibre about 350 mm long designed to be terminated at an equipment panel or internal bulkhead, where connection to the main fibre system is made. This encapsulation is used for the CQX62 and CQX63 LEDs, the BPW44 p-i-n-diode. The 375CQY laser and the 368BPY avalanche photodiode have a similar packages.

In the encapsulation of Fig.21(b) an optical-fibre bar extends to the end of the metal ferrule; this package forms part of a standard BNC, TNC or RIM-SMA optical-fibre connector. This encapsulation is used for the CQX60 and CQX61 LEDs and the BPW45 photodiode. Connection may be made to devices in either encapsulation with a loss of about 1.5 dB.

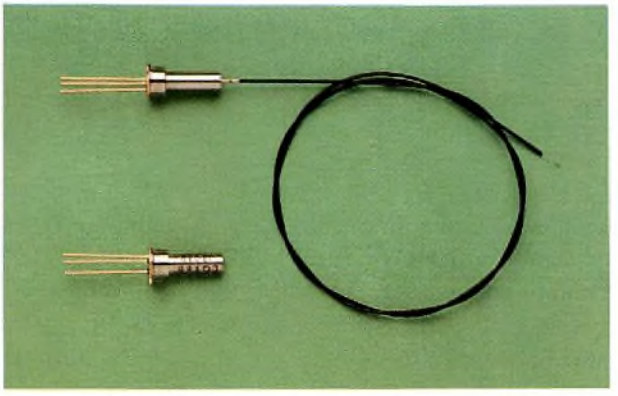

Fig.21 Encapsulations used for active fibre-optic devices. (a) Package with fibre 'pigtail'; (b) package with short, thick fibre which is designed to form part of an active connector

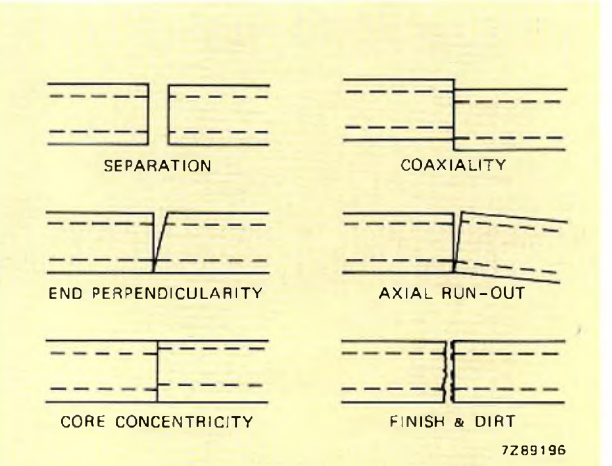

Fig.22 Factors affecting losses in fibre-to-fibre joints

COUPLING OPTICAL FIBRES

In order to assemble a practical fibre-optical communications system, it must be possible to make connections to and between optical fibres. For maintenance purposes, some of the connections will have to be demountable.

In essence, the optical coupling of two fibres is achieved by ensuring that their ends are clean and of adequate optical quality, and then holding them concentrically close together. Figure 22 shows a number of the fibre-to-fibre joint defects that can contribute to connection loss.

Fibre-to-fibre connectors

Demountable connectors are available for both single and multiple-fibre cables. Their essential features are two aligning and holding terminations for the fibres, and a connecting bush. Most commercially-available fibre connectors are based on the mechanical arrangements of coaxial types, such as those of Fig.23. Connectors for thick step-index fibres made from plastic materials are also available.

A low-loss connection between graded-index or monomode fibres requires an extremely precise mechanical arrangement. Simple ferrule constructions in standard SMA or DIN housings are generally insufficient.

Figure 23 shows two types of fibre-to-fibre connectors suitable for step-index fibres: one for a fibre cable and the other for a single or double-coated fibre for use inside equipment. Both connectors achieve alignment accuracy by means of a watch jewel.

Welding (fusing) together fibres is an attractive, low-cost solution in cases where demountability is not required, as in buried trunk cables. Losses as low as 0.1 dB can be achieved by this method (Ref. 14).

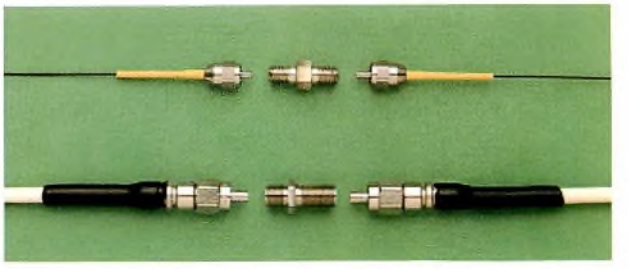

Fig.23 Demountable connectors for optical fibres: (upper) connector for coated fibres; (lower) connector for fibre cable with strain-relieving sleeve

Coupling fibres to active elements

Efficient coupling of light sources and detectors to system fibres has been greatly simplified by the introduction of device packages with integral coupling fibres as shown in Fig.21. All active optical elements can, in principle, be mounted in one of these two encapsulations.

The fibre-pigtail package allows the designer to position a device freely on a printed-circuit board. This is a major advantage where parasitic inductances and stray capacitance can affect system performance. Such a situation would be found on racked p.c. boards in telephone exchanges.

The fibre-bar package, Fig.21(b), for active connectors, Fig.24, is mainly used in short-haul data links where the active elements are LEDs and p-i-n diodes.

Efficiency of coupling between LEDs or lasers and optical fibres can be improved by the use of small lenses.

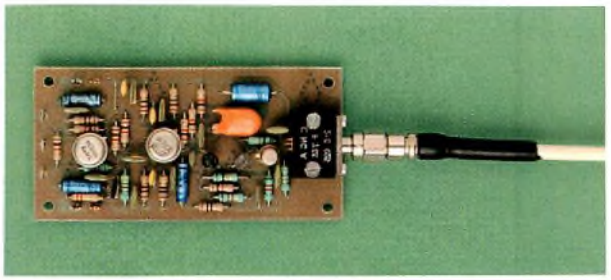

Fig.24 Active fibre connector using package of Fig.21(b)

SYSTEM-DESIGN CONSIDERATIONS

The essential properties of a fibre-optic communication system are bandwidth and attenuation.

Bandwith

Assuming Gaussian pulses, the bandwidth can be estimated simply by summing the various system time constants:

$$\tau_{tot}^2 = \tau_s^2 + \tau_f^2 + \tau_d^2 \qquad (14)$$

Here, τ_{tot} is the overall system time constant, τ_s is the time constant of the light source and driver, τ_d is the time constant of the system fibre, and τ_d is the time constant of the detector and receiver input circuit.

The light-source time constant is the rise or fall time, whichever is the longer. The optical-fibre time constant is the sum of the time constants due to colour and mode dispersion:

$$\tau_f^2 = \ell^2(\tau_c^2 + \tau_m^2) \qquad (15)$$

where ℓ is the fibre length, τ_c is the phase delay per unit fibre length due to colour dispersion and τ_m is the phase delay per unit length due to mode dispersion.

Once the time constant has been calculated, the overall modulation bandwidth of the system is

$$B = 1/(2\tau_{tot}) = 1/(2T) \qquad (16)$$

where T is the minimum pulse length available for digital transmission.

Signal attenuation

The maximum permissible signal attenuation in a fibre-optic system is

$$A_{max} = \frac{P_{s\,max}}{P_{d\,min}} \qquad (17)$$

where P_s is the optical power available from the light source and P_d is the power coupled to the photodetector. A more powerful light source is equivalent to a more sensitive detector.

About 1 mW to 3 mW of optical power can be coupled into a graded or step-index fibre from a semiconductor laser, depending on coupling efficiency, fibre numerical aperture and laser performance.

The power coupled into a fibre from a LED can be calculated from Eq.9 for a step-index fibre. Due to the Lambertian character of the source, the influence of the numerical aperture is much greater than with a laser. Coupled power varies, in practice, from 10 μW to 100 μW.

The main limitations on the sensitivity of a p-i-n diode-equipped receiver are set by shot and thermal noise. Optimum performance is obtained using a high-resistance transimpedance amplifier, a silicon FET input stage, and a differentiator to compensate for the low-pass characteristic of the input stage (Ref.15). At modulation frequencies above a few tens of megahertz, better results will be obtained with a good bipolar or GaAs FET input stage.

Figure 25 gives the sensitivity of a silicon FET-equipped p-i-n diode receiver as a function of diode load resistor R_L for a bit-error rate of 10^{-10} at a transmission speed of 20 Mbits/s. An input capacitance of 2 pF and a FET noise equivalent series resistance of 300 Ω are assumed.

Due to the internal multiplication factor M, an avalanche photodiode is much more sensitive than a p-i-n diode. The sensitivity of a receiver equipped with

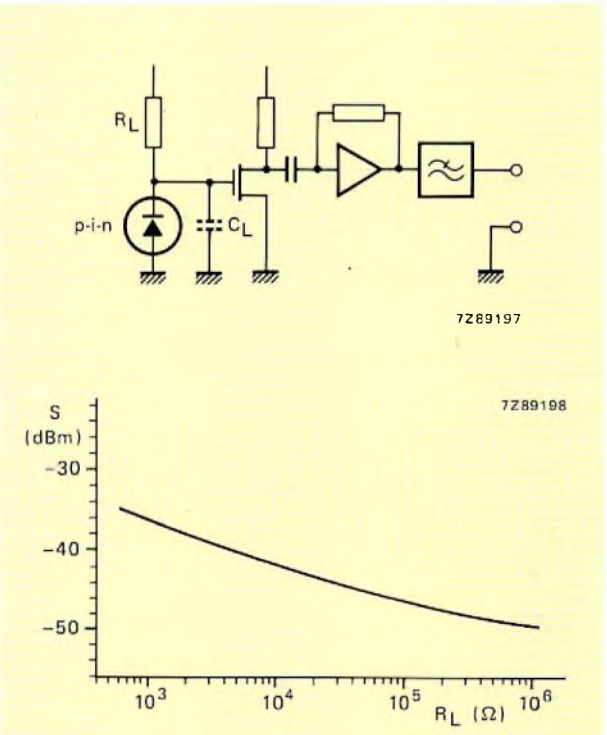

Fig.25 Sensitivity S of p-i-n diode receiver as a function of diode load resistor R_L, with outline circuit diagram; R_{eq} is the equivalent series noise resistance of the FET

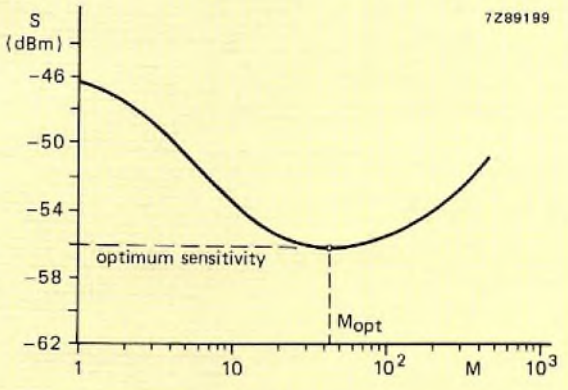

Fig.26 Sensitivity of receiver using an avalanche photodiode, as a function of avalanche multiplication factor M

an avalanche diode detector is plotted in Fig.26 as a function of avalanche multiplication factor M. A load resistor of 100 kΩ and an excess noise factor of 2+0.02M are assumed; other details are as for Fig.25.

In order to achieve a bit-error rate of 10^{-10} in digital transmission, a signal-to-noise ratio of 22 dB is required. For analogue TV transmission, acceptable picture quality requires a signal-to-noise ratio of at least 45 dB and, consequently, more optical power.

Range

The maximum range of a fibre-optic system is set by either bandwidth or attenuation. The ranges achievable with various source, fibre and detector combinations are plotted as a function of bit rate in Fig.27.

APPLICATIONS

Optical communications systems compete with millimeter waveguide, coaxial and twisted-pair transmission lines. Glass-fibres are certainly attractive in prospect compared with moderate and high-quality coaxial cables. Whether they will replace twisted-pair lines depends on the price of copper.

The extra cost of the optoelectronic interface devices often outweighs the cost advantage of the glass-fibre cable, particularly in short-haul systems. However, an optical system should not necessarily be regarded as a one-to-one replacement for a copper-line system. The use of multiplexing techniques to take advantage of the large information-carrying capacity of glass-fibre cables can greatly reduce the cost per channel.

In hazardous or noisy environments, glass-fibre cables often do not require the coding and decoding equipment, interfence suppressors, heavy shielding or isolation transformers necessary with copper lines. Fibre-optic systems are inherently interference insensitive. Due to their low weight and small size, a given cable duct can accommodate more optical cables than metal ones.

System feasibility can best be judged economically. Compare the value-in-use of the existing system with the actual cost of an optical replacement, taking all costs, direct and indirect, into account.

Telecommunications

Telephone trunk lines and television distribution require levels of performance best achieved with lasers, graded-index fibres and avalanche diode detectors. Particularly on the basis of cost per channel, fibre-optic cables will be cheaper than coaxial cables. In addition, due to the very low attenuation of optical fibres, few or no repeaters will be required.

A 32 Mbits/s optical link has been demonstrated that has a range of 53 km between repeaters, compared to the 1.5 km of an equivalent coaxial system.

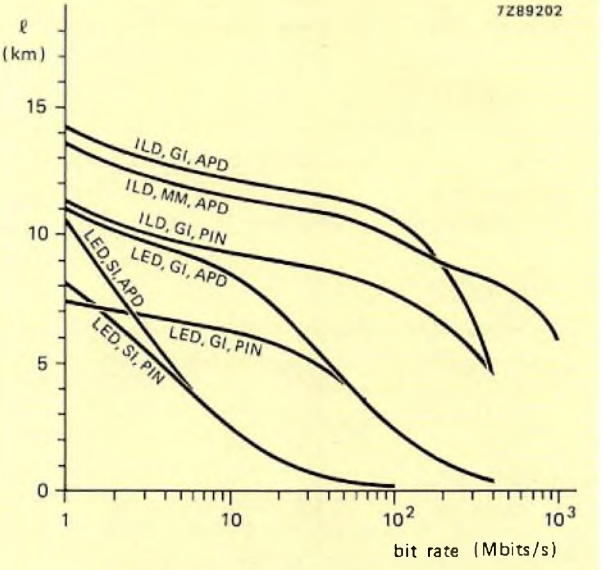

Fig.27 Bit rate as a function of range/repeater spacing ℓ for fibre-optic systems using various source-fibre-detector combinations; A = 5 dB/km, λ = 880 nm. SI, step-index fibre (τ_m = 50 ns/km); GI, graded-index fibre (τ_m = 0.5 ns/km); MM, monomode fibre; ILD, laser diode; LED, light-emitting diode; PIN, p-i-n photodiode; APD, avalanche photodiode

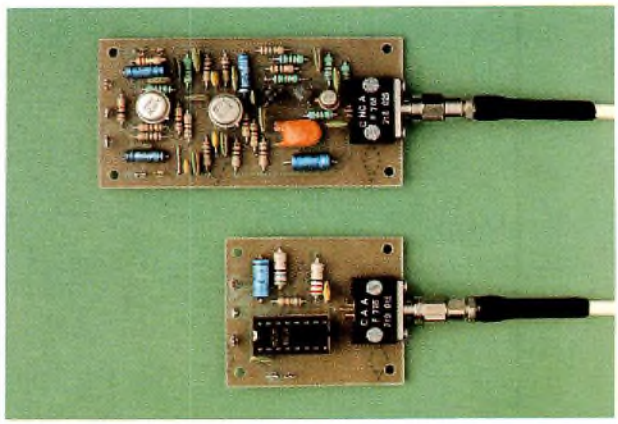

Fig.28 Short-haul fibre-optic data link

Defence

The immunity to interference, low weight, compactness and difficulty of tapping make fibre-optics especially attractive for both military and general high-security applications.

Data processing

Fibre-optic systems are ideal for linking computers to peripherals. Here, speed is the most important property.

Industrial control

Systems using LEDs, step-index fibres and p-i-n diode detectors are ideal for monitoring and control purposes in industrial plants, where distances are short and information is transferred at relatively slow speeds.

Optical wiring

The small size and immunity to crosstalk of optical fibres make them attractive in prospect for internal wiring in such applications as automobiles, data-processing equipment and telephone exchanges.

Wideband home service

Using optical fibres, a wideband network to deal with the increasing flow of information to and from the home becomes a practical possibility. One or two fibres could be used to carry TV and radio programmes, telephony, viewdata, telebanking, public utilities metering, and similar services. Several projects with this in view are already in progress or under consideration: Hi-Ovis in Japan, BIGFON in the Federal Republic of Germany, DIVAC in The Netherlands, and Biarritz in France. If the idea is widely taken up, its impact on the market for fibre-optic components will be dramatic.

Prototype short-haul link

Figure 28 shows a design for a short-haul fibre-optic data link. The range is 500 m and the bandwidth sufficient for digital transmission at 10 Mbits/s (Ref. 16). The transmitter uses a CQX61 LED as light source; the receiver detector is a BPW45 p-i-n diode.

REFERENCES

1. Bell, A. G. 1881. On the production and reproduction of sound by light. *Proc. Am. Assn, Adv. Sc. 29:* 115-136.
2. Cade, C. M. 1962. Eighty years of photophones. *Brit. Comm. and El. 9:* 112-115 (No. 2).
3. Snitzer, E. 1961. Cylindrical dielectric waveguide modes. *J. Opt. Soc. Am. 51;* 491-505 (No. 5).
4. Miller, S. E. et al. 1973. Research towards optical fiber transmission systems. *Proc. IEEE. 61:* 1703-1751 (No. 2).
5. Kawakami, S. and Nishizawa, J. I. 1968. An optical waveguide with optimum distribution of the refractive index with reference to waveguide distortion. *IEEE Trans. MTT. 16:* 814-818 (No. 10).
6. Christian, T. S. 1975. Radiometry, photometry and optoelectronic devices. *E.A.B. 32:* 125-136 (No. 4).
7. Payne, D. N. et al. 1975. Zero material dispersion in optical fibres, *Electronics Letters 11:* 176-178 (No. 8).
8. Chang, C. T. 1979. Minimum dispersion at 1.55 μm for single mode step index fibres. *Electronics Letters 15:* 765-767 (No. 23).
9. Allan W. B. 1973. *Fibre optics, theory and practice.* 29-33. Plenum Press, London and New York.
10. Miya, T. et al. 1979. Ultimate low loss single mode fibre at 1.55 μm. *Electronics Letters 15:* 106-108 (No. 4).
11. Ass, H. M. J. M. v. et al. 1976. The manufacture of glass fibres for optical communication. *Philips Tech. Rev. 36:* 182-189 (No. 7).
12. Panish, M. B. 1976. Heterostructure injection lasers. *Proc. IEEE 64:* 1521-1535 (No. 10).
13. Webb. P. P. et al. 1974. Properties of avalanche photodiodes. *RCA Rev. 35:* 234-278 (No. 6).
14. Franken A. J. J. et al. 1978/1979. Experimental semi-automatic machine for hot splicing glass fibres for optical communication. *Philips Tech. Rev. 38:* 158-159 (No. 6).
15. Personick, S. D. 1973. Receiver design for digital fibre optic communications systems. *BSTJ 52:* 843-886 (No. 6).
16. Otten H. J. M. 1978. A short haul digital fibre-optic link using OF842/843 high radiance LED and OF844 p-i-n photodiode. *Philips' Application Report ETT7808.*

Purpose-designed ferrite toroids for isolated current measurement in power electronic equipment

J. A. HOULDSWORTH

We have recently developed a D.C. Current Transformer (DCCT) system for three-phase current measurement in our Pulse-Width Modulation (PWM) variable speed drive for a.c. motors (see Refs.1, 2, 3, and 4). The system incorporates two purpose-designed ferrite toroids which have been introduced to provide the transformer cores. Although this DCCT system has been designed for a specific purpose, its ability to provide accurate isolated current measurement at low cost means that it has the potential for widespread industrial use. This article covers the general theory of the DCCT, the design and performance of a DCCT using our ferrite toroids, single-phase and three-phase applications, and the use of bifilar windings to reduce magnetisation losses.

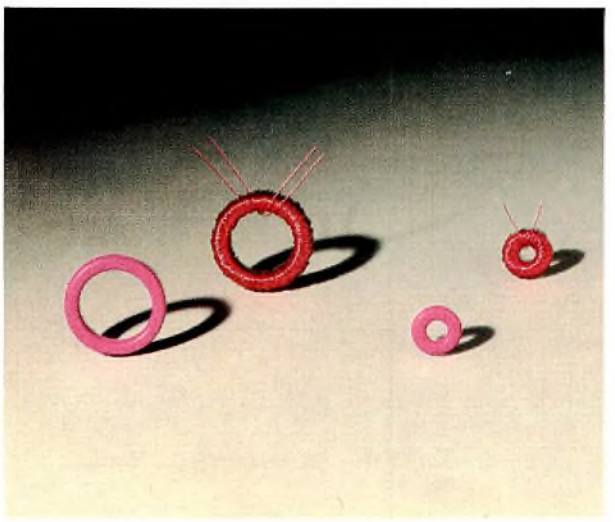

Fig.1 Ferrite toroids for DCCT applications: 12.7 mm toroid (right), 25.4 mm toroid with bifilar winding (left)

The two purpose-designed ferrite toroids, ordering codes 4313 020 18280 and 4313 020 18290*, have external diameters of 12.7 and 25.4 mm respectively. They are nylon-coated, and are manufactured using 3C8 (A16) Ferroxcube material. This material is a particularly good choice for DCCT applications owing to its high values of B_{sat} and μ_r, small hysteresis window, and good temperature performance. Figure 1 shows examples of the toroids, both in the unwound state, and ready wound for DCCT applications. Details of the important physical and magnetic dimensions of the toroids are given in Table 1.

D.C. CURRENT TRANSFORMER

The mechanical construction of a d.c. current transformer is shown in Fig.2, and the basic circuit diagram of a DCCT system is shown in Fig.3. The transformer consists of a pair of identically-wound ferrite toroids, with secondary windings connected in anti-phase series as shown in Fig.3, and a common primary winding passing through the centre of both toroids. To measure the current in the primary winding, a voltage pulse waveform is applied across the secondary windings; this produces a voltage signal V_0 across the sensing resistor R_3 proportional to the current in the primary.

Theory of operation

A primary (load) current I_p produces a magnetic field strength H within each toroid of magnitude:

$$H = \frac{n_p I_p}{\ell_e}, \qquad (1)$$

*UK ordering codes FX3848 and FX3849 respectively

TABLE 1

Physical and magnetic dimensions of DCCT ferrite toroids

Nominal external diameter mm	Minimum internal diameter mm	Effective magnetic length mm	Effective magnetic area mm^2
12.7	5.4	27.6	9.68
25.4	17.1	68.9	15.1

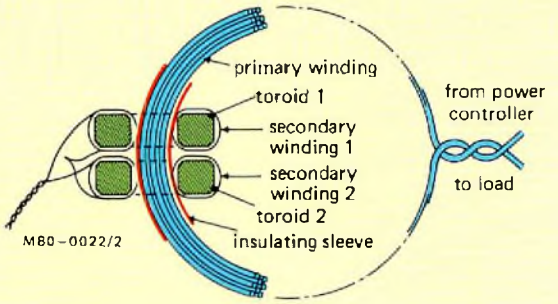

Fig.2 Mechanical construction of D.C. Current Transformer

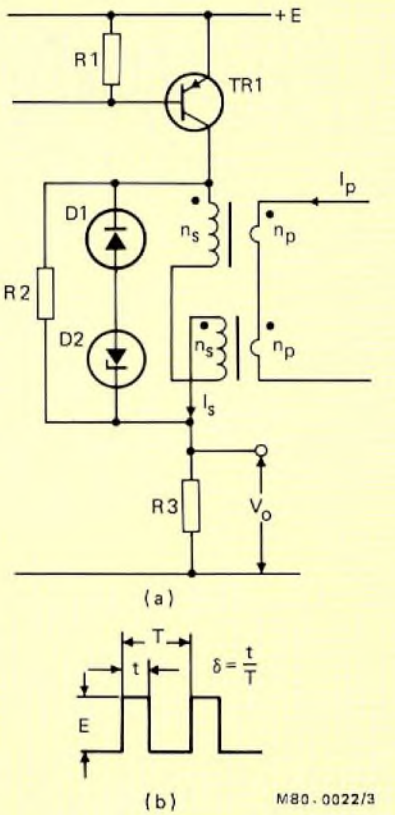

Fig.3 (a) Basic circuit of DCCT system
(b) Voltage pulse waveform applied to secondary windings

where n_p is the number of primary turns, and ℓ_c is the toroid effective magnetic length. The magnitude of H sets the magnetic operating point – the same for both toroids – on the ferrite material B/H characteristic, while the direction of the primary current determines the operating quadrant. For simplicity of explanation, a d.c. primary current which gives +B/+H (first) quadrant operation is considered first (see Fig.4). Figure 4 is a simplified B/H characteristic, the hysteresis being omitted for clarity.

By applying a voltage pulse of predetermined voltage-time product (Et) across the two anti-phase series-connected secondary windings, there is a resultant change in flux density ΔB of:

$$\Delta B = \Delta B_1 + \Delta B_2 = \frac{Et}{n_s A_e}, \qquad (2)$$

where ΔB_1 is the change in flux density for toroid 1, ΔB_2 the change for toroid 2, n_s is the number of secondary turns per toroid, and A_e is the toroid effective magnetic area. Because of the anti-phase connection of the toroids, ΔB_1 and ΔB_2 will be opposite in direction. Since the toroids are connected in series, the two secondary currents must be equal, so that equal (but

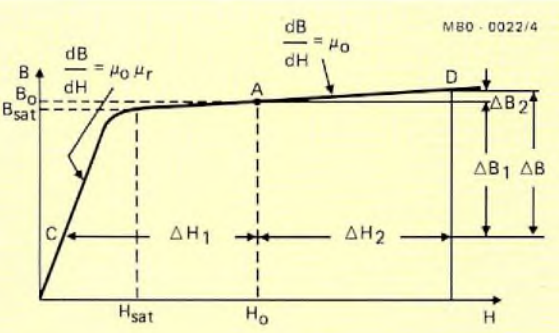

Fig.4 Simplified B/H characteristic

opposite) magnetic field strength changes ΔH, are produced in each toroid. Thus:

$$\Delta H_1 = \Delta H_2 = \frac{n_s I_s}{\ell_e}, \quad (3)$$

where I_s is the secondary current common to both secondary windings.

The effect of these changes in magnetic field strength is shown in Fig.4. The operating point of toroid 2 moves from A to D, that is toroid 2 goes further into saturation, while toroid 1 becomes desaturated, moving from A to C. If it is assumed that the quiescent operating point A is well into saturation, so that H_o is very much larger than H_{sat}, and that the relative permeability of the ferrite material μ_r is large, then H_o is approximately equal to ΔH_1. However:

$$H_o = \frac{n_p I_{p(o)}}{\ell_e}, \quad (4)$$

where $I_{p(o)}$ is the value of primary current producing a magnetic field strength H_o, and:

$$\Delta H_1 = \frac{n_s I_{s(pk)}}{\ell_e}, \quad (5)$$

where $I_{s(pk)}$ is the peak value of secondary current, which occurs at point C, corresponding to the end of the applied voltage pulse. Therefore:

$$\frac{n_p I_{p(o)}}{\ell_e} = \frac{n_s I_{s(pk)}}{\ell_e},$$

or:

$$I_{s(pk)} = \frac{n_p}{n_s} I_{p(o)}. \quad (6)$$

The value of the secondary current at the operating point C (in the region $0 \leqslant H \leqslant H_{sat}$) is therefore proportional to the primary current. Thus by detecting the peak value of the secondary current, a signal $V_{o(pk)}$ proportional to the primary current is obtained.

By changing the direction of the primary current, the quiescent magnetic operating point of the two toroids is moved to the $-B/-H$ (third) quadrant. The voltage pulse (Et) across the secondary windings now desaturates toroid 2 and drives toroid 1 further into saturation. The operating equations are essentially identical to those obtained for the first quadrant, but with ΔH_1 replaced by ΔH_2. Thus the DCCT output provides an isolated signal which is proportional to the modulus of the amplitude of the instantaneous current being measured.

Maximum current range

For linear operation H_o cannot be less than H_{sat}, so that the minimum value of primary current which can be measured with reasonable linearity is given by:

$$I_{p(min)} = \frac{H_{sat} \ell_e}{n_p}. \quad (7)$$

The upper limit on primary current, consistent with linear operation, is determined by the need for the point C (Fig.4) to be on the unsaturated portion of the B/H characteristic. From this requirement it can be shown that:

$$I_{p(max)} = \left(H_{sat} + \frac{\Delta B}{2\mu_o}\right) \frac{\ell_e}{n_p}. \quad (8)$$

Therefore the maximum linear measurable current range is given by:

$$\frac{I_{p(max)}}{I_{p(min)}} = 1 + \frac{\Delta B}{2\mu_o H_{sat}}. \quad (9)$$

Bandwidth

The bandwidth of the DCCT system is inversely proportional to the period of the switching frequency, or δ/t (see Fig.3b). The Sampling Theorem dictates that to resolve a signal of frequency f, requires a switching frequency of at least 2f, and in practice a factor of at least ten times is used to give reasonable waveform fidelity.

DESIGN PROCEDURE FOR TOROID WINDINGS

Figure 5 shows a simplified flowchart of the general design procedure for specifying toroid windings in DCCT applications. A value for ΔB of 250 mT is assumed, being a good design value for 3C8(A16) material. Details of the primary windings are calculated first, subject to the specification of the required primary current range. The secondary winding details are then calculated, having specified or calculated the required bandwidth, voltage pulse amplitude (E), and duty cycle (δ). In selecting a value of n_s to start the design of the secondary winding, it is important to remember that the maximum value of the secondary current $I_{s(max)}$, given by:

$$I_{s(max)} = \frac{n_p}{n_s} I_{p(max)}, \quad (10)$$

must not exceed the peak current rating of the switching transistor (TR_1 in Fig.3).

DCCT PERFORMANCE

The DCCT performance is determined primarily by the magnetic properties of the toroid and the temperature dependence of the sensing circuit. Figure 6 shows a typical measured B/H characteristic for the 25.4 mm toroid, and this figure is now used to demonstrate two

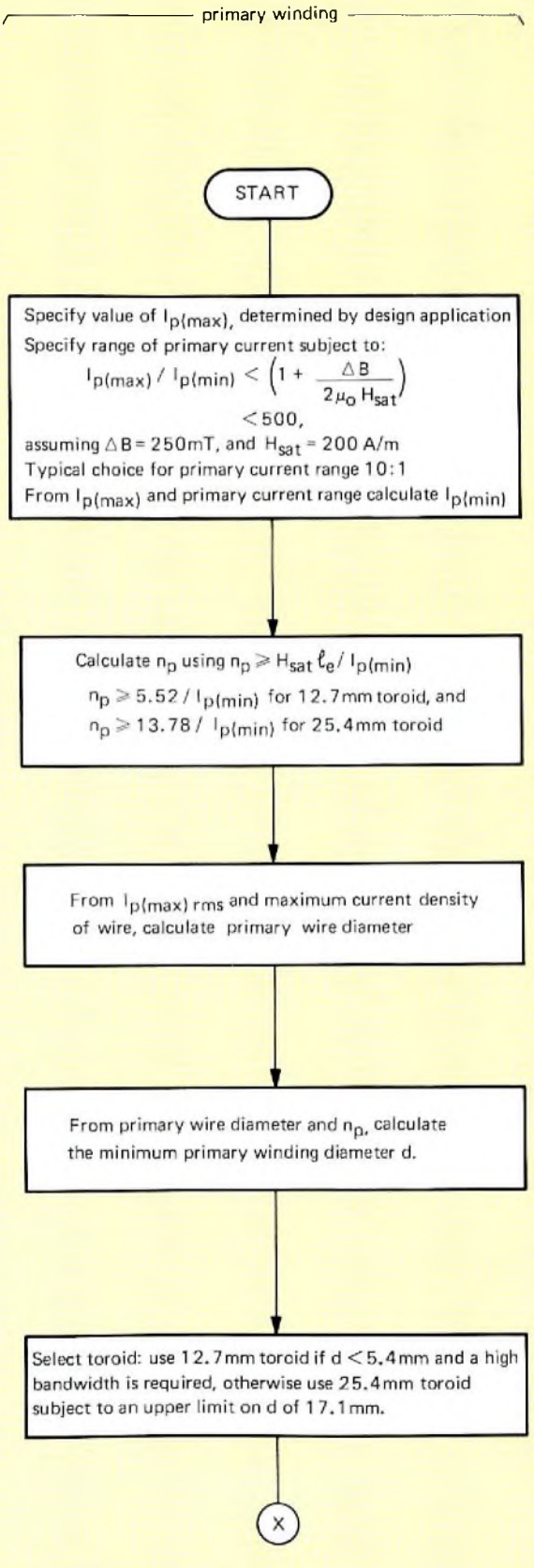

Fig.5 Simplified flowchart of toroid winding design for DCCT applications

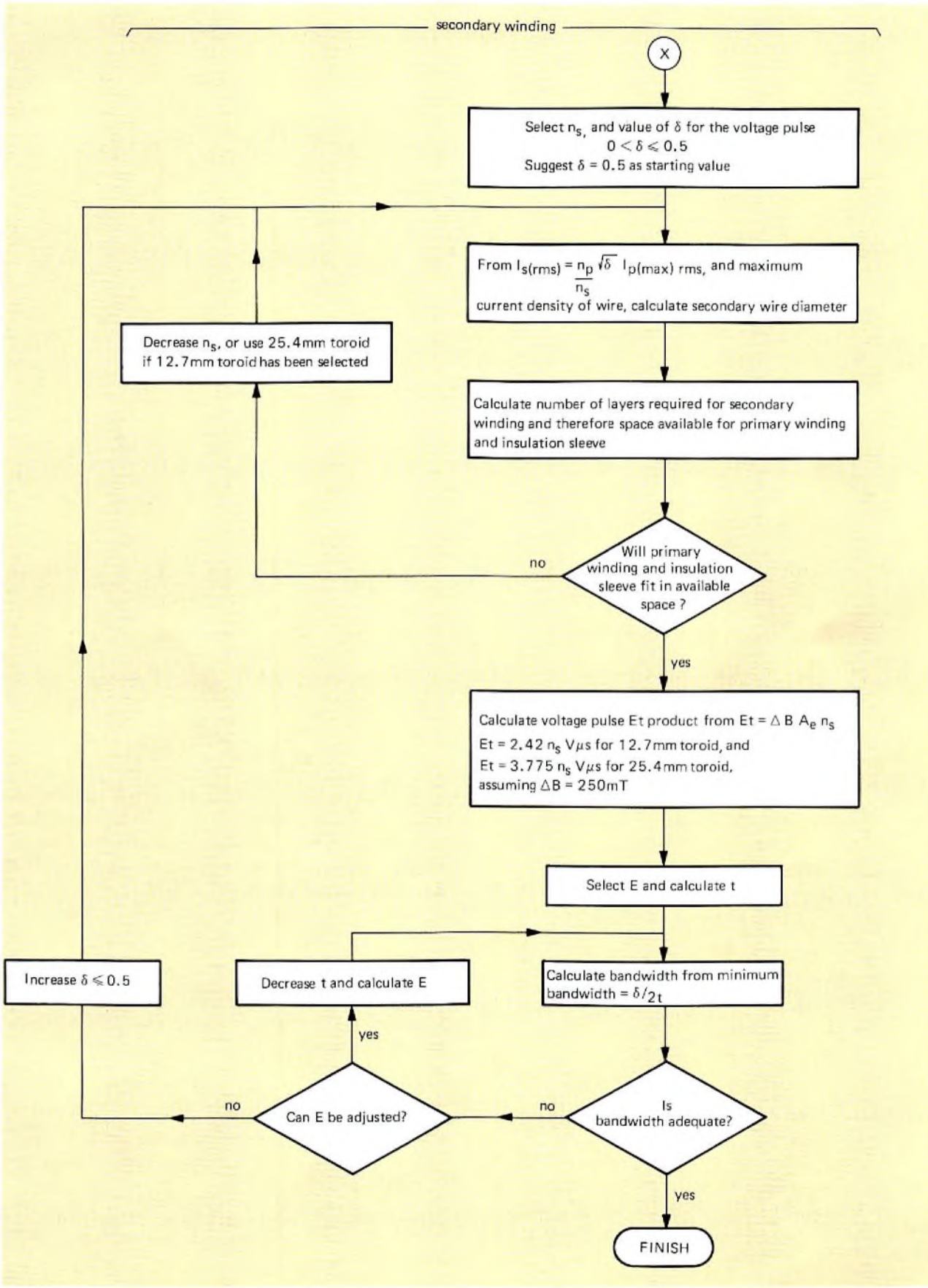
secondary winding
X
Select n_s, and value of δ for the voltage pulse
$0 < \delta \leq 0.5$
Suggest $\delta = 0.5$ as starting value
From $I_{s(rms)} = \frac{n_p}{n_s}\sqrt{\delta}\ I_{p(max)}$ rms, and maximum current density of wire, calculate secondary wire diameter
Decrease n_s, or use 25.4mm toroid if 12.7mm toroid has been selected
Calculate number of layers required for secondary winding and therefore space available for primary winding and insulation sleeve
Will primary winding and insulation sleeve fit in available space ?
no
yes
Calculate voltage pulse Et product from $Et = \Delta B\ A_e\ n_s$
$Et = 2.42\ n_s\ V\mu s$ for 12.7mm toroid, and
$Et = 3.775\ n_s\ V\mu s$ for 25.4mm toroid,
assuming $\Delta B = 250mT$
Select E and calculate t
Increase $\delta \leq 0.5$
Decrease t and calculate E
Calculate bandwidth from minimum bandwidth = $\delta/2t$
yes
no
Can E be adjusted?
no
Is bandwidth adequate?
yes
FINISH

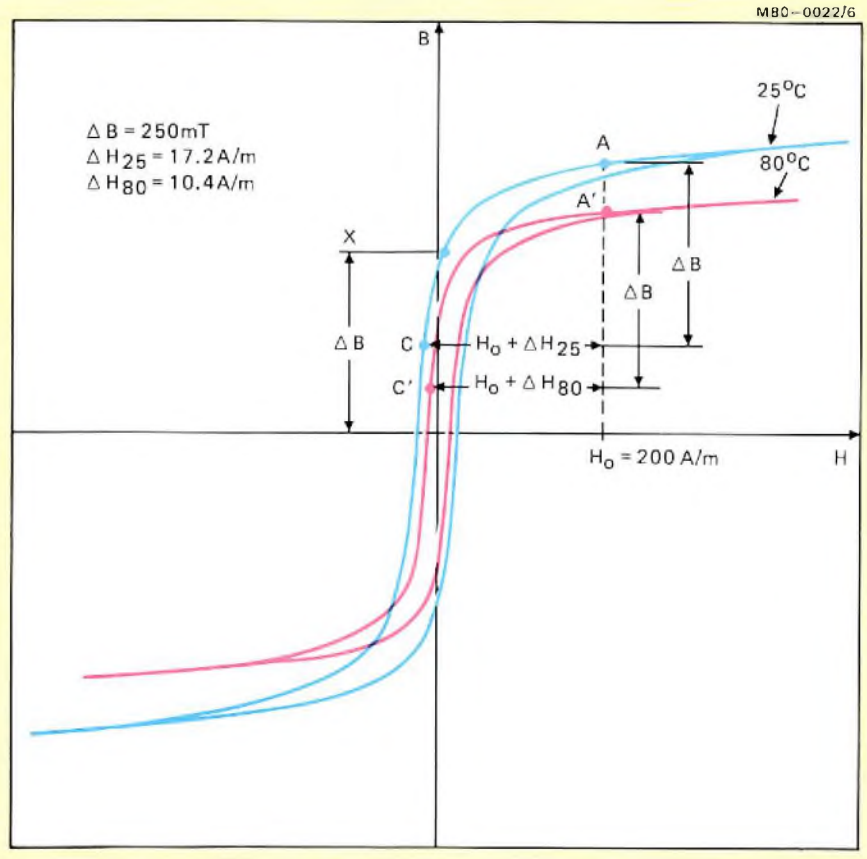

Fig.6 B/H characteristic for 3C8(A16) material, measured using a 25.4 mm toroid

aspects of DCCT performance: the worst-case static error (loss of linearity between $I_{p(o)}$ and $I_{s(pk)}$), and the temperature drift due to the change in the B/H characteristic.

Linearity

The linear relationship between peak secondary current, and primary current (Eq.6), is based on the assumption that ΔH_1 is equal to H_o (see Fig.4). The static error in the peak secondary current as a measure of primary current at temperature T is therefore defined as:

$$\frac{(H_o + \Delta H_T) - H_o}{H_o} = \frac{\Delta H_T}{H_o}, \qquad (11)$$

where ΔH_T is the final magnetic field strength in the unsaturated toroid.

Referring to Fig.6, and using the minimum value of magnetic field strength (and hence the minimum primary current) of H_o = 200 A/m (corresponding to $H_o = H_{sat}$), then for operation at 25°C, the magnetic operating point moves from A to C as a result of a ΔB change of 250 mT, so that the worst-case static error is given by:

$$\frac{\Delta H_{25}}{H_o} = \frac{17.2}{200} = 8.6\%.$$

As H_o increases, there will be a slight reduction in ΔH_{25} so that an upper limit on the value of the static error for any value of H_o can be estimated by using the value of ΔH_{25} corresponding to H_o = 200 A/m. For H_o = 2000 A/m, this gives:

$$\frac{\Delta H_{25}}{H_o} = \frac{17.2}{2000},$$

$$= 0.86\%.$$

Thus for H_o significantly larger than 200 A/m, the linearity between $I_{p(o)}$ and $I_{s(pk)}$ is excellent.

Drift

The drift due to a temperature change $(T_1 - T_2)$ is defined as the change in static error between these two temperatures; that is:

$$\frac{(H_o + \Delta H_{T1})}{H_o} - \frac{(H_o + \Delta H_{T2})}{H_o} = \frac{\Delta H_{T1} - \Delta H_{T2}}{H_o}. \qquad (12)$$

Referring to Fig.6, for $H_o = 200$ A/m and $\Delta B = 250$ mT, then the magnetic operating points move from A to C, and A′ to C′ for 25 and 80°C operation respectively. The drift caused by this temperature variation is therefore given by:

$$\frac{\Delta H_{25} - \Delta H_{80}}{H_o} = \frac{17.2 - 10.4}{200} = 3.4\%.$$

Clearly, as in the previous linearity calculation at fixed temperature, large values of H_o reduce the error caused by temperature drift. Figure 7 shows the typical variation of $V_{o(pk)}$ with primary current I_p over a 60°C temperature change for the circuit of Fig.3, using a 12.7 mm toroid, and a 3.9 Ω sensing resistor.

The fold-back in the $V_{o(pk)}/I_p$ characteristic, which occurs for low values of I_p, corresponds to those values of H_o which are less than that at point X on Fig.6. For such values the ΔB change moves the operating point into the third quadrant.

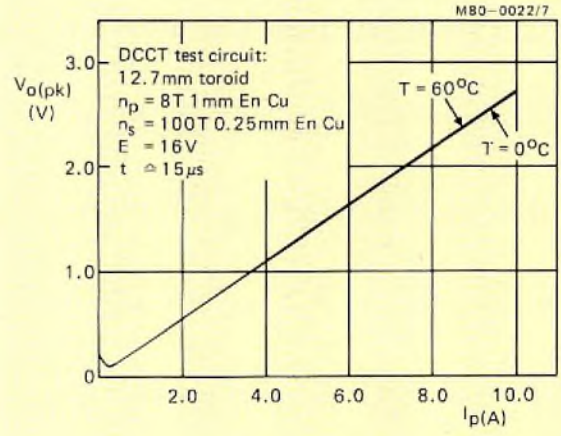

Fig.7 Peak output voltage versus primary current

SINGLE-PHASE A.C. AND D.C. APPLICATIONS

The basic circuit of Fig.3 can be used for single-phase a.c. or d.c. current measurement applications where an isolated current measurement is required from a single current-carrying conductor. Typical applications include single-phase a.c. phase (or line) control, and d.c. motor control systems.

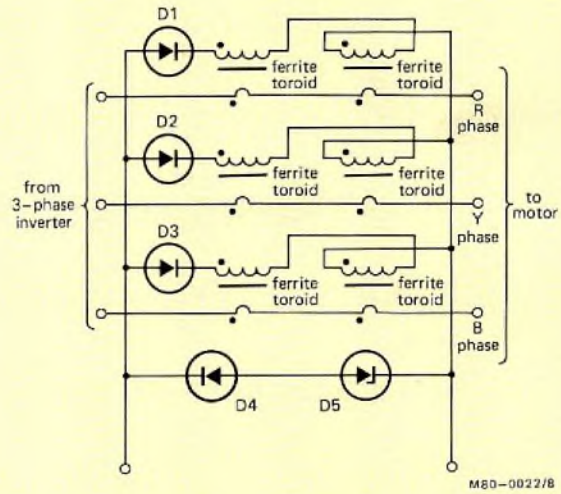

Fig.8 Toroid connections for three-phase DCCT

THREE-PHASE A.C. MOTOR DRIVE SYSTEMS

For three-phase current measurements, three pairs of toroids are used to sense current in the three load conductors (see Fig.8), together with a common switching stage and common sensing resistor. This three-phase DCCT circuit provides an isolated output which is proportional to the sum of the moduli of the three-phase lines, so that:

$$V_{o(pk)} \propto \left(|I_R| + |I_Y| + |I_B| \right), \qquad (13)$$

and the output is therefore the full-wave rectified current waveform with a current ripple frequency of six times the supply frequency (see Fig.9).

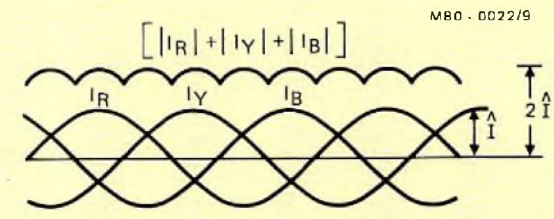

Fig.9 Sum of moduli for three-phase current waveforms

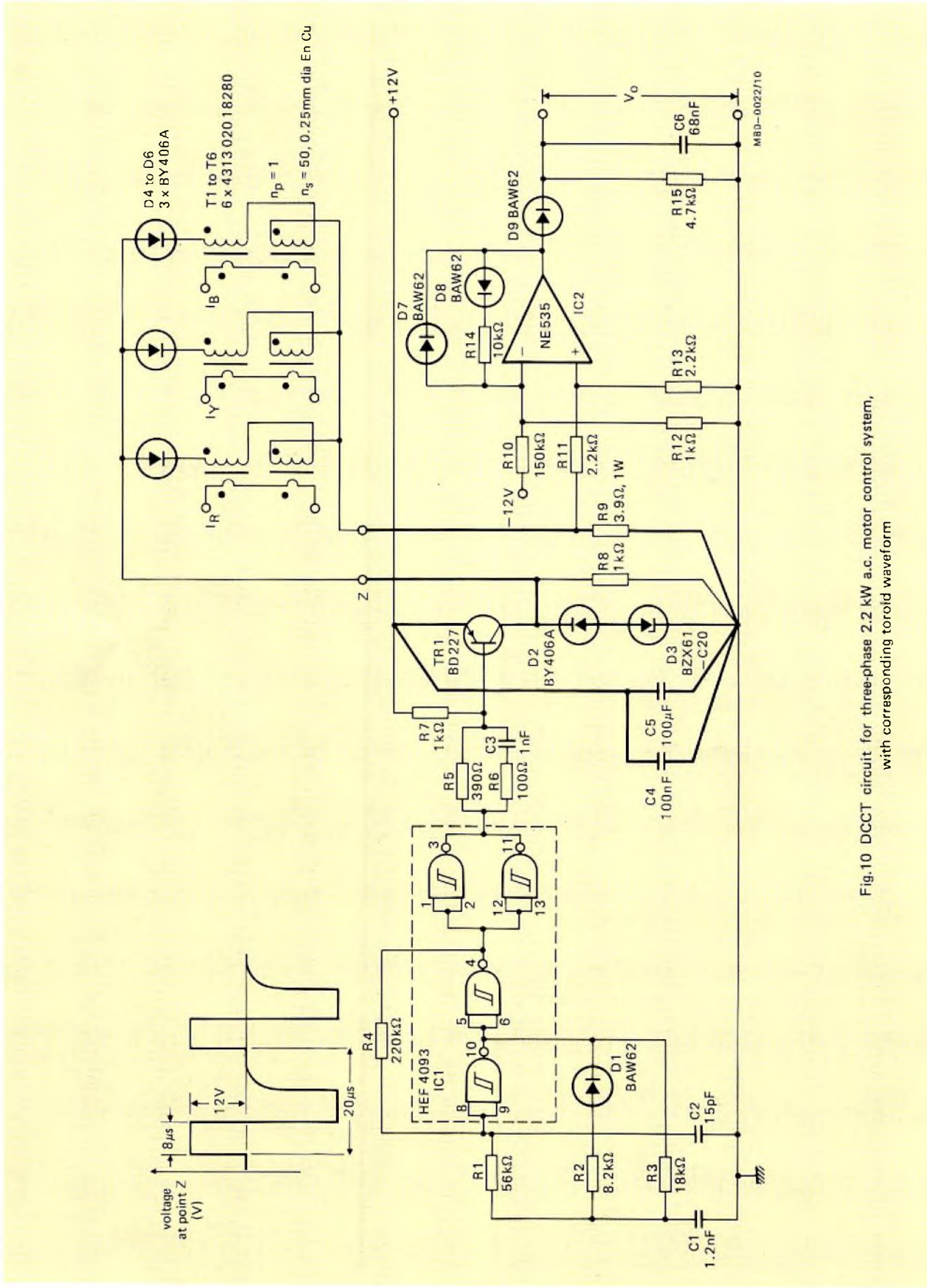

Fig.10 DCCT circuit for three-phase 2.2 kW a.c. motor control system, with corresponding toroid waveform

The diodes in series with the toroid secondaries, D_1, D_2, and D_3 (Fig.8), prevent inductive circulating currents. The toroid configuration of Fig.8 is particularly useful in three-phase a.c. motor control circuits where accurate high-bandwidth, isolated three-phase current measurement is required at an economic price. Assuming

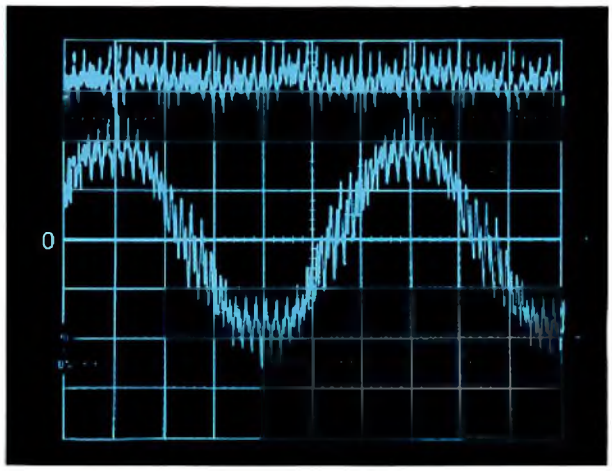

Fig.11 Typical D.C. Current Transformer waveforms: Upper trace $V_{o(pk)}$, lower trace one phase of a.c. motor current

all six toroids have the same number of primary and secondary turns, then the common driving and sensing circuits ensure that no sub-harmonics are produced in the measured output signal $V_{o(pk)}$. This is a common problem in most other currently-available three-phase current measurement circuits and is caused by imbalance in the transfer ratios. Figure 10 shows a complete DCCT circuit suitable for our three-phase a.c. motor control system (Refs.1, 2, 3, and 4). Typical output waveforms of this system are shown in Fig.11.

ENERGY SAVINGS

For the circuit of Fig.3a, the toroid magnetising energy is dissipated in the voltage regulator diode D_2. Alternatively, this energy may be recovered if a bifilar secondary winding is used. This is particularly suited to the larger 25.4 mm toroid, where the magnetising energy is quite significant and the toroid internal diameter is large enough to accommodate a second winding (see Fig.1). By using a bifilar secondary winding, energy savings of approximately 50% can be achieved.

This article is the fifth in a series covering various aspects of our PWM variable speed drive. The next article in the series will be devoted to the electrolytic capacitors developed for application in the d.c. link.

REFERENCES

1. HOULDSWORTH, J.A. and ROSINK, W.B., 'Introduction to PWM speed control system for 3-phase AC motors', Electronic Components and Applications, Vol.2, No.2, February 1980, pp.66 to 79.
2. BURGUM, F. and NIJHOF, E.B.G., 'Inverter circuit for PWM motor speed control system', Electronic Components and Applications, Vol.2, No.3, May 1980, pp.130 to 142.
3. STARR, B.G. and van LOON, J.C.F., 'LSI circuit for AC motor speed control', Electronic Components and Applications, Vol.2, No.4, August 1980, pp.219 to 229.
4. ROSINK, W.B., 'Analogue control system for an AC motor with PWM variable speed drive', Electronic Components and Applications, Vol.3, No.1, November 1980, pp.6 to 15.

INAUGURATION OF STEREO/DUAL SOUND FOR TV TRANSMISSIONS

The Berlin radio/tv exhibition (Funkausstellung) to be held in August will mark a new departure in tv sound: selected West German transmitters will commence broadcasting two sound channels instead of one. For receivers adapted to take advantage of it the new system will offer two new options: stereo sound, and the possibility of listening to a motion-picture sound track in the original language or dubbed in another. With the aid of headphones, two persons watching the same programme will even be able to listen to sound tracks in different languages. Existing receivers not adapted to the new system will receive only the normal monophonic or monolingual sound. Modulation of both the monophonic and the stereo sound will be to high-fidelity standards.

In anticipation of this new development the next issue of Electronic Components and Applications will contain an article describing intergrated circuits for decoding the transmission identification signals and separating the two sound channels. It will also describe both economical and high-fidelity stereo circuits for use with the new transmissions, together with the appropriate integrated circuits.

Microprocessor peripheral for viewdata

R. E. F. BUGG

In recent years the capability of the conventional tv receiver has been enhanced by the development of two complementary systems that provide for the display of digitally encoded alphanumeric and graphical information. The systems have the generic names teletext and viewdata*; these use a similar word format for transmission and an identical page format for display, but differ fundamentally in their mode of transmission. This article describes a purpose-designed LSI circuit, type SAA5070, which has been developed for use in viewdata receivers. Before describing the SAA5070 in detail it is helpful to review the characteristics of teletext and viewdata and the features of the associated receivers. The original development work on teletext and viewdata was concentrated in the UK, and the details given in this review relate to UK teletext and viewdata systems. Alternative systems introduced, or under development, in other countries do differ from UK teletext and viewdata. However, such differences are generally minor, and in particular they do not limit the application of the SAA5070 which is a highly versatile circuit suitable for use in all existing viewdata systems.

* Teletext and viewdata are also described as broadcast videotext and interactive videotex, and strictly speaking teletext and viewdata are limited to UK usage only with other specific names used in other countries. However, the wider meaning of teletext and viewdata is generally understood, and has been adopted in this article.

TELETEXT

Teletext, which is operated in the UK by the BBC (British Broadcasting Corporation) and IBA (Independent Broadcasting Authority), uses the broadcast television signal to carry digitally-encoded alphanumeric data (see Ref.1 for a full UK teletext specification). The data is carried on unused lines above the normal displayed picture. Two lines per field are used at present, but in future this could be increased up to a maximum of 16 lines. Ninety-four standard alphanumeric characters are transmitted, which can be in any one of six colours – red, green, blue, yellow, cyan, and magenta – or white.

The teletext page format allows up to 24 rows and 40 columns of standard characters to be displayed. In addition to the normal display of alphanumeric characters, teletext allows for the display of simple graphics. These are produced by assembling small illuminated rectangles in any one of the six available colours, each one-sixth of the space occupied by a standard alphanumeric character. Typical teletext pages are shown in Fig.1.

Each teletext character is transmitted as one 8-bit word consisting of seven data bits plus a parity bit. The bit rate is 6.9375 Mbits/s which allows a 40 character row of teletext display to be carried on one television line. Using two lines per field, a full teletext page may be transmitted in less than a quarter of a second (see Ref.2 for a full description of the transmission system).

The existing UK teletext services (Ceefax for the BBC and Oracle for the IBA) each carry several hundred pages of information, advice, news, and entertainment. The pages are transmitted sequentially, and when a viewer selects a particular page he must await its arrival. The

index page from BBC's Ceefax service

weather page from IBA's Oracle service

Fig.1 Typical teletext pages

access time for a page will depend on the number of pages being transmitted, and on the amount of information carried on each page; for Ceefax it currently averages about 12 s.

Teletext receiver

We have been involved with teletext since its inception, developing a laboratory-prototype receiver for the acquisition and display of Ceefax and Oracle transmissions. Following this early experience, we developed a set of four dedicated LSI circuits for use in a production teletext receiver design. The resulting receiver gives high performance combined with flexibility and economy.

A simplified block diagram of the system is shown in Fig.2. It comprises the four dedicated ICs VIP (SAA5030), TAC (SAA5040), TIC (SAA5020), and TROM (SAA5050), a page memory of two standard 1 K x 4 static RAMs, and three low-power Schottky

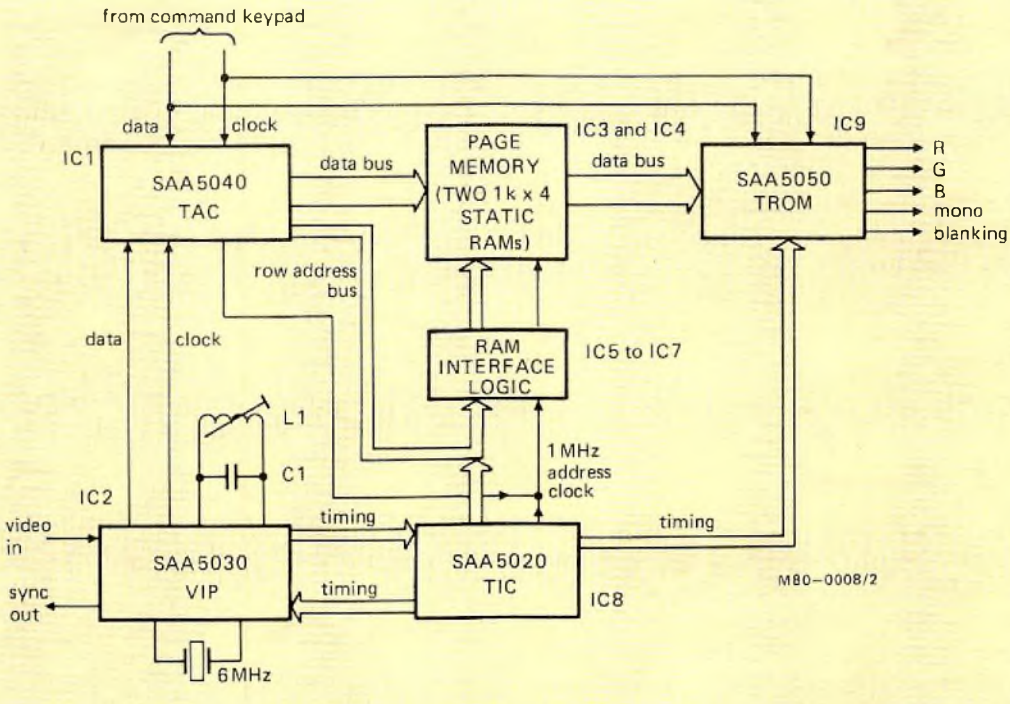

Fig.2 Simplified block diagram of teletext receiver

TTL ICs which interface the page memory. Teletext provides a wide range of display options, and the receiver is therefore controlled by a command keypad, usually a remote control system with an infrared link.

The basic functions of the four dedicated ICs are now briefly described. A fuller description of the ICs and the receiver design is given in Ref.3.

SAA5030 VIP video input processor

The video signal is input to the VIP (IC_2 in Fig.2) where it is sliced by means of an adaptive data slicer circuit. A clock signal is generated from the sliced data using the external 6.9375 MHz tuned-circuit ($L_1 C_1$), and this signal is used to serially clock the data into the TAC (IC_1 in Fig.2). A 6 MHz display system clock is also included in IC_2, the output of which is divided in IC_8 to produce a pulse every 64 μs. This signal is passed back to IC_2 where it is used to phase-lock the timing system of the teletext display with the incoming television picture signal.

SAA5040 TAC teletext data acquisition and control

The TAC (IC_1 in Fig.2) has two principal sections: a data acquisition section that processes the teletext data so that it can be written into the page memory, and a control section that processes control information from the command keypad. The control information identifies the required page and operates the various display options that are available with teletext.

The data acquisition section of TAC divides the data from VIP into its component parts and checks the data for errors. The row address of the incoming data line (one of twenty-four) is fed by this section to the 5-bit row address bus, and the character data is fed through the data bus to the page memory as a sequence of 40 7-bit parallel words.

SAA5020 TIC timing chain

The TIC (IC_8 in Fig.2) generates all the timing signals for the teletext display. It consists of a series of divider stages which subdivides the 6 MHz signal from VIP. During display a 1 MHz clock signal steps the character addresses in the page memory. Column address counters in the RAM interface are cleared at the end of each row. Every ten lines during the display TIC steps the row address forward by one to access the next row of characters in the memory.

SAA5050 TROM teletext read-only memory

The basic function of TROM (IC_9 in Fig.2) is to convert the 7-bit character data stored in the page memory into the corresponding video signals. These comprise a monochrome-only signal and RGB signals for a colour receiver. The blanking output signal enables the television video signal to be blanked, or partially blanked out when a teletext newsflash or subtitle is to be displayed.

Additional circuits in TROM enable various control functions to be performed. These function are determined by control characters received from the page memory. Examples of these control functions are the selection of graphics or alphanumerics, 'flashing' words, or boxes.

VIEWDATA

Viewdata is the generic term for systems which disseminate and retrieve computer-based information using a telephone line for communication and a television set for display. The world's first public viewdata service was developed by British Telecom, which has given the name Prestel* to its viewdata system (see Ref.4 for a specification of Prestel).

While viewdata has many similarities with teletext, page format and data encoding for example, the use of telephone lines for data transmission results in two very significant differences between the two systems. With viewdata, data can be transmitted from the user to the computer; this contrasts with the purely passive nature of teletext. In addition, unlike teletext where the number of pages is constrained by the need to provide an acceptably-low access time, the page capacity of viewdata is limited only by the storage capacity of the viewdata computer.

The Prestel system has a data base with a capacity of several hundred thousand pages, providing a comprehensive information service for business and domestic users. Pages can be selected directly if the page numbers are known. Alternatively, a simple system using few commands enables the user to identify any required page.

The use of this system is illustrated in Fig.3. The user is initially presented with the index page, and one of several categories of information is chosen by pressing the corresponding single digit page number on the command keypad. A further index page is then displayed, and this process is continued until the desired page is reached.

The limitations imposed by the bandwidth of the standard telephone line means that the data rate for viewdata is relatively slow in comparison to teletext:

*Prestel is a registered trademark.

Fig.3 Typical sequence of Prestel displays, illustrating the page selection process

1200 baud, corresponding to 120 characters per second on the receive channel (computer to receiver), and 75 baud on the return channel. However, the response from the computer is virtually instantaneous, resulting in a negligible access time. The word format is shown in Fig.4. Data is transmitted asynchronously, and each 8-bit word is preceded by a start bit (LOW) and terminated by a stop bit (HIGH). A system of Frequency-Shift Keying (FSK) is used. On the receive channel, a logic HIGH is represented by a 1.3 kHz tone and a logic LOW by 2.1 kHz. On the return channel the frequencies are 390 and 450 Hz respectively.

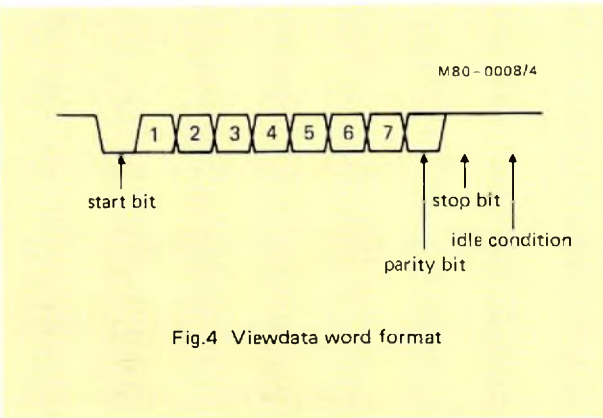

Fig.4 Viewdata word format

Our involvement with teletext is matched by a similar commitment to viewdata. We are a major supplier of viewdata modules, and have now produced a full LSI viewdata receiver system. The system is based on a microprocessor from the standard 8048 family, and the purpose-designed LSI circuit, type SAA5070, which forms the subject of this article. The SAA5070 has been given the name LUCY, derived from the phrase 'line coupling unit'. The LUCY chip is primarily a microprocessor peripheral device, intended to integrate as many as possible of the fixed hardware functions of a viewdata receiver on the telephone line side. It is manufactured in N-channel MOS and encapsulated in a 40-pin dual-in-line package. The detailed description of the IC is preceded by an examination of the performance requirements and design of a viewdata receiver.

Viewdata receiver

The design of a viewdata receiver will be determined partly by the viewdata system specification and partly by the facilities required by the user of the receiver. A wide range of designs is therefore possible, and viewdata receivers are invariably microprocessor based, partly to cope with this potential variety. However, for all viewdata systems there will be a number of basic features that any receiver must have for the reception and display of viewdata; these may be summarised as follows.

- Provide the signals necessary to establish the telephone connection
- Receive and process serial data from the telephone line, and transmit outgoing data on the return channel
- Write the display data into a page memory and generate the page display signals
- Receive and process user control instructions
- Store and retrieve the user identification code and the telephone numbers of viewdata data bases

Figure 5 shows a simplified block diagram of a viewdata receiver based on the LUCY integrated circuit that provides all these basic features. The receiver consists of two main sections: a display section and a data acquisition and control section. The display section consists of the page memory, the character generator (SAA5050 TROM), the timing chain (SAA5020 TIC), and the page memory interface logic. The data acquisition and control section consists of an 8049 microprocessor, the LUCY chip, and an electrically-alterable ROM (EAROM) holding the identification code and data base telephone numbers. The Line Terminating Unit (LTU), interposed between LUCY and the telephone line, provides safety and isolation components, filters the received and return channel signals, and contains the dialling relays.

User control instructions from a command keypad are fed to the receiver via an IBUS (information bus) input on LUCY. The dialling function is controlled by three relays on the LTU; the signals to activate these relays are provided by LUCY. The FSK signal from the telephone line is filtered and squared-up in the LTU before being input to LUCY. Under the control of the microprocessor the data words are parallel-loaded onto the data bus of the viewdata receiver and assigned to the appropriate location in the page memory. The generation of the page display signals is the same as for teletext, with the TROM converting the character data in the page memory into the RGB signals required to display the character data on a tv screen.

SAA5070 LUCY

A simplified block diagram indicating the internal organisation of the SAA5070 is shown in Fig.6. Each section of the IC can communicate with the microprocessor via a register (of up to eight bits) which is connected to an internal bus. In addition to the registers associated with a particular section of LUCY, there are four registers which affect the whole IC: two status registers, a mode register, and a command register. These determine the current status of the device, dictate the mode of operation, or initiate a specific function. The IC incorporates the following features.

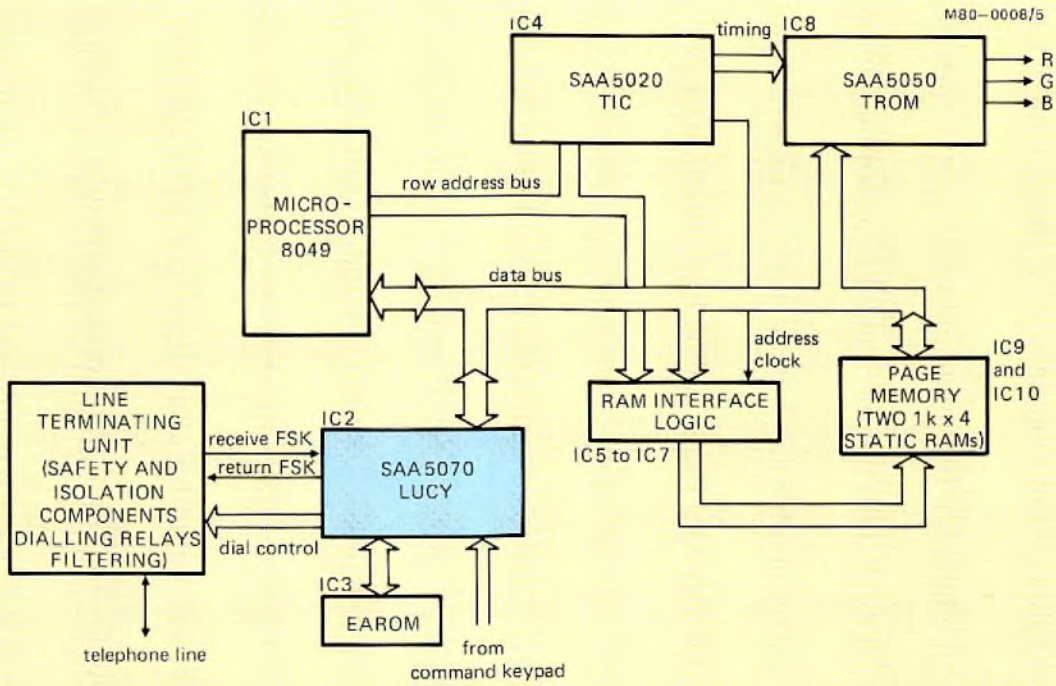

Fig.5 Simplified block diagram of basic viewdata receiver

- Microprocessor interface
- Autodialling circuit for British Telecom and European requirements
- Timer circuits (60 and 1.5 s time-outs)
- 1200 baud demodulator and asynchronous receiver
- 75/1200 baud modulator and asynchronous transmitter
- Tape recorder modem (modified 'Kansas City' standard)
- Tape recorder asynchronous receiver/transmitter
- IBUS receiver and receiver/transmitter
- General-purpose input/output ports for other subsystems (such as an EAROM)

The SAA5070 is partitioned for flexibility of use. This permits the use of an external modem, as required by a number of national telephone authorities, and allows simultaneous but independent operation of the tape recorder interface and the line interface. A full description of the IC is given in Ref.3.

Microprocessor interface

The controlling microprocessor communicates with the SAA5070 via an 8-bit multiplexed address and data input/output port (pins 26 to 33). An internal read or write pulse ($\overline{R}$ and $\overline{W}$) is produced by gating the external read or write pulses $\overline{RD}$ and $\overline{WR}$ (see Fig.6) with the chip select pulse $\overline{CS}$. One of the internal registers of the IC is enabled onto the internal bus by gating the internal read or write pulses with the appropriate output of the register address decoder ($\overline{SR0}$ to $\overline{SR12}$). The register address is taken from the four least significant data bits latched on the falling edge of Address Latch Enable (ALE).

Autodial section

A simplified diagram of the dialling relays located in the LTU is shown in Fig.7. Dialling is initiated by closing the Seize-line relay RL_2, and simultaneously disconnecting the telephone handset via RL_1. The Seize-line relay is activated by a signal from one of the LUCY general-purpose input/output ports (see below) otherwise all the timing signals necessary to drive the relays are provided by the autodial section of LUCY. Dialling impulses, at the rate of 10 per second, are generated in the Imp relay. During impulsing, the Don relay is closed to short-circuit the telephone line. The impulsing ratio can be altered to cover both UK and European requirements. There is a timer associated with the dialling circuit which can be used to time out 1.5 or 60 s. The 60 s timer might typically be used to release the telephone line if connection is not made within 60 s of dialling the last digit.

Line demodulator and carrier detect

The input to the line demodulator, via the FSKIN pin, consists of the FSK signal from the telephone line, which has been squared and bandpass filtered in the LTU. Via

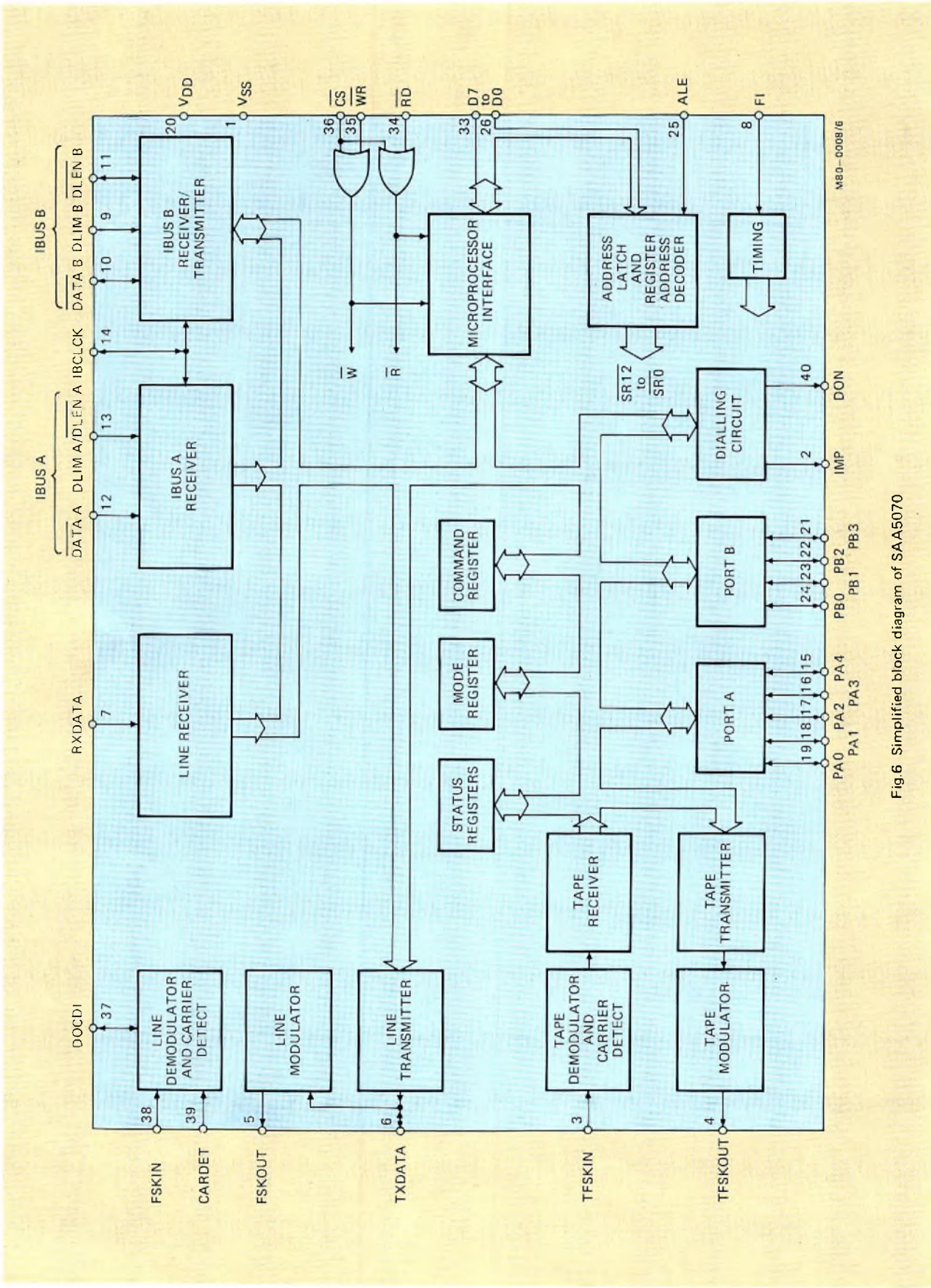

Fig.6 Simplified block diagram of SAA5070

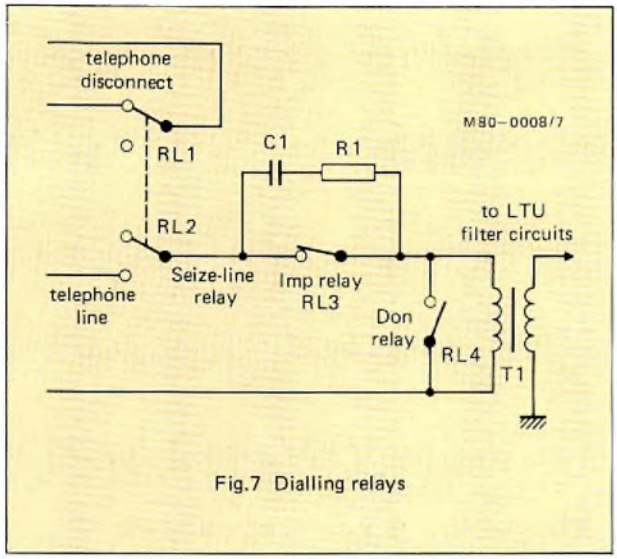

Fig.7 Dialling relays

the DOCDI pin, the demodulator outputs a signal of varying mark/space ratio which is then filtered and limited to give a digital signal for the RXDATA pin.

At the end of the dialling process, a carrier signal (a 1.3 kHz tone) is transmitted from the computer to the receiver. When this carrier has been detected, a return carrier is sent to the computer, which on detecting the return carrier completes the connection process by sending the sign-on page. At the start of a call, supervisory tones such as the dial tone, ringing tone, and number unobtainable tone, will be present on the line. These tones are rich in harmonics which lie in the 1.3 to 2.1 kHz passband. If the signals corresponding to these tones were input to LUCY via the 1.3 to 2.1 kHz bandpass filter, then it is possible that the filtered signal would be mistaken for the 1.3 kHz carrier, causing the terminal to malfunction. To avoid this possibility, the FSKIN pin is initially disabled, and the received signal is input to the CARDET pin of LUCY with minimal filtering only. This allows the fundamental frequency to be recognised by the IC so that supervisory tones will not be mistaken for the 1.3 kHz carrier. When a carrier signal has been detected on the CARDET pin for a net time of 2 s, the FSKIN pin is enabled and the received signal switched from the CARDET pin to the FSKIN pin.

Line receiver

The line receiver is designed to work with either seven data bits and a parity bit, or with eight data bits and no parity. If parity is used, then odd or even parity detection may be selected.

The signal data is shifted into a serial-to-parallel shift register via the RXDATA pin. When all ten bits (see Fig.4) have been received, the start and stop bits are stripped off, and the 8-bit word is loaded into a holding register, ready to be accessed by the microprocessor.

Line transmitter

The data format of the transmitted signal is identical to that of the received signal. Odd or even parity may be selected, and if the parity check is disabled, an 8-bit data word may be used. Two transmission rates are available: 75 baud for viewdata transmissions, and 1200 baud which can be used for private communication systems.

The output of the line transmitter will normally go directly to the line modulator. However, if LUCY is used with an external modem, then the line transmitter output is brought to the TXDATA pin. This pin is connected internally to the modulator input and can act as the data input if the transmitter is off-chip, as could be the case with an external keyboard.

Line modulator

The modulator produces a serial delta-modulated bit stream, which is lowpass filtered in the LTU to provide a suitable FSK signal for the telephone line (see Fig.8). The serial bit stream is generated by a 92-bit pattern stored in an internal ROM. This bit pattern has been carefully chosen so that the harmonics of the modulator output signal which fall in the 1.3 to 2.1 kHz passband are much lower than the fundamental, thereby permitting the use of a relatively simple filter design.

The frequency coding of the FSK signal is dependent on the transmission bit rate. At 1200 baud, a HIGH is represented by 1.3 kHz and a LOW by 2.1 kHz, while at 75 baud, HIGH and LOW signals are represented by 390 Hz and 450 Hz respectively.

Tape section

A tape recorder, for storing viewdata pages, is a useful addition to the basic viewdata receiver of Fig.5. The operation of the LUCY tape interface is similar to the

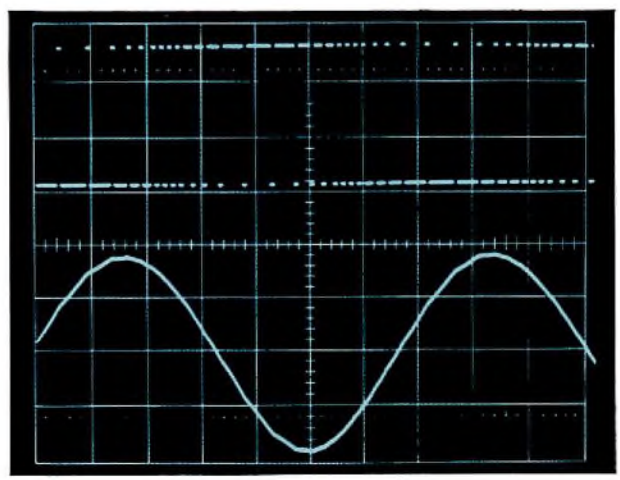

Fig.8 Delta-modulated 390 Hz return channel signal:
(a) upper trace — serial bit stream
(b) lower trace — serial bit stream after lowpass filtering

operation of the telephone line interface but is physically separate and works independently. This means that it is possible to record one stream of data while receiving a separate stream of data from the data base.

The tape data modulation system is a modified form of the 'Kansas City' standard. A HIGH is represented by one cycle of 1.3 kHz, and a LOW by two cycles of 2.6 kHz. The modulator output requires only minimal external lowpass filtering to produce data suitable for audio cassette tape recorders. The bit rate is 1300 baud on both record and replay, and the data format is identical with that for viewdata. The parity check may be odd or even, and parity can be disabled if an 8-bit data word is required. The data rate of 1300 baud is slightly faster than the 1200 baud line receive rate, allowing incoming data from the line to be transferred (via the microprocessor) directly onto tape, independently of possible tolerances in the line receive rate.

To overcome the tendency of cassette recorders to attenuate higher frequencies, the 1.3 kHz signal contains 2 μs wide attenuating pulses every 12 μs. After external filtering, this reduces the 1.3 kHz signal by 3 dB relative to the 2.6 kHz signal.

Data is output via the TFSKOUT pin and input via the TFSKIN pin. Because the modulation is in phase with the data, a clock may be extracted from the signal on replay, and this permits a wide tolerance on replay speeds. A carrier detect circuit is included which enables the tape receiver if a tape carrier signal (1.3 or 2.6 kHz) is received for 100 ms. If the carrier is lost for 100 ms, then the receiver is disabled.

IBUS A receiver and IBUS B receiver/transmitter

All three IBUS circuits (receiver A, receiver B, and transmitter B) are general-purpose in that they are capable of handling variable length codes of 1 to 12 bits. Each of the three circuits has two 8-bit registers, which are accessed by two successive read or write operations to the same address.

The IBUS circuits have been designed to be compatible with the various bus structures currently in use, incorporating two-wire to three-wire conversion and a 62.5 kHz clock input/output pin to accept or provide a 62.5 kHz clock as required. Receiver A may be set to receive two- or three-wire IBUS messages. For three-wire operation the data clock is derived from the 62.5 kHz clock on the IBCLCK pin. Receiver B/transmitter B is composed of a two-wire receiver and a transmitter which produces all the signals necessary for two- or three-wire IBUS transmission.

User control code conversion is a typical use of these circuits. A single remote control command is fed to receiver A. The command is read and code-converted by the microprocessor. If required, this code-conversion can result in a string of command instructions. These are then written back into LUCY and output via transmitter B.

Port A and Port B

These are general-purpose input/output ports. Port A has five outputs and Port B has four. Typically, the outputs of Port A provide a direct interface to an electrically-alterable ROM, holding the user identification code and data base telephone numbers, while one of the pins of Port B can be used to output the signal controlling the Seize-line relay in the dialling circuit.

EXTENDED SPECIFICATION RECEIVERS

As mentioned above, even within the same viewdata system specification, such as UK Prestel, differing user requirements can result in receiver designs which differ greatly in performance and the range of facilities offered. The LUCY integrated circuit is suitable for use in basic receiver designs, such as that shown in Fig.5, but offers a host of additional facilities as well. Figure 9 shows a block diagram of an extended specification viewdata receiver which illustrates the range of facilities potentially available with LUCY. In addition to the features shown in Fig.5, the extended specification receiver could incorporate the following facilities.

- A tape recorder for storing viewdata and teletext pages
- An alphanumeric keyboard for message writing and editing
- Teletext acquisition and control circuits so that the receiver has full teletext/viewdata capability
- Multipage memory – giving rapid access to, and easy manipulation of, stored pages
- A hard-copy printer

Figures 5 and 9 illustrate some of the flexibility of LUCY, but they can only tell half the story since the full performance of a LUCY-based viewdata receiver will be determined by the microprocessor software. The LUCY integrated circuit is thus highly adaptable, a characteristic that is likely to become increasingly important as viewdata is developing in a very diverse manner.

Figure 10 shows a LUCY-based viewdata decoder board developed for the French interactive videotex system Antiope. This system is generally similar to Prestel but differs in the treatment of character attributes. By simply changing the software in the microprocessor, the decoder of Fig.10 can be used for the reception of Prestel – an attractive illustration of the flexibility of LUCY and microprocessor-based design.

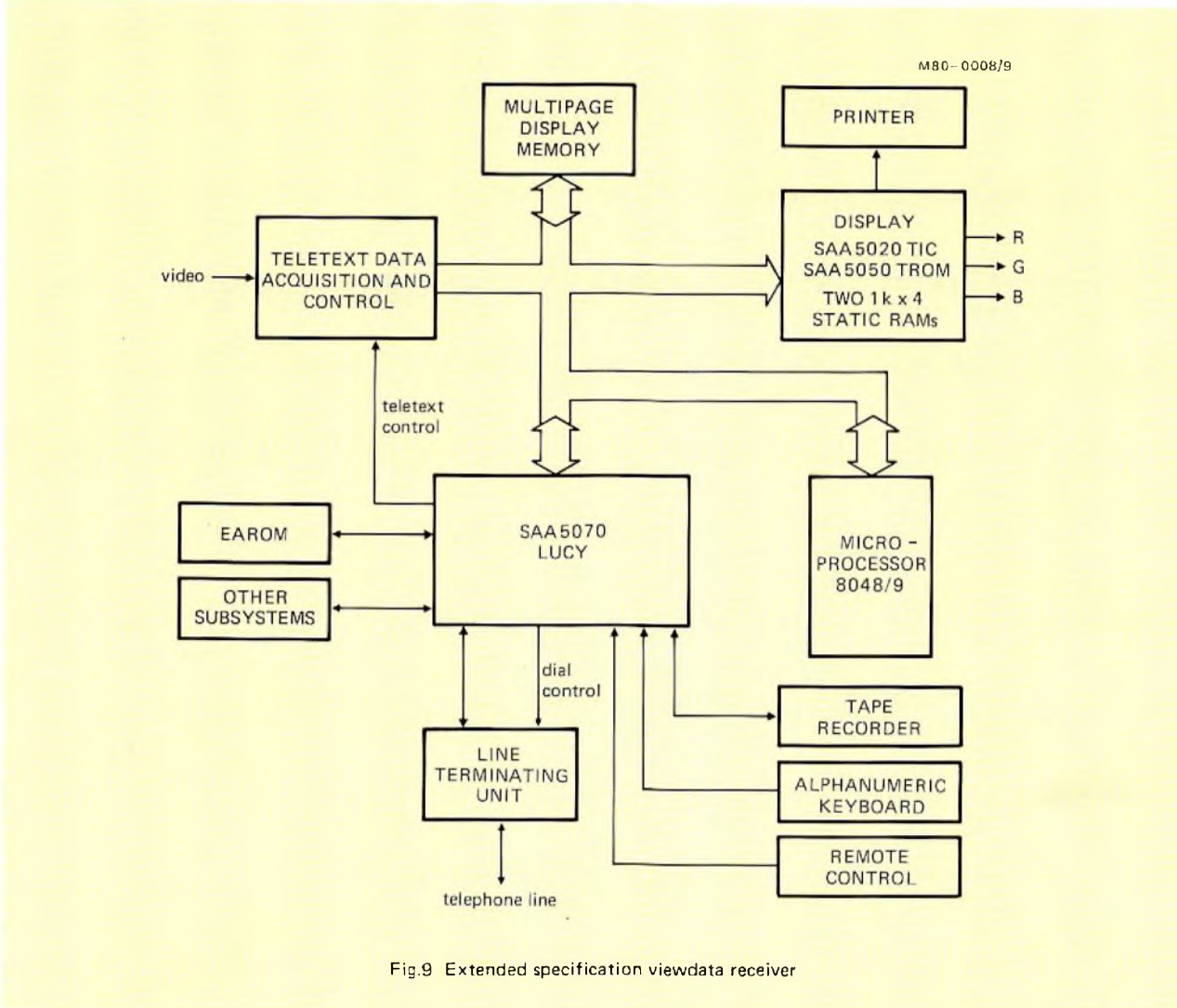

Fig.9 Extended specification viewdata receiver

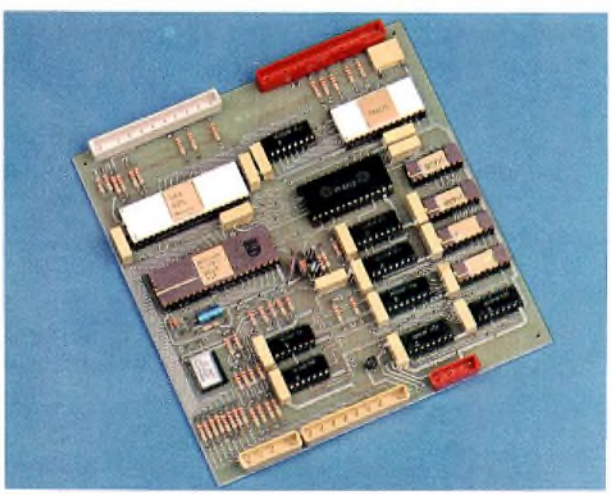

Fig.10 LUCY-based decoder board designed for the French interactive videotex system Antiope

REFERENCES

1. 'Broadcast Teletext Specification', BBC/IBA/BREMA, September 1976.
2. DAVIES, H.Q.N., 'Survey of teletext transmission systems and Mullard decoders', Mullard Technical Communications, Vol.14, No.134, April 1977, pp.143 to 158.
3. Mullard Technical Publication M81-0001, Mullard Limited, 1981.
4. 'The Prestel Terminal Specification, Edition 1', British Telecom, December 1980.

Part 2 – Design calculations

Ceramic permanent magnets for d.c. motors

H. J. H. VAN HEFFEN

FERROXDURE CERAMICS IN PERMANENT-MAGNET MOTORS

This article uses the same symbols and terminology as Part 1 (E.C.A. Vol.3 No.1), and the equation number sequence started there is here continued.

Preliminary considerations

Available materials

Grades of anisotropic Ferroxdure are available with values of remanance from 250 mT to 400 mT and values of intrinsic coercivity from 240 kA/m to 360 kA/m. Materials are made with various combinations of remanence and coercivity: high remanence and low coercivity, as for FXD370; low remanence and high coercivity, as for FXD270. All these can be produced in shapes suitable for permanent-magnet motors. For each design, there are cost/performance trade-offs to be made that depend on the grade of material used and the magnet shape required.

Magnet requirements

The basic requirements of magnets for permanent-magnet motors are:

- that they can supply the total flux required at a given operating temperature
- that they can tolerate the reverse m.m.f. due to the stall current at that temperature.

Motor specification

Both the total flux required and the m.m.f. to be tolerated depend on the motor design; however, a number of designs are possible within the requirements of a given motor specification. These designs must share the same parameters that determine the motor specification. These parameters can be classified as follows.

- *Specific parameters* that set the requirements and operating conditions.
- *Primary parameters* that can be derived unambiguously from the specific parameter by established formulae.

A motor design that satisfies these requirements is itself characterised by

- *secondary or design parameters* that apply only to that design. These do not follow directly from the motor specification: some variation is possible so that their actual values are, to some extent, determined by the designer.

Table 1 lists the specific, primary and some of the secondary parameters of a motor. The primary parameters are derived from the specific parameters using the following expressions:

$$C = M_n/M_0 \quad (16)$$

$$C_m = (\eta_{m(n)} - C)(E - E_b)/n\eta_{m(n)} \quad (17)$$

$$I_0 = 2\pi M_0/C_m \quad (12)$$

$$I_n = 2\pi M_n/(C_m\eta_{m(n)}) \quad (11)$$

$$R = (E - E_b)/I_0 \quad (64)$$

$$R_e = R_i + R_c \quad (65)$$

$$R_a = R - R_e \quad (66)$$

$$E_c = nC_m \quad (9)$$

$$\eta_{(n)} = (\eta_{m(n)} - C)(E - E_b)/E \quad (29)$$

$$\eta_{e(n)} = \eta_{(n)}/\eta_{m(n)}. \quad (24)$$

TABLE 1
Specific, primary and secondary motor parameters

Specific parameters

E, E_b, M_0, M_n, n, P_{DR}, R_c, R_i, $\eta_{m(n)}$ and their temperature dependence

Primary parameters

C, C_m, E_c, I_0, I_n, R, R_a, R_e, $\eta_{e(n)}$

Secondary parameters

a, D_c, F, g, p, S_n, S_0, w, Z and the dimensions of rotor, magnets and housing, together with the grade of permanent-magnet material.

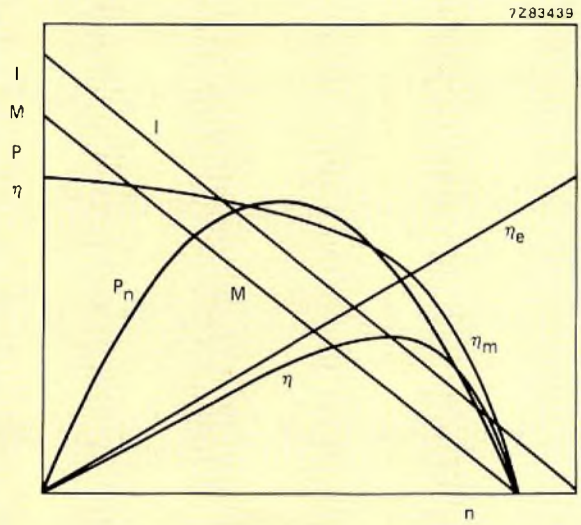

Fig.1 The variation of a number of motor characteristics with rotation rate n

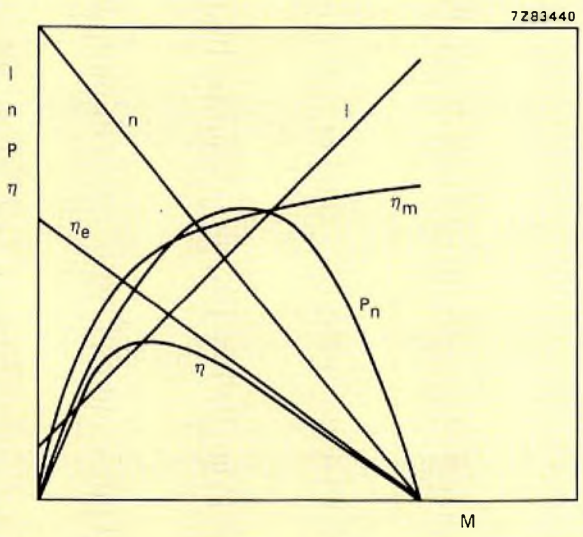

Fig.2 The variation of a number of motor characteristics with generated torque M

Figure 1 shows how a number of the parameters vary with n, and Fig.2 how they vary with M.

The design process now comprises determining the values of the secondary parameters. These will be such that, within the limits of their own interdependence, they make for a design that satisfies any economic, production, or application-oriented limitations. These may be the use of existing laminations, minimum cost, minimum weight, or the optimisation of some other characteristic. Moreover, it is the choice of secondary parameters that ensures that irreversible demagnetisation of the stator magnets cannot occur at maximum (stall) current over the working-temperature range of the motor.

Influence of the specific parameters

Let us now examine two designs that satisfy the same motor specification. Both specific and primary parameters are, of course, the same for both designs, but each has its own set of secondary parameters:

parameter	*design 1*	*design 2*
Φ_{tot}	$\Phi_{tot\,1}$	$\Phi_{tot\,2}$
Z	Z_1	Z_2
α'	α'_1	α'_2
F	F_1	F_2
a	a_1	a_2

It follows from eqs. (7) and (31) that

$$\frac{Z_1\Phi_{tot\,1}}{a_1} = \frac{Z_2\Phi_{tot\,2}}{a_2}. \qquad (67)$$

From eq. (33)

$$F_1 = I_0\alpha'_1 Z_1/(8\pi a_1 q) \qquad (68)$$

$$F_2 = I_0\alpha'_2 Z_2/(8\pi a_2 q). \qquad (69)$$

Combining eq. (67) with eq. (69) yields

$$F_2 = \frac{I_0\alpha'_2 a_2 \Phi_{tot\,1} Z_1}{8\pi a_2 a_1 \Phi_{tot\,2} q} = \frac{I_0\alpha'_2 \Phi_{tot\,1} Z_1}{8\pi a_1 \Phi_{tot\,2} q}. \qquad (70)$$

Substituting eq. (68) in eq. (70) yields

$$\frac{\Phi_{tot\,1} F_1}{\alpha'_1} = \frac{\Phi_{tot\,2} F_2}{\alpha'_2} \qquad (71)$$

That is, for any design to a given motor specification,

$$\frac{\Phi_{tot} F}{\alpha'} = \text{constant}.$$

Since, from eqs (7) and (31)

$$\Phi_{tot} = aC_m/Z \qquad (72)$$

and, since

$$F = I_0\alpha' Z/8\pi aq \qquad (33)$$

it follows that

$$\frac{\Phi_{tot} F}{\alpha'} = \frac{aC_m I_0 Z}{8\pi aZq} = I_0 C_m/(8\pi q). \qquad (73)$$

Substitution in eq. (73) by means of eq. (12) yields

$$\Phi_{tot} F/\alpha' = M_0/(4q). \qquad (74)$$

If the motor parameters were specified at t_1, then for another temperature t_2 we can write, from eq. (34)

$$\Phi_{tot(t2)} = \Phi_{tot(t1)} \left\{ 1 + \frac{(t_2 - t_1)Br}{100} \right\}$$

from eq. (37)

$$F_{(t2)} = F_{(t1)} \frac{R_{a(t1)} + R_{c(t1)} + R_{i(t1)}}{R_{a(t2)} + R_{c(t2)} + R_{i(t2)}}$$

and, from eq. (38),

$$M_{0(t2)} = M_{0(t1)} \left\{ 1 + \frac{(t_2 - t_1)\tau Br}{100} \right\} \times \times \frac{R_{a(t1)} + R_{c(t1)} + R_{i(t1)}}{R_{a(t2)} + R_{c(t2)} + R_{i(t2)}}$$

from which it is apparent that

$$F_{(t)}\Phi_{tot(t)} = \alpha' M_{0(t)}/(4q). \qquad (75)$$

That is, for q = 1, throughout the operating temperature range of the motor:

The product of the total flux through the motor and the effective back m.m.f. induced by the starting current must equal one quarter of the product of the winding angle and the starting torque generated at that temperature.

Since the total flux is supplied by the stator magnets, whereas the back m.m.f. is generated by the rotor, eq. (75) unites both components of the motor specification. Of the specific parameters, in fact, only M_0 and α' affect this relationship, and, of these, α' is generally predetermined by the choice of two, four, or more poles for the motor.

THE VOLUME OF PERMANENT-MAGNET MATERIAL

Practical considerations

Substitution in eq. (75) by means of eqs (56) and (57) yields the volume of the permanent magnets needed for a permanent-magnet motor:

$$V_f = \frac{\alpha' M_{0(t)} (1 + d_s/D_{is})}{2fqB_{r(t)} [\gamma_0 I_{cJ(t)} - B_{r(t)} \delta/(\mu_0 d)]}. \qquad (76)$$

Since

$$d_s = d - \delta \qquad (77)$$

eq. (76) can also be written

$$V_f = \frac{\alpha' M_{0(t)} [1 + (d - \delta)/D_{is}]}{2fqB_{r(t)} [\gamma_0 H_{cJ(t)} - B_{r(t)} \delta/(\mu_0 d)]}. \qquad (78)$$

That is, the volume of magnetic ceramic required in a permanent-magnet motor is a function of

- material characteristics B_r, H_{cJ}, γ_0
- motor specification parameters M_0, α'
- magnet dimensions D_{is}, d_s
- air-gap length δ
- magnetic-circuit leakage and reluctance factors f, q.

In practice, an average value for air-gap length δ is found to be 0.0008 m. Taking $\gamma_0 = 0.83$ and, with $\mu_0 = 4\pi \times 10^{-7}$ H/m, the volume of ceramic permanent-magnets required is

$$V_f \cong \frac{\alpha' M_{0(t)} [1 + (d - 0.0008)/D_{is}]}{2fqB_{r(t)} (0.83H_{cJ(t)} - 636.44B_{r(t)}/d)}. \qquad (79)$$

Some impression of the effects of d and D_{is} on the volume of the various grades of Ferroxdure ceramics is given by the three-dimensional presentation of Fig.3 Here, the volume at 20 °C is given for unity winding angle and unity starting torque; product fq is also taken as unity – a value close to that encountered in practice.

In Fig.3 the relationship between the volume of material and dimensions d and D_{is} is shown for FXD 270

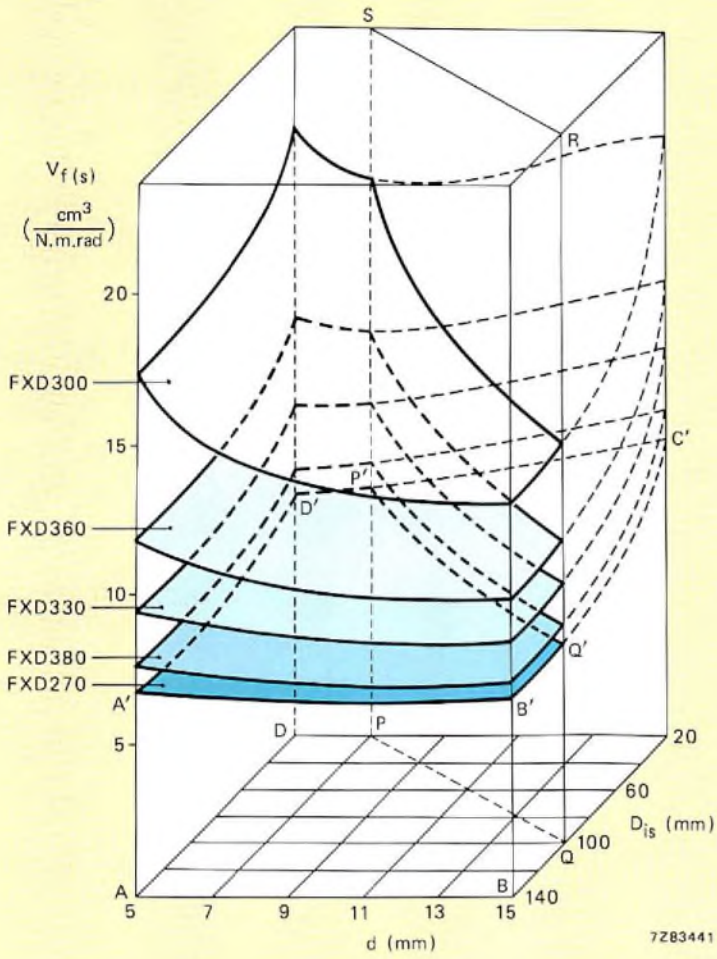

Fig.3 Three-dimensional representation of the specific volume (volume for unit torque and winding angle) of various grades for Ferroxdure ceramics as functions of d and D_{is}.

by surface A′B′C′D′. Not all the combinations of these dimensions will occur in practice: a motor with a D_{is} value of 20 mm and a magnet plus air gap thickness d of 15 mm, for example. Consequently, base surface ABCD has been delimited by line PQ so that the surfaces of volume are also restricted to practical values by plane PQRS; this restriction is, of course, somewhat arbitrary. In the case of the FXD 270 surface, only area A′B′Q′P′D′ represents examples likely to be encountered in practice.

Contributing factors

In order to examine the effect of the various system parameters on the volume of magnet material required, it is helpful to simplify eq. (79) by reducing it to three terms:

– a factor G that defines the segment geometry,

$$G = 1 + (d - 0.0008)/D_{is} \qquad (80)$$

– a factor $Q_{d(t)}$ that describes the performance of the magnet material at a given temperature,

$$Q_{d(t)} = 2B_{r(t)}(0.83H_{cJ(t)} - 636.44B_{r(t)}/d) \qquad (81)$$

– and a factor $f_{m(t)}$ that reflects the motor specification and the amount by which the magnets overhang the rotor,

$$f_{m(t)} = \alpha' M_{0(t)}/(fq). \qquad (82)$$

In this way, eq. (79) reduces to

$$V_f = Gf_{m(t)}/Q_{d(t)}. \qquad (83)$$

Where the specific volume, the volume for unity torque and unity winding angle (1 radian), is sufficient, eq. (83) itself may be reduced to

$$V_{f(s)} = G/Q_{d(t)}. \qquad (84)$$

It is the specific volume that is shown in Fig.3.

OPTIMISING MATERIAL VOLUME

The effect of dimensions

Figure 4 shows the relationship between the value of $Q_{d(t)}$, which is inversely proportional to material volume, and rotor-to-housing distance d plotted from eq.(81) for a number of grades of anisotropic Ferroxdure. It is evident that there is a limiting value of $Q_{d(t)}$ for each grade of ceramic magnet material which is reached for large values of d. Note, too, that the value of $Q_{d(t)}$ changes rapidly at small values of d, and, thus, so does the volume of material required.

Dimension d is, however, also present in factor G, eq.(80). The variation of G with d is, of course, a straight line whose slope is determined by the value of D_{is}, Fig.6. The effect of d on the volume of magnet material is small at large values of D_{is}.

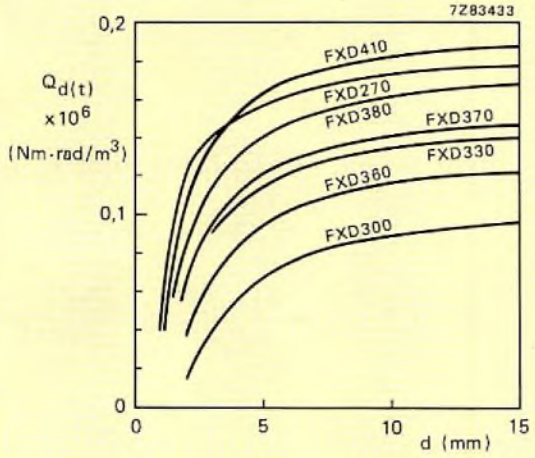

Fig.4 Variation of $Q_{d(t)}$ with d plotted from eq. (81) for various grades of Ferroxdure

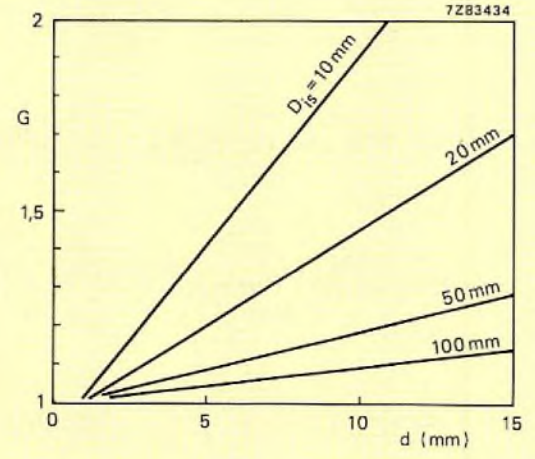

Fig.5 Variation of G with d from eq. (80)

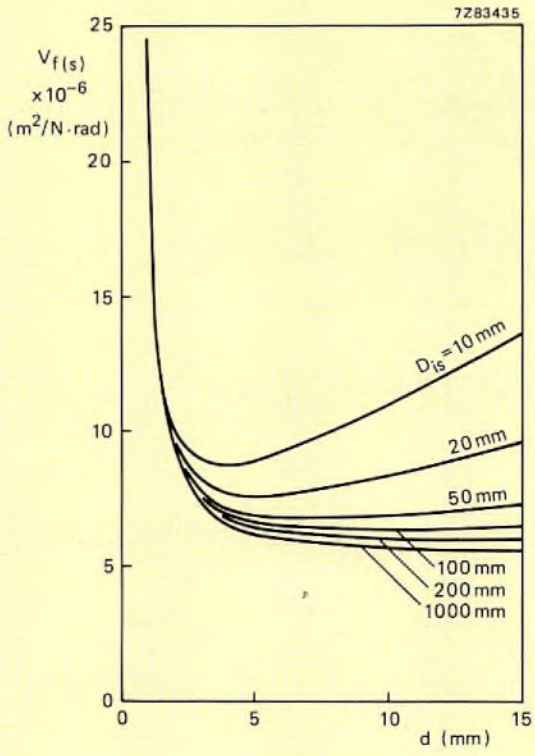

Fig.6 Specific volume $V_{f(s)}$ of Ferroxdure 270 as a function of d with D_{is} as a parameter

The combined effect of d and D_{is} on both $Q_{d(t)}$ and G yields the specific volume $V_{f(s)}$ for a given grade of material, as is shown by Fig.3. The specific volume is plotted for FXD 270 as a function of d and for various values of D_{is} in Fig.6, which is a number of sections through Fig.3. There it is apparent that specific volume decreases with increasing D_{is}, and that for smaller motors (D_{is} less than about 100 mm) there is a value of d for which $V_{f(s)}$ is minimum. At values of D_{is} above about 100 mm no minimum value of $V_{f(s)}$ is apparent at practical values of d.

Effect of material properties

Equation (81) may be rewritten

$$Q_{d(t)} = 1.66B_{r(t)}H_{cJ(t)} - 1272.88B^2_{r(t)}/d. \qquad (85)$$

Differentiating yields

$$\frac{dQ_{d(t)}}{dB_{r(t)}} = 1.66H_{cJ(t)} - 2545.76B_{r(t)}/d \qquad (86)$$

From this it is evident that there will be a maximum value of $Q_{d(t)}$ when

$$B_r(t) = 6.52 \times 10^{-4} H_{cJ}(t)d. \qquad (87)$$

This means that, for each value of d, there is a magnet material that has the general properties (γ_0 and μ_{rec}, for example) of anisotropic Ferroxdure with combinations of H_{cJ} and B_r for which minimum magnet volume is obtained. In fact, for each value of H_{cJ} there is a value of B_r for which V_f is minimum. Some of these combinations are listed in Table 2, where it can be seen that these ideal materials have very much larger values of B_r than are encountered in practice.

Figure 7 shows the H_cJ and B_r coordinates of some practical materials together with the theoretically minimum values of H_cJ on curves for two values of $Q_d(t)$. It can be seen that, owing to the shape of the curves, the theoretical minima are in fact negligibly smaller than the values that can actually be obtained with present-day materials.

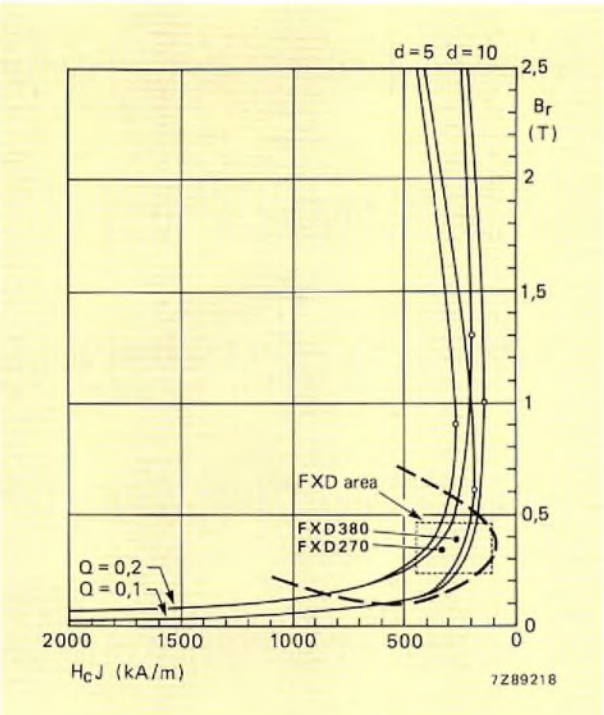

Fig.7 B_r as a function of H_cJ for $Q = 0.1\,Nm/cm^3$ and $Q = 0.2\,Nm/cm^3$, $d = 5\,mm$ and $d = 10\,mm$; the open points are points of $(H_cJ)_{min}$. The dashed curved indicates the region of practical interest, and the dotted rectangle the area in which the coordinates of present-day Ferroxdure materials are

TABLE 2
Optimum material characteristics for minimum magnet volume at a number of values of d

H_{cJ} (kA/m)	B_r (T)		
	d = 3 mm	d = 5 mm	d = 10 mm
100	0.196	0.326	0.652
200	0.391	0.652	1.304
300	0.587	0.978	1.956
400	0.782	1.304	2.608
500	0.978	1.630	3.260

CONCLUSIONS

Manipulation of the standard motor-design relationships highlights a number of potentially-interesting correlations between motor specification, motor construction and performance. It also sheds additional light on the importance of the characteristics of the permanent-magnet material for the stator.

Emphasis here has been on the amount of magnetic material used. However, this is but one aspect of the overall design and one of the directions in which trade-offs can be made by the designer.

ACKNOWLEDGEMENTS

The author would like to express his appreciation to P. J. Schophuizen and F. A. J. Wouters for the work that they carried out in connection with this study.

REFERENCES

1. Wullkopf, H. 1964. Der magnetischen Fluss in Gleichstrommotoren bei Verwendung von Permanentmagneten aus Ferroxdure. *Valvo Berichten X.*
2. 1974. *D.C. motors with Ferroxdure permanent magnets.* Philips' Application Book.
3. Haes, E. 1974. *Recoil lines for Ba and Sr FXD materials in the 2nd quadrant.* Internal report.
4. Schophuizen, P. J. 1979. *Temperature coefficient for the H_{cJ} in Ferroxdure.* Private communication.

Abstracts

Integrated circuits for car radios

A family of integrated circuits designed to meet the performance requirements for car a.m./f.m. stereo radio/cassette players accommodates both commonly followed concepts for f.m. channel demodulation: ratio detector and quadrature detector. A complete design for each concept is given together with performance data.

Fibre-optic communications

Advances in glass and semiconductor technology make wideband optical communication a feasible alternative to waveguide and coaxial cables. With present-day light sources, photodetectors, optical fibres and coupling devices, repeater spacings of the order of 1 km are practical at data rates up to 10 Mbit/s. Apart from bandwidth, the advantages of fibre-optic communication include high immunity to interference, crosstalk, and unauthorized tapping.

Purpose-designed ferrite toroids for isolated current measurement in power electronic equipment

The saturable cores in a pulsed d.c. current transformer (DCCT) system developed for use in pulse-width modulation a.c. motor control are purpose-designed ferrite toroids. The ability of the DCCT to provide accurate isolated current measurement at low cost gives it the potential for widespread industrial use beyond the specific purpose for which it was developed. This article discusses the theory, design, and performance of DCCT systems using the purpose-designed toroids in single and three-phase applications.

Microprocessor peripheral for viewdata

The SAA5070 is a large-scale integrated circuit designed as a microprocessor peripheral device in viewdata receivers and intended to integrate as many as possible of the fixed hardware functions on the telephone line side. This article describes features of the IC in detail, together with its use in viewdata receivers using microprocessors of the 8048 family.

Ceramic permanent magnets for d.c. motors

Part 2 – Design calculations

Using equations developed in Part 1 (E.C.A. Vol. 3 No. 1), it is shown how the volume of magnetic material required depends on the motor specification, the segment geometry, and the performance of the magnet material at a given temperature. Calculation based on this dependence can be used to optimise the volume of magnetic material for a given motor specification.

Integrierte Schaltungen für Autoradios

In einer Familie von integrierten Schaltungen, die für den Einsatz in AM/FM-Stereo-Autoradio/Recorder entwickelt worden sind, werden zwei Konzepte für die FM-Demodulatoren verwendet: Ratio-Detektor und Quadraturdemodulator. Für jedes dieser Konzepte wird ein kompletter Schaltungsentwurf mit den zugehörigen technischen Daten und Eigenschaften angegeben.

Glasfaser-Übertragung

Fortschritte in der Glas- und Halbleitertechnologie machen optische Breitbandübertragungen zu einer attraktiven Alternative zu Hohlleitern und Koaxialkabeln. Die gegenwärtig verwendeten Lichtquellen, Fotodetektoren, Glasfaser-Leitungen und Konnektoren ermöglichen Verstärkerabstände von 1 km bei einer Datenübertragungsrate bis zu 10 Mbit/s. Neben grosser Breitbandigkeit zeichnen sich Glasfaser-Übertragungen durch eine hohe Sicherheit gegen Störungen, Übersprechen und heimliches Anzapfen aus.

Speziell entwickelte Ferrit-Ringkerne für potentialfreie Strommessungen

Für ein Messwandlersystem (DCCT-System) zur potentialfreien Strommessungen bei Anlagen zum Betrieb von drehzahlgeregelten Wechselstrommotoren mit Impulsbreiten-Modulation wurden spezielle Ferrit-Kerne entwickelt. Die möglichkeit mit einem solchen Messwandlersystem preiswert potentialfreie Strommessungen durchführen zu können, ermöglicht darüber hinaus den Einsatz dieses Systems in einem weiten Bereich industrieller Anwendungen. In diesem Artikel werden die Theorie, der Entwurf und die Arbeitsweise des mit speziell entwickelten Ferrit-Kernen arbeitenden Messwandlersystems diskutiert.

Mikroprozessor-Peripherieschaltung für Bildschirmtext

Die Schaltung SAA5070 ist eine hochintegrierte Schaltung, die als Mikroprozessor-Peripherie in Bildschirmtext-Empfängern entwickelt wurde mit dem Ziel, eine möglichst grosse Anzahl der festliegenden Hardware-Funktionen auf der Telefonleitungsseite in einer Schaltung zu integrieren. Dieser Beitrag umfasst eine detaillierte Beschreibung der Eigenschaften dieser Integrierten Schaltung in Verbindung mit deren Einsatz in Bildschirmtext-Empfängern, die einen Mikroprozessor der Familie MCS-48™ verwenden.

Keramische Permanentmagnete für Gleichstrommotoren

Teil 2 – Entwurfsberechnung

Unter Verwendung der in Teil 1 hergeleiteten Gleichungen wird gezeigt, wie das erforderliche Volumen des Magnetmaterials von der Motorspezifikation, den Abmessungen der Segmente und den Eigenschaften des Magnetmaterials bei einer vorgegebenen Temperatur abhängt. Die auf dieser Abhängigkeit fussende Berechnung kann zur Optimierung des Magnetvolumens bei einer gegebenen Motorspezifikation dienen.

Circuits intégrés pour auto-radio

Cette famille de circuits intégrés est conçue pour répondre aux impératifs de performances des combinés auto-radio stéréophoniques m.a./m.f./lecteurs des cassettes et emploie les deux concepts couramment utilisés pour la démodulation du canal m.f.: la détection de rapport et la détection quadratique. On trouvera une étude complète de chaque concept ainsi que les performances.

Communication par fibres optiques

Les progrès de la technologie du verre et des semiconducteurs font de la communication optique à large bande une solution de remplacement acceptable pour les guides d'ondes et câbles coaxiaux. Les sources lumineuses, photodétecteurs, fibres optiques et dispositifs de couplage actuels rendent practicable un espacement des récepteurs de l'ordre de 1 km avec un débit atteignant 10 Mbit/s. En plus de la largeur de bande, la communication par fibres optiques présente l'avantage d'une grande immunité aux parasites, à la diaphonie et à la captation non autorisée des messages.

Toroïdes de ferrite personnalisés pour la mesure de courants isolés dans les matériels électroniques de puissance

Les noyaux saturable dans un système de transformation de courant continu pulsé (DCCT) destiné à la commande de moteurs alternatifs par modulation de largeur d'impulsion sont des toroïdes de ferrite personnalisés. L'aptitude du DCCT à permettre à peu de frais la mesure de courants isolés lui donne des possibilités étendues d'emploi dans l'industrie, qui dépassent l'application spécifique pour laquelle il a été mis au point. L'article expose la théorie, la construction et le fonctionnement des systèmes DCCT équipés des toroïdes personnalisés dans des applications en monophasé et triphasé.

Périphérique de microprocesseur pour télétexte

Le SAA5070 est un circuit intégré à grande échelle destiné à servir de dispositif périphérique de microprocesseur dans les récepteurs de télétexte et à incorporer un aussi grand nombre que possible des fonctions de matériel fixes du côté ligne téléphonique. L'article décrit en détail les caractéristiques du circuit intégré, ainsi que son emploi dans les récepteurs de télétexte équipés de microprocesseurs de la famille 8048.

Aimants permanents céramiques pour moteurs à courant continu

2ème Partie – Calculs de réalisation

Les équations étudiées dans la 1ère partie (E.C.A., Vol. 3, No. 1) montrent les relations qui existent entre le volume nécessaire de matériau magnétique et les caractéristiques fonctionnelles du moteur, la géométrie des segments et le comportement du matériau magnétique à une température donnée. Le volume de matériau magnétique pour un moteur de caractéristiques données peut être optimalisé à l'aide de calculs basés sur ces relations.

Circuitos integrados para auto-radios

Una familia de circuitos integrados, especialmente diseñados para equipos de radio-casette am/fm estéreo para el automovil, combina los dos conceptos seguidos normalmente para la demodulación del canal de fm: detector de relación y detector de cuadratura. En este artículo se da un diseño completo para cada concepto junto con datos de funcionamiento.

Transmisión por fibras ópticas

Los avances en las tecnologías del vidrio y de semiconductores hacen que la transmisión óptica de banda ancha sea una alternativa factible frente a las guías de ondas y cables coaxiales. Con las fuentes de luz actuales, fotodetectores, fibras ópticas y dispositivos de acoplamiento, se logra espaciar los repetidores unos 1 km, para una velocidad de transmisión de 10 Mbit/s. Otras ventajas de la transmisión por fibras ópticas son: elevada inmunidad a interferencias, diafonía e imposibilidad de acceso a la informacion.

Ferritas toroidales para medidores de corriente aislados en equipo de potencia

Los núcleos saturables en un sistema transformador de CC. (DCCT), desarrollados para usar en control de motores de ca con modulación de anchura de impulsos (PWM) son toroides de ferrita especialmente diseñados. La facilidad de los DCCT para proporcionar unas mediciones de corriente aisladas a bajo coste, les proporciona un amplio abanico de posibilidades en el campo industrial, además del específico propósito para el que fueron diseñados. Este artículo expone la teoría diseño y características de los sistemas DCCT, que utilizan los toroides especialmente en aplicaciones monofásicas y trifásicas.

Microprocesador periférico para viewdata

El SAA5070 es un circuito integrado a gran escala, diseñado como periférico en receptores viewdata en un intento de integrar al máximo posible las functiones fijas pertenecientes al hardware de entrada de las líneas telefónicas. Este artículo describe con detalle las características del CI conjuntamente con su uso en los receptores viewdata donde se usan microprocesadores de la familia 8048.

Imanes permanentes cerámicos para motores de c.c.

Parte 2 – cálculos de diseño

Utilizando las ecuaciones desarrolladas en la parte 1 (E.C.A. Vol. 3, No. 1), se demuestra que el volumen del material magnético necesario depende de las especificaciones del motor, de la geometría del segmento y de las características del material magnético a una determinada temperatura. Las células basadas en esta dependencia se pueden utilizar para optimizar el tamaño del material magnético para una determinada especificación del motor.

Authors

B. P. Bahnsen was born in Hamburg, West Germany, in 1934. After taking his degree in electrical engineering in 1962 he joined the Application Laboratory of Valvo G.m.b.H. in Hamburg as a member of the radio and telecommunications group where, for the past eight years, he has specialized in r.f. and decoder parts of radio receivers.

R. E. F. Bugg was born at Aylesbury, Buckinghamshire, in 1949 and took his B.Sc in electrical engineering at Imperial College, London, in 1970. After graduation he joined Mullard Ltd, where he initially worked in the tv section and, later, in the text-handling group where he now is. He has been associated with teletext since its beginning and holds several patents related to it.

Arnold Garskamp was born in Rotterdam, The Netherlands in 1936 and graduated in electrical and radio engineering in 1967. After military service, he joined the Central Application Laboratory of Elcoma in Eindhoven where he was involved in the application of semiconductors in radio and audio circuits. For the past eight years, he has concentrated on design techniques for radio circuits intended for subsequent integration. He cooperated in the design of the f.m. i.f. system TEA5560 which is described in this issue.

H. J. H. van Heffen was born in The Hague in 1930 and joined Philips in 1949. While employed at the Research Laboratory he studied organic chemistry with the Royal Netherlands Chemical Society and Philips Technical Institute. In 1960 he transferred to the ceramics laboratory of the Electronic Components and Materials Division where, till 1970, he was engaged in the development of hard ferrites. Since then, as a member of the commercial department, he has been concerned with technical applications of magnetic ceramics.

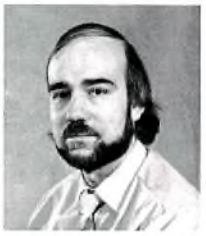

John Houldsworth obtained an honours degree in electronics from the University of Salford and joined the power group of Mullard Applications Laboratory in 1969. In 1970 he undertook a sponsored research course at the University of Manchester Institute of Science and Technology and earned an M.Sc. in control engineering. Since 1971 he has engaged in innovative work in power electronics and most recently on speed control of industrial three-phase induction motors. He is team leader of the motor control group at the Systems Applications Centre for Power at Mitcham. He is a chartered engineer and a member of the IEE, where he serves on the Power-Electronic Equipment Committee, P6.

Henk J. M. Otten was born at Sint Oedenrode, The Netherlands, in 1946 and graduated in electronic engineering at the University of Technology, Eindhoven, in 1973. After joining the Central Application Laboratory of Philips Elcoma Division he became engaged in the development of integrated circuits for tv receivers and, later, of components for fibre-optic communication. At present he is concerned with the design and application of components for electronic telephone equipment.

Electronic components and materials

for professional, industrial and consumer uses

from the world-wide Philips Group of Companies

Argentina: FAPESA, Av. Crovara 2550, Tablada, Prov. de BUENOS AIRES, Tel. 652-7438/7478.
Australia: PHILIPS INDUSTRIES HOLDINGS LTD., Elcoma Division, 67 Mars Road, LANE COVE, 2066, N.S.W., Tel. 427 08 88.
Austria: ÖSTERREICHISCHE PHILIPS BAUELEMENTE Industrie G.m.b.H., Triester Str. 64, A-1101 WIEN, Tel. 62 91 11.
Belgium: M.B.L.E., 80, rue des Deux Gares, B-1070 BRUXELLES, Tel. 523 00 00.
Brazil: IBRAPE, Caixa Postal 7383, Av. Brigadeiro Faria Lima, 1735 SAO PAULO, SP. Tel. (011) 211-2600.
Canada: PHILIPS ELECTRONICS LTD., Electron Devices Div., 601 Milner Ave., SCARBOROUGH, Ontario, M1B 1M8, Tel. 292-5161.
Chile: PHILIPS CHILENA S.A., Av. Santa Maria 0760, SANTIAGO, Tel. 39-40 01.
Colombia: SADAPE S.A., P.O. Box 9805, Calle 13, No. 51 + 39, BOGOTA D.E. 1., Tel. 600 600.
Denmark: MINIWATT A/S, Emdrupvej 115A, DK-2400 KØBENHAVN NV., Tel. (01) 69 16 22.
Finland: OY PHILIPS AB, Elcoma Division, Kaivokatu 8, SF-00100 HELSINKI 10, Tel. 1 72 71.
France: R.T.C. LA RADIOTECHNIQUE-COMPELEC, 130 Avenue Ledru Rollin, F-75540 PARIS 11, Tel. 355-44-99.
Germany: VALVO, UB Bauelemente der Philips G.m.b.H., Valvo Haus, Burchardstrasse 19, D-2 HAMBURG 1, Tel. (040) 3296-1.
Greece: PHILIPS S.A. HELLENIQUE, Elcoma Division, 52, Av. Syngrou, ATHENS, Tel. 915 311.
Hong Kong: PHILIPS HONG KONG LTD., Elcoma Div., 15/F Philips Ind. Bldg., 24-28 Kung Yip St., KWAI CHUNG, Tel. 12-24 51 21.
India: PEICO ELECTRONICS & ELECTRICALS LTD., Ramon House, 169 Backbay Reclamation, BOMBAY 400020, Tel. 295144.
Indonesia: P.T. PHILIPS-RALIN ELECTRONICS, Elcoma Div., Panim Bank Building, 2nd Fl., Jl. Jend. Sudirman, P.O. Box 223, JAKARTA, Tel. 716 131.
Ireland: PHILIPS ELECTRICAL (IRELAND) LTD., Newstead, Clonskeagh, DUBLIN 14, Tel. 69 33 55.
Italy: PHILIPS S.p.A., Sezione Elcoma, Piazza IV Novembre 3, I-20124 MILANO, Tel. 2-6994.
Japan: NIHON PHILIPS CORP., Shuwa Shinagawa Bldg., 26-33 Takanawa 3-chome, Minato-ku, TOKYO (108), Tel. 448-5611.
(IC Products) SIGNETICS JAPAN, LTD, TOKYO, Tel. (03)230-1521.
Korea: PHILIPS ELECTRONICS (KOREA) LTD., Elcoma Div., Philips House, 260-199 Itaewon-dong, Yongsan-ku, C.P O. Box 3680, SEOUL, Tel. 794-4202.
Malaysia: PHILIPS MALAYSIA SDN. BERHAD, Lot 2, Jalan 222, Section 14, Petaling Jaya, P.O.B. 2163, KUALA LUMPUR, Selangor, Tel. 77 44 11.
Mexico: ELECTRONICA S.A. de C.V., Varsovia No. 36, MEXICO 6, D.F., Tel. 533-11-80.
Netherlands: PHILIPS NEDERLAND B.V., Afd. Elonco, Boschdijk 525, 5600 PB EINDHOVEN, Tel. (040) 79 33 33.
New Zealand: PHILIPS ELECTRICAL IND. LTD., Elcoma-Division, 2 Wagener Place, St. Lukes, AUCKLAND, Tel. 894-160.
Norway: NORSK A/S PHILIPS, Electronica, Sørkedalsveien 6, OSLO 3, Tel. 46 38 90.
Peru: CADESA, Rocca de Vergallo 247, LIMA 17, Tel. 62 85 99.
Philippines: PHILIPS INDUSTRIAL DEV. INC., 2246 Pasong Tamo, P.O. Box 911, Makati Comm. Centre, MAKATI-RIZAL 3116, Tel. 86-89-51 to 59.
Portugal: PHILIPS PORTUGESA S.A.R.L., Av. Eng. Duharte Pacheco 6, LISBOA 1, Tel. 68 31 21.
Singapore: PHILIPS PROJECT DEV. (Singapore) PTE LTD., Elcoma Div., Lorong 1, Toa Payoh, SINGAPORE 1231, Tel. 25 38 811.
South Africa: EDAC (Pty.) Ltd., 3rd Floor Rainer House, Upper Railway Rd. & Ove St., New Doornfontein, JOHANNESBURG 2001, Tel. 614-2362/9.
Spain: COPRESA S.A., Balmes 22, BARCELONA 7, Tel. 301 63 12.
Sweden: A.B. ELCOMA, Lidingövägen 50, S-11584 STOCKHOLM 27, Tel. 08/67 97 80.
Switzerland: PHILIPS A.G., Elcoma Dept., Allmendstrasse 140-142, CH-8027 ZÜRICH, Tel. 01/43 22 11.
Taiwan: PHILIPS TAIWAN LTD., 3rd Fl., San Min Building, 57-1, Chung Shan N. Rd, Section 2, P O. Box 22978, TAIPEI, Tel. (02)-5631717.
Thailand: PHILIPS ELECTRICAL CO. OF THAILAND LTD., 283 Silom Road, P.O. Box 961, BANGKOK, Tel. 233-6330-9.
Turkey: TÜRK PHILIPS TICARET A.S., EMET Department, Inonu Cad. No. 78-80, ISTANBUL, Tel. 43 59 10.
United Kingdom: MULLARD LTD., Mullard House, Torrington Place, LONDON WC1E 7HD, Tel. 01-580 6633.
United States: (Active devices & Materials) AMPEREX SALES CORP., Providence Pike, SLATERSVILLE, R.I. 02876, Tel. (401) 762-9000.
(Passive devices) MEPCO/ELECTRA INC., Columbia Rd., MORRISTOWN, N.J. 07960, Tel. (201) 539-2000.
(IC Products) SIGNETICS CORPORATION, 811 East Arques Avenue, SUNNYVALE, California 94086, Tel. (408) 739-7700.
Uruguay: LUZILECTRON S.A., Avda Rondeau 1576, piso 5, MONTEVIDEO, Tel. 91 43 21.
Venezuela: IND. VENEZOLANAS PHILIPS S.A., Elcoma Dept., A. Ppal de los Ruices, Edif. Centro Colgate, CARACAS, Tel. 36 05 11.

A19

Printed in The Netherlands